FIBRE DYNAMICS IN THE AIR-LAID NONWOVEN PROCESS

A thesis submitted in accordance with the requirements for the degree of Doctor of Philosophy

by

Alireza Pourmohammadi

being an account of work carried out under the supervision of

Professor C. A. Lawrence

University of Leeds

School of Textile Industries

June, 1998

The candidate confirms that the work submitted is his own and that appropriate credit has been given where reference has been made to the work of others.

To:

My wife, simin

and

my son, mohammad

Abstract

Nonwoven manufacturing processes, generally speaking, aim to produce fabric more economically than can be achieved by traditional means of fabric formation namely weaving and knitting. Although all nonwovens are made by assembling fibres into some type of web, there are various ways of producing webs. The most common web forming methods are : carding (parallel-laid and cross-laid), meltblown, spunbonded, wet-laid and air-laid.

This study focuses on the air-laid web process. The main objective of the reported work is to further develop the understanding of the dynamics of fibre flow in the air-laid web forming process by deriving a theoretical model which relates fibre properties (fineness, length, density) and process variables to fibre movement in the stripping zone of the process.

Having read the literature and obtaining the necessary background about fibre dynamics in the air flow, a new theoretical model has been developed which describes the movement of fibres along the teeth of the opening roller and their passage along the channel. This model gives an insight into the general behaviour of fibres when the key process variables (such as air speed, cylinder speed, angle of teeth, length of the teeth,...) are altered.

In an attempt to verify the theoretical model, high speed cine photography was used to visualise the flow of fibres through the system. Analysis of photographs gave good agreement with the main theoretical findings of the model in respect of the trajectory of fibres within the stripping zone of the air-laid web forming process.

ACKNOWLEDGEMENT

First and foremost praise to Allah, who taught man that he knew nothing. Thanks to Him for all the bounty bestowed upon mankind.

I would like to express my gratitude to my supervisor Professor C.A.Lawrence, whose support throughout the project has been unerring and his comments, advice and general encouragement has been of great worth and importance.

I am gratefully indebted to Dr. G.A.V Leaf and R. Hill for their valuable discussions and continuous interest by which I benefited during the theoretical part of this thesis.

I wish to thank Dr. G.A.V. Leaf and Dr. S. Russell for their thorough reading of the draft copies of this text and for helpful suggestions and amendments, which contributed greatly to the final text.

Thanks are also due to Miss L. Seymour (secretary of Prof. Lawrence), Mrs. V. Whitehead (Departmental Librarian), Mr. E. Hampshaw (of Nonwoven Lab.), J.Peckam and H.S. Rait (of Eng. workshop) and also to all my friends and colleagues, who have been of great assistance and support throughout this research.

My thanks are extended to the Ministry of Culture and Higher Education of Islamic Republic of Iran for giving me the opportunity and support to carry out this study.

Finally, I unreservedly express my sincere and loving thanks to my wife, Simin, for her unstinting patience and support during the whole period of this study and to my little son Mohammad. I owe a debt of gratitude to my parents and my brother and sister who have been a constant source of encouragement. I dedicate this thesis to all my family in the appreciation of their forbearance.

Contents

List of Figures

Chapter one

Chapter Two

Chapter Three

Chapter Four

Chapter Five

Chapter Six

List of Tables

Chapter one

Chapter Four

Chapter Five

Chapter Six

Introduction

The demand made by industry on machine manufacturers for uniform web strength in all directions, constitutes a major problem for conventional carding equipment due to the directional fibre orientation in the web. Balanced strength can only be attained when an equal fibre distribution in all directions can be achieved. In other words, total randomisation.

In order to reach the above goal, aerodynamic web formation provides the means of producing randomisation in the web. Air-laid web forming technology enables the manufacture of high quality webs in the web weight range 20-3000 g/m^2. These webs are then utilised for variety of applications due to their random structure, which exhibits an isotropic strength distribution and good softness. This technology is a growing area of the nonwoven industry and the aim of the present work is to establish a fundamental understanding of the system to be used to allow the possible improvement of the performance of the process.

To be able to carry out the present work an air lay machine was modified so that an acceptable web, in terms of regularity ,could be obtained. In this study the dynamic behaviour of fibres in the system were theoretically modelled and a high speed camera was used to visualise the fibre motion in the stripping zone of the air-laying machine.

Outline of the Research Work

⌖ A general background about the nonwoven industry, the applications of products and also a concise history of air-laid technology is given in Chapter One.

⌖ In Chapter Two a fundamental understanding of the fibre dynamic through an air flow is described/~~established~~ by referring to the published literature.

⌖ A theoretical model which relates fibre properties (fineness, length, density) and process variables to the fibre motion in stripping zone is explained in Chapter Three.

⌖ The experimental air-laid machine and all the modification is described in Chapter Four.

⌖ The photographic part of the work is substantially stressed with a comprehensive explanation of the high speed camera ,which is used in this work for providing the pictures from the fibre motion, in Chapter Five.

⌖ Chapter Six discusses the Numerical results from the theoretical model and the results from the analysis of the films taken by high speed camera. Finally the conclusion and recommendation for future work is given in Chapter Seven.

AIMS AND OBJECTIVES OF THE PRESENT WORK

The objectives of the present study may be summarised as follows:

1) To establish a fundamental understanding of the dynamics of fibre flow through an air-laid web forming process.

2) To derive a model or models which relate fibre properties (fineness, length, density) and process variables to fibre movement in the transport channel of the air-laid process.

3) To experimentally validate the numerical results obtained from the theoretical model.

Chapter one

A General Background to the Nonwoven Industry

1.1 Introduction

The Nonwoven industry first began to establish itself in the immediate post-war period, and it has been showing steady growth for many years. Forecasts for the near future are optimistic and anticipate a total of 2.6 million tonnes for the global nonwoven demand by the year 2001 [Shariq 98]. Generally speaking, nonwoven fabric manufacture aims to produce fabrics more economically than can be achieved by traditional means of fabric production, mainly weaving and knitting. They are essentially high production processes and as originally conceived they aim to cut the production cost by : a) minimising the intermediate steps between raw material and the end use product (that is, fibre to fabric in one operation), b) using waste and other cheap low grade materials which can not be used in the traditional fabric formation methods.

1.2 Nonwoven end-uses categories

The applications of Nonwoven fabrics can be divided into two categories, namely *disposable* and *durable.* Disposable items are used once and then thrown away , whereas durable goods generally remain in place through the lifetime of the particular application. Figure (1.1) shows the end-use consumption of Nonwoven fabrics in the three main regions of the world which produce the overwhelming majority of nonwovens (that is over 88 % of the more than 2.1 million metric tons, total tonnage used in the manufacture of Nonwoven fabrics in 1994) [Shariq 96].

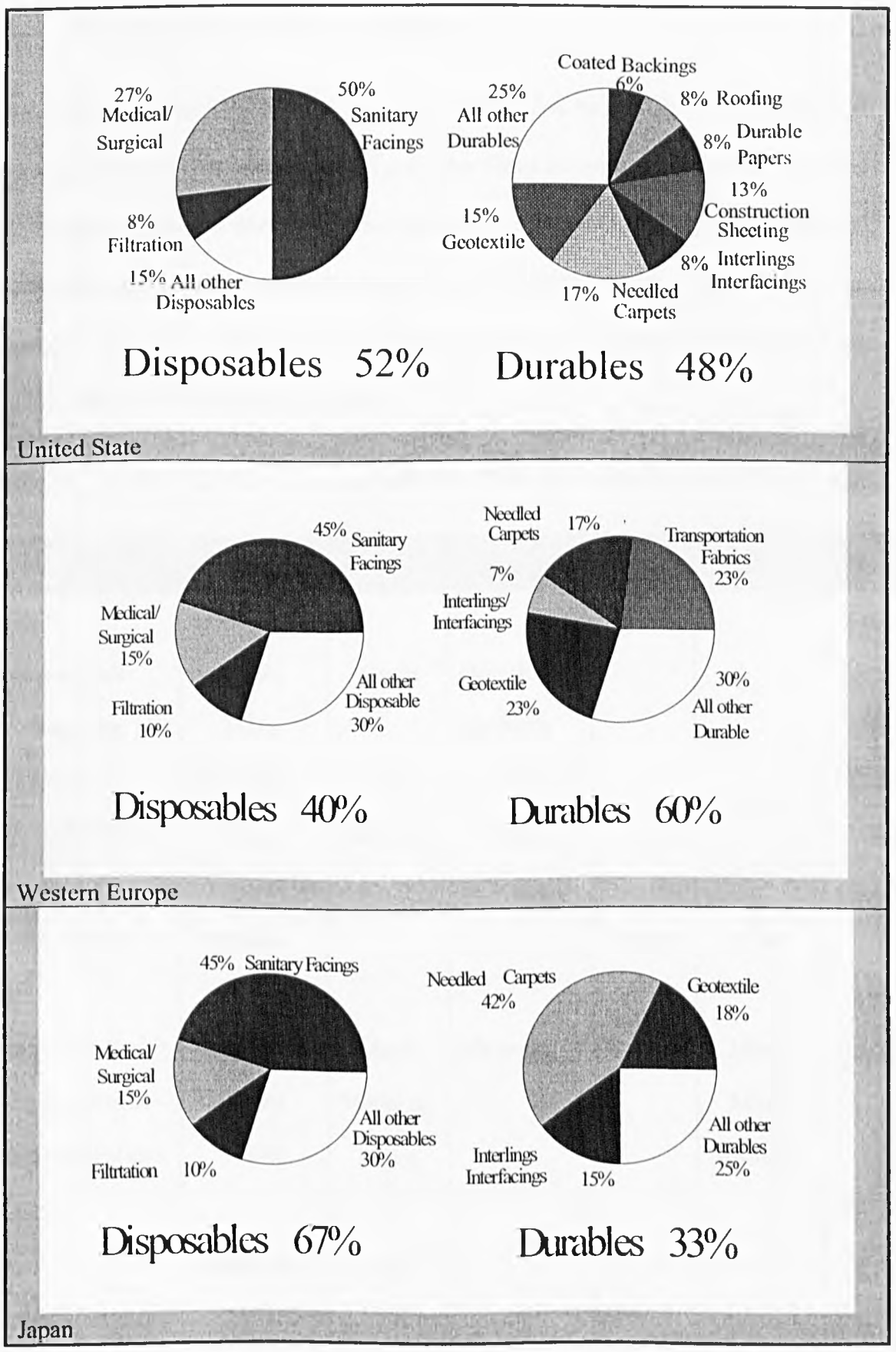

Figure (1.1) Consumption of nonwovens by end-use application

1.3 Fibre type used in nonwoven industry

Both natural and synthetic (staple or filament) fibres can be used in the production of Nonwoven fabrics. Polypropylene and polyester fibres are now the main fibres used by the industry. These two fibres compete heavily with each other in many of the same end uses, with polypropylene having the competitive advantage because of its slightly lower fibre and fabric cost. Table (1.1) summarises the use of different fibre types in the various Nonwoven production categories.

Table (1.1) End uses for nonwoven fabrics by fibre and product segment (Shariq 98)

	PP	Polyester	Rayon	PE	Nylon	Cotton
Disposable						
Diaper Coverstock	Major	Minor	Occasional			
Feminine Hygiene	Major		Moderate			
Surgical/Medical	Moderate	Major	Major			Moderate
Wipes & Roll Towels	Minor	Moderate	Major			Major
Filtration Media	Major	Major	Minor			Minor
Disposable Apparel	Moderate			Major	Minor	
Durable						
Interlinings/Interfacing	Minor	Major	Moderate		Minor	Occasional
Furniture Construction	Major	Moderate			Minor	
Transportation Fabrics	Minor	Major			Moderate	
Geotextiles						
Roofing	Occasional	Major				
Agricultural uses	Major	Major				

1.4 Methods of manufacturing nonwoven fabrics

In general, the manufacture of nonwoven fabrics consists of two basic stages, namely, web formation and consolidation of the formed web.

1.4.1 Web formation

The main web forming methods may be classified as wet-laid , polymer-laid and dry-laid.

1.4.1.1 Dry-laid

In dry laid nonwovens , discontinuous fibres are formed into parallel , two dimensional isotropic or three dimensional, randomly oriented structures by mechanical or aerodynamic means. These webs may be subsequently consolidated by mechanical , chemical or thermal bonding methods.

1.4.1.2 Polymer-laid

Polymer laid technology transforms polymer solutions or melts into fabric in one continuous operation. Manufacturing steps include obtaining uniform polymer extrusion, fabric formation and consolidation. There are two commercially successful systems in this category, namely spunbonded and meltblown nonwovens.

Spunbonded nonwovens are composed of continuous filaments which have been extruded in web form onto a collection belt and subsequently consolidated by mechanical, chemical or thermal means.

Meltblown nonwoven manufacturing processes are similar to the spunbond process in using melt extrusion. However , upon passage through the extrusion orifice , the molten polymer is accelerated by high velocity hot air jets which attenuate the filament streams

to microdenier size and propel individual fibres to a collection surface. As the fibres are in a tacky state on the collection screen, cohesive web structures are produced. Spunbond and meltblown technologies can both be categorised as melt spinning techniques. However, it is well known that the meltblown process can produce ultrafine filaments (1-10 microns for Polypropylene) and the spinning speed, which is based on the average filament diameter and throughput per hole per minutes, can be as high as 30,000 m/min [Lu 96]. On the other hand , the spunbond processes usually produce filaments in the range 15-40 microns and the highest speed that can be reached is about 4500 m/min [Lu 96].

1.4.1.3 Wet laid nonwoven

In the wet forming process , fibres are suspended in water , brought to a forming unit where the water is drained off through a screen, after which the fibres are deposited on a wire screen. Finally ,the fibres are removed from the wire to be dried.

Figure (1.2) shows that the dry laid web process is the largest and fastest growing method in manufacturing nonwoven fabric and polymer laid is the second largest method [Shariq 96].

1.4.2 Web consolidation

Basically there are three types of web consolidation techniques, which are: *mechanical*, *chemical* and *thermal*

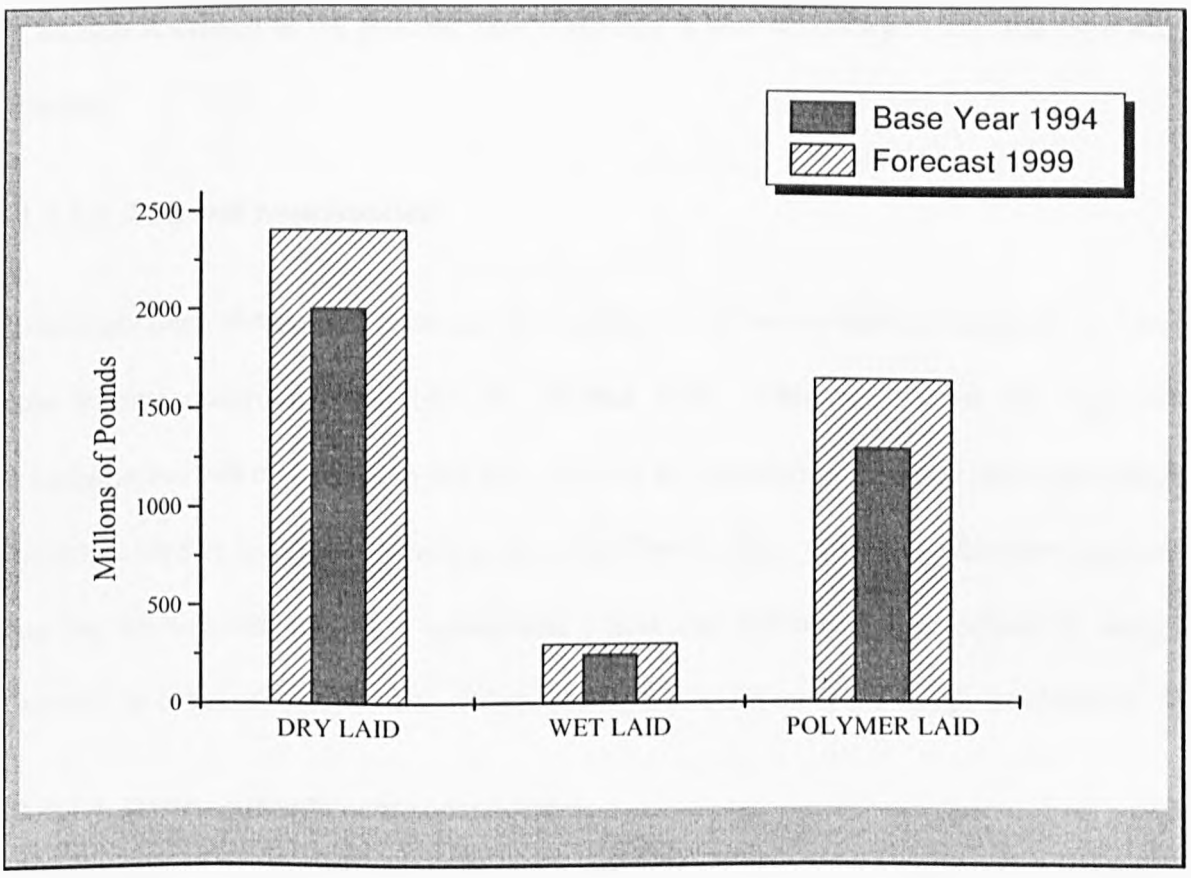

Figure (1.2) Growth in nonwoven web production by process

1.4.2.1 Mechanical consolidation

This method of consolidation includes needlepunching, stitch bonding, and hydroentanglement. Needle-punched fabrics are made by the transfer of fibres from one face of the web towards the other face , this causing an interlocked structure to be produced. The transfer of fibres is caused by barbed needles and the structure of these needles can have a crucial effect on fabric properties.

1.4.2.2 Chemical consolidation

Chemical consolidation is a process of adding a chemical material to a formed web. The addition of binders to the formed web can be through the following processes : saturation (liquid), spray (liquid or powder), foam (liquid). Although application of the

chemical is critical in the process, heat treatment is also necessary to dry and cure the binder.

1.4.2.3 Thermal consolidation

Thermal consolidation processes use the application of heat or heat and pressure to fuse the formed nonwoven web into the finished web. Fibres of almost any type or configuration can be bonded in this way, as long as a portion of the fibre has a thermally sensitive surface which can adhere to the other fibres. Basic processes which are applied on the formed web are : a) calendering , heat and pressure being applied by using smooth or patterned rolls b) hot air-heat , using a convection or a through air chamber.

1.4.2.4 Hydroentanglement consolidation

In this method fibre entanglement can be achieved by the application of fine , high pressure columnar water jets. As the water passes through the web, fibre segments are moved from top to bottom of the web and it is claimed that the high turbulence at the support screen enhances the fibre-to-fibre entanglement. Until recently, hydroentanglement output was almost exclusively of soft and light materials weighing up to 120 g/m^2 without chemical additives. More recently the use of higher jet pressures, up to 300 bar, has made it possible to produce webs weighing up to 400 g/m^2 [Ward 97].

In respect of the subject of the present work, dry laid (particularly air laid) web formation needs to be considered in more detail.

Chapter Two

Literature Review

2.1 Principle of air-laid web formation system

The basic principle of almost all aerodynamic web formation systems is shown in figure(2.1). A pre-formed batt is fed to a high speed, rotating cylinder covered by saw-tooth clothing. As a result of centrifugal force and the application of an air stream, which may rely on suction, blowing or a combination of both, the fibres are detached from the cylinder surface. The air stream conveys the fibres to a screen (either a perforated drum or a screen conveyor) where the carrier air is dissipated and the web is formed.

The quality of the web is directly related to the degree of opening of the fibre materials used in the preliminary web and also to the air stream which has to convey the individual fibres to the screen surface without agglomerating them along their flight path. Apparently , depending on the fibre specifications, a certain volume of air will be required to meet these requirements.

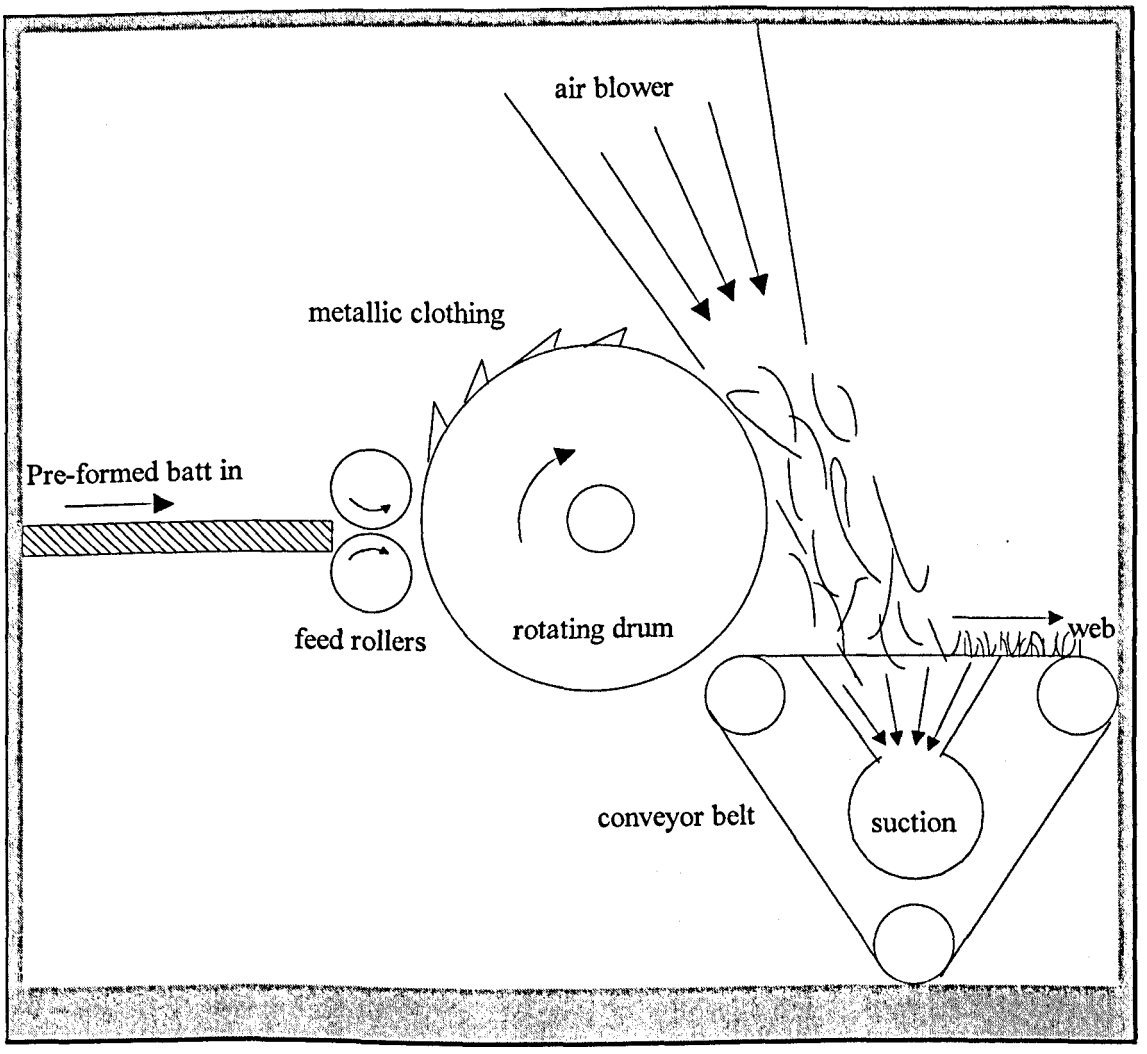

Figure (2.1) Basic principle of air-laid web formation system

2.2 History of air-laid web formation technology

Although the first patent involving the air-laid process dates back to 1882 (US patent 480,588) it was not until the 1940's that the first commercial unit was developed by the Curlator Corporation (now, known as the Rando Machine Corporation). In this machine a pre-web sheet passes through a nose bar/ high speed opening drum and is opened into relatively individual fibres by injecting air , these fibres are transported via a fibre duct and are deposited onto a perforated drum[see Fig. 2.2]. This machine is known as the Randowebber.

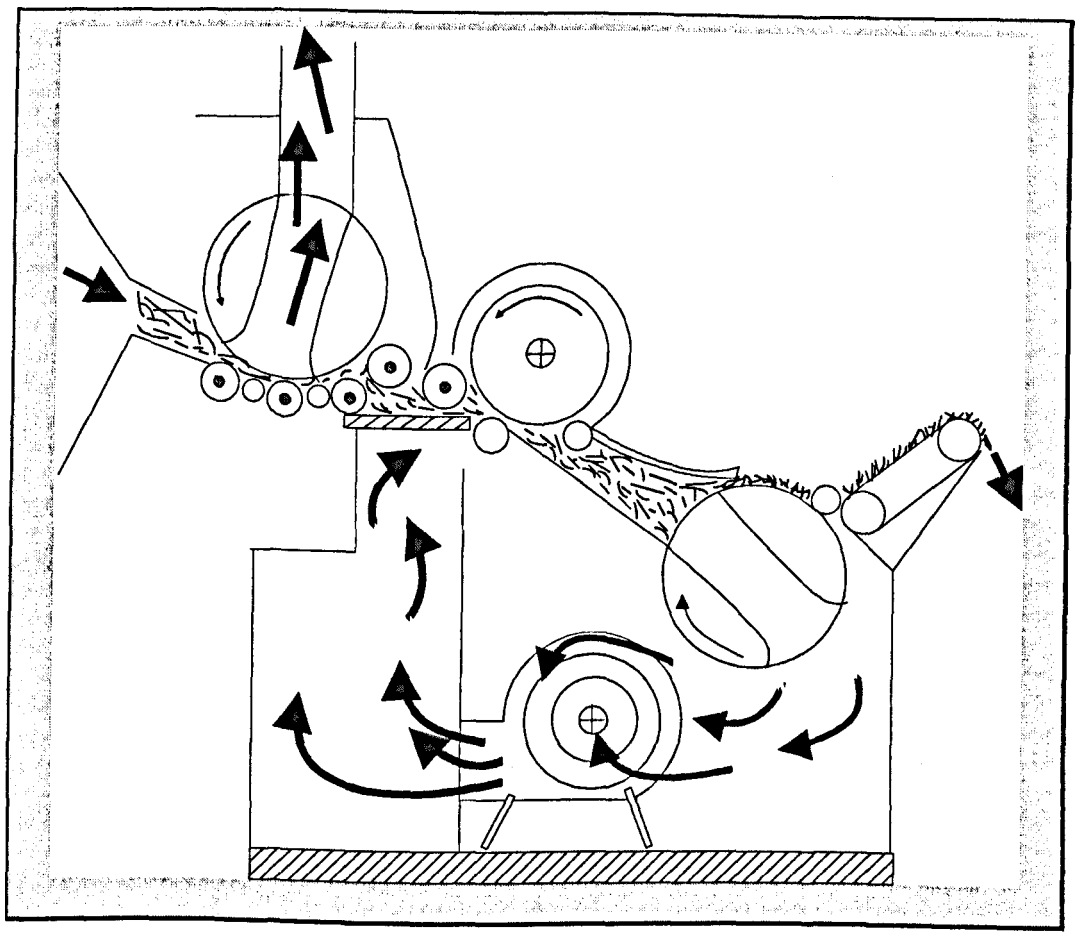

Figure (2.2) The Curlator Random card

Plummer [1949] explained that it is preferable to ensure that fibres longer than 40 mm, are aligned before presenting them to the air forming machine. One way of doing this is to form the web pre-sheet on one or more standard card. Alternatively, a number of card slivers can be laid side by side to form a layer which, as a whole, may be fed to a feed roller operating with a nose plate (see Fig. 2.3).

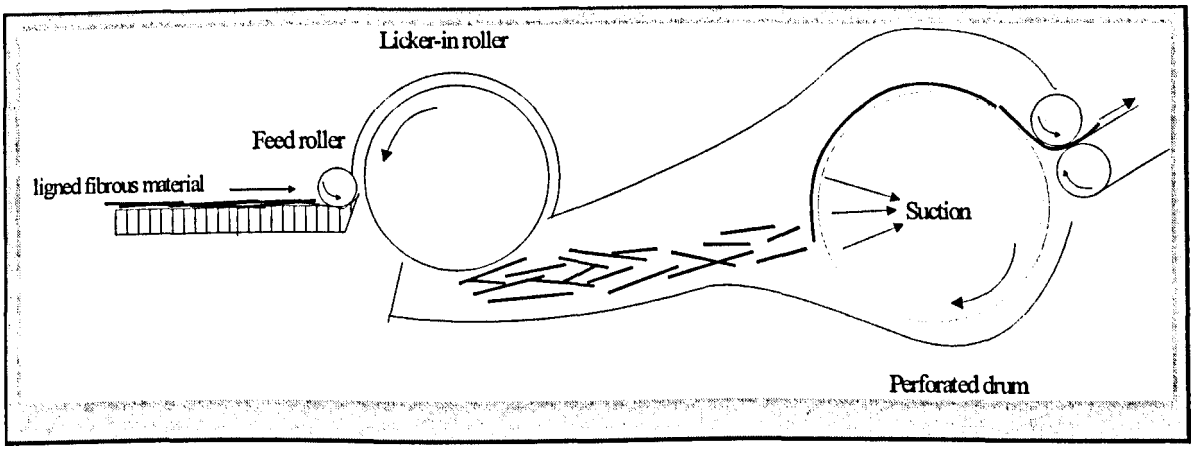

Figure (2.3) Plummer's apparatus for making air-laid web

The aligned fibrous material is then fed to a licker-in roller which is clothed with metallic wire and rotates at a constant speed of 1200-5000 r.p.m. The fibres are detached from the teeth of the licker-in roller by the centrifugal force with the aid of a suction fan located at the other side of the transfer duct. The air velocity at the point where it passes over the surface of the licker-in is equal or greater than that of the peripheral speed of the roller.

Later in the 1950's a Finnish inventor, H.J.Hieldt developed an air forming technique that involved the use of an electrostatic current to help in guiding the fibres.

In 1958, a patent was issued to James d' Arcy Clark [1958] for forming fibrous material using air-laying and consolidating the fibres into a web or sheet . This apparatus used an elongated cylindrical housing having a fibre feed opening in the upper end through which fibres were introduced to the system. To achieve a uniform dispersion of fibres in the air, a series of air inlets were provided in one row across the housing [see Fig. 2.4]. Some of them were arranged in a fixed angular position (to direct their streams of air tangential into the housing), while others are positioned to direct their stream of air

at variable angles. There was a reciprocating nozzle positioned at a level below the fixed nozzles.

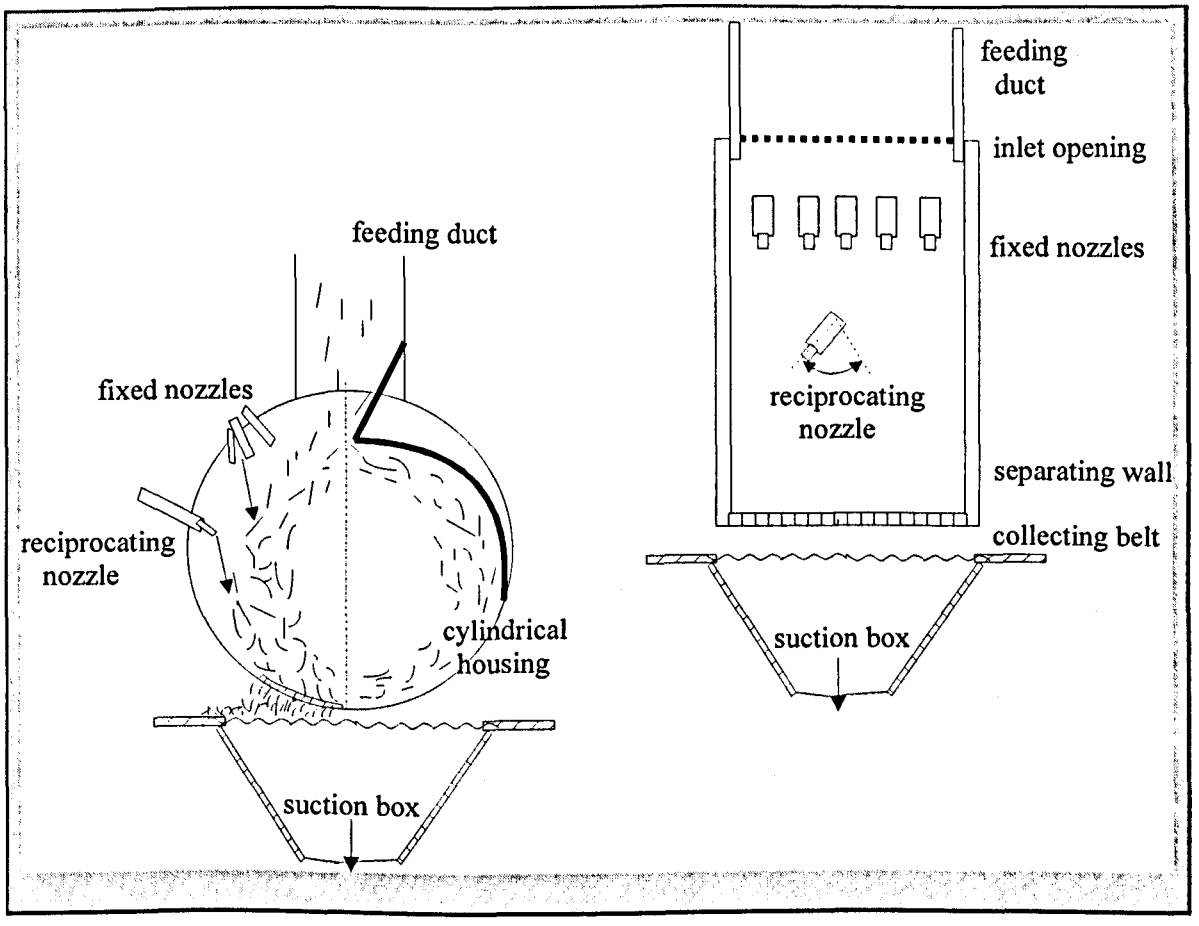

Figure (2.4) James d'Arcy Clark apparatus

In 1964, Fehrer [1964] issued a patent describing an apparatus which enabled the formation of a uniform web of hair or fibres of all kinds by very simple mechanical means.

The apparatus comprised a rotating opening drum for separating fibrous material into individual fibres and a conveyer belt onto which the individual fibres were deposited in the form of a web. The key point of this method is that the fibres land only under the action of gravity and are uniformly distributed throughout the cross-section of the wall [see Fig. 2.5]. He stressed that the fibres can be ejected from the opening drum in steeper or wider parabolic trajectory paths until they move in a free fall zone. He also

emphasised that the uniform distribution can be obtained when an appropriately dispersed material settles gradually .

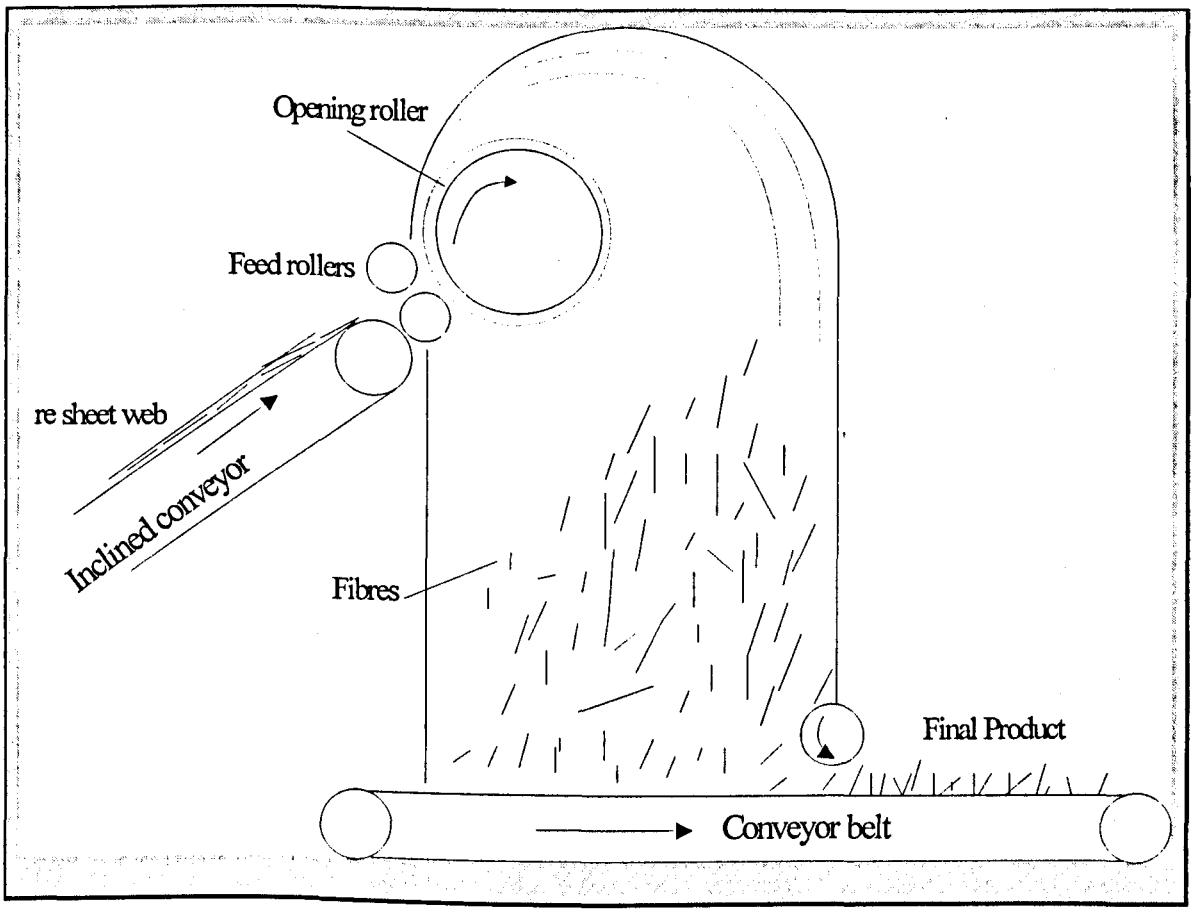

Figure(2.5) E.Fehrer patent in 1964

In the early 1970's the Japanese company Honshu, developed a process for making a variety of air-laid nonwovens using wood pulp and synthetic fibres.

In 1979 Karl Kroyer [1979] from Denmark invented a method for Dry-laying a web of fibrous material. Referring to figure (2.6), the fibres and air flow are passed through the vibrating screen; onto the forming belt through which the air is drawn by the suction box.

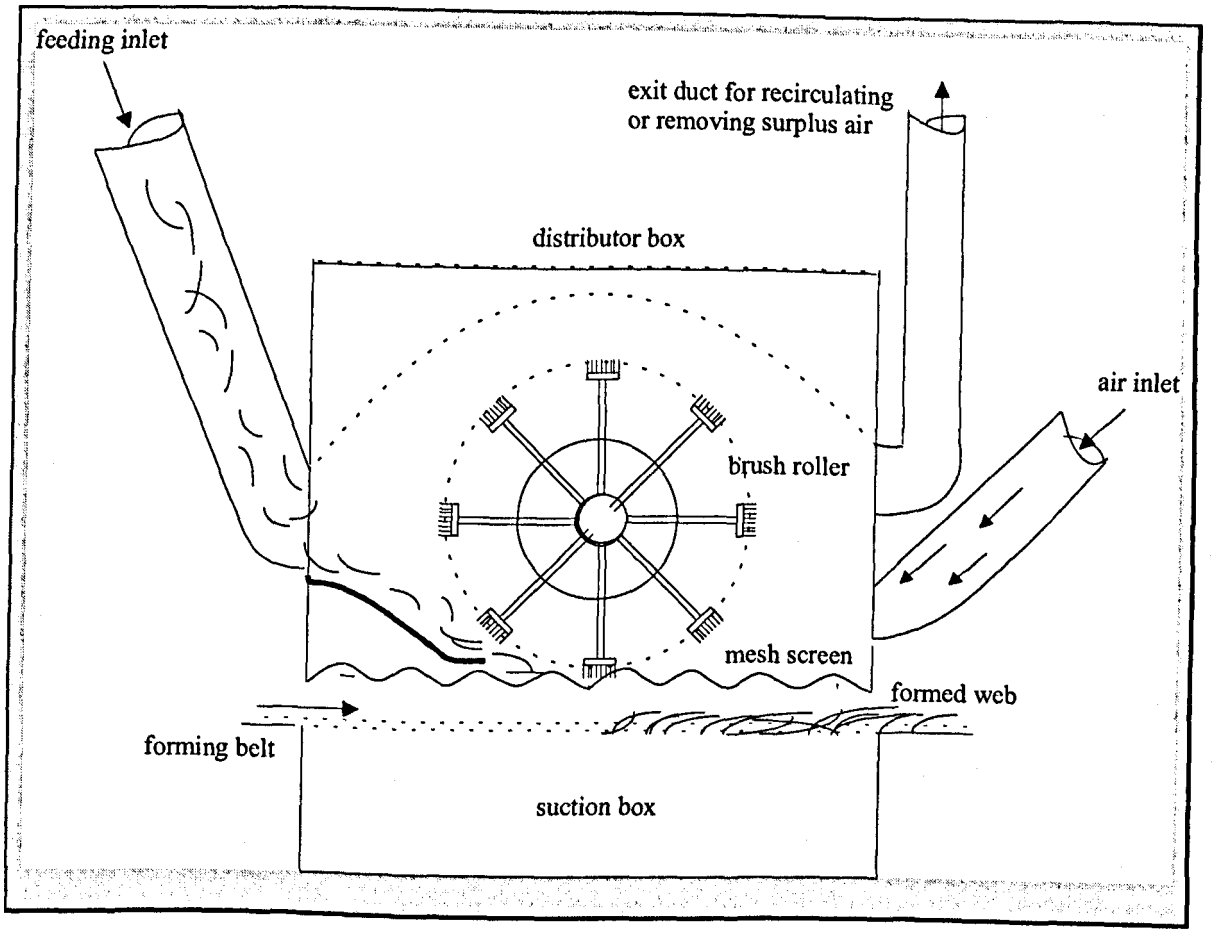

Figure (2.6) Karl Kroyer method for air-laid web formation

The outstanding point of this invention is the way of fibre deposition. It is believed that the passage of fibres through the screen is due to :

a) The vibration of the screen . The amplitude and frequency of vibration are controlled by the screen tension, the speed of rotation and height of the brush roller, b) The centrifugal and aerodynamic effect of the brush roller, c) The positive net air pressure inside the enclosure, d) The vacuum box.

It is claimed that by passing the cellulosic fibres through a vibrating screen a web with an suitable cross-sectional profile and substantially free of conglomerated fibres or thin spots can be produced.

Today, Dan-web forming International Ltd. , founded by ex-Kroyer associates , and Fehrer (Austria) are the most important suppliers of air-laid technology. The Fehrer company offers a variety of air-laid web forming processes, such as the V12 , V21/K12 , K12, K21 machines. The latest version is known as K21 which provides webs in the range 10-200 g/m^2 and high speed production up to 150 m/min.

From a commercial viewpoint the air-laid web formation technology offers the following features [Wolf 1990]:

a) Optimum use of raw material

Air forming systems are designed to optimise the use of increasingly costly raw materials. For example in some cases a "sandwich" structure may be produced on the forming belt with high-cost, high-performance material on the outside and low-cost filler materials on the inside. This approach is capable of using a broad range of fibres such as short cellulosic fibre, glass fibre, recycled wool, synthetic and special fibres such as ceramic and aramids fibres.

b) Environmental friendliness

Generally speaking, an air forming system is a "clean" process and does not create air and water pollution, chemical waste or in-plant pollution problems.

c) Economics

In most cases, the operating costs are below those of other nonwoven processes. Additionally, the absolute capital investment is significantly less than that of the wet-laid or spunbond process.

d) Simplicity

The air forming system does not require highly skilled operators. It is also easy to start up and shut down and has low maintenance demands.

The above commercial considerations explain the increasing importance of the technology.

Figure 2.7 shows the demand and supply of air-laid fabrics [Pivko 1995]. It is evident that about 100,000 tons of additional capacity will be required by the year 2000. As the demand for air-laid fabrics has increased over the last decade, the process has improved significantly from its earlier days.

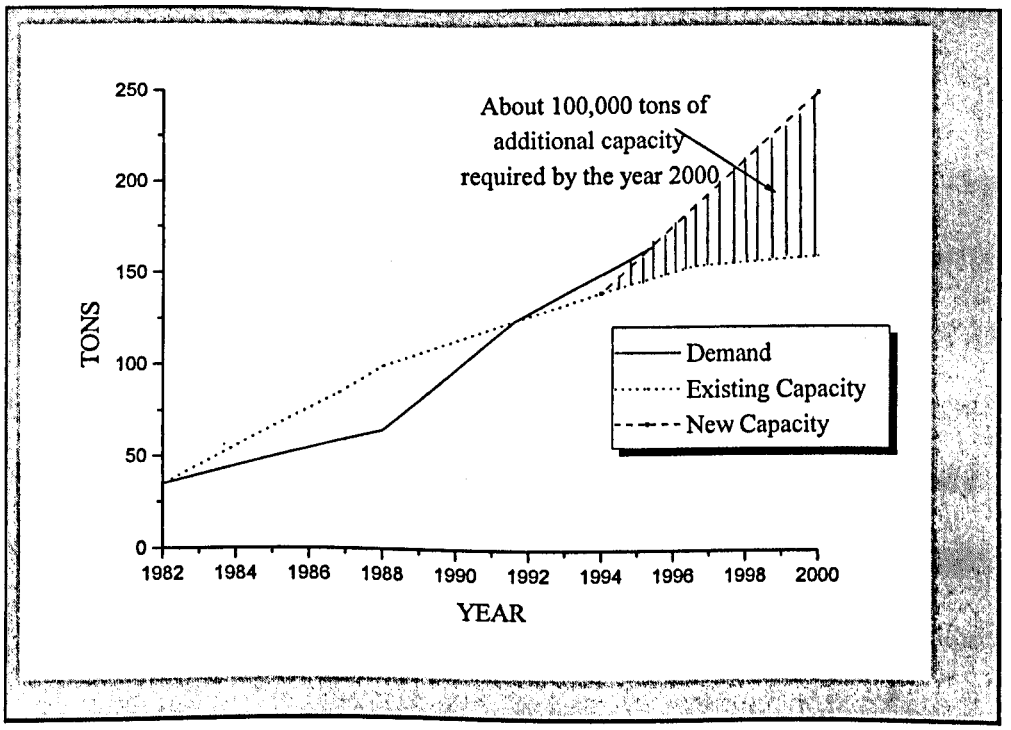

Figure (2.7) Air-laid global demand and supply 1982-2000

Because of the similarity of the available air-laid machine at the University of Leeds and the Fehrer K12 air-laid system, the principle of the K12 air-laid machine is briefly explained in the following section.

2.3 The K12 air-laid machine

The development of aerodynamic nonwoven machinery has advanced in step with the raw material available. The increasing importance of synthetic fibres and the industry's need to produce good quality webs in the lower weight range (below 150 g/m^2) were the reasons leading to a new generation of air-laid nonwoven machinery in the late 1960's. The K12 random-web machine , which was first marketed in 1968, was one of the machines developed as a result of this advanced technology.

The K12 machine was specially developed for use with synthetic fibres. However, it was intended to have great flexibility and to be compatible with fibres such as cotton, recycled wool as well as special fibres, such as para, meta aramids and ceramic fibres.

Figure (2.8) shows a schematic diagram of the K12 air-laid machine. A pre-formed batt is fed to the rapidly rotating main cylinder by means of an inlet roller and a nose bar, where the initial fibre opening takes place. Two pairs of worker/stripper rollers on the main cylinder situated between the nose bar and the fibre exit point complete the opening of the pre-web into individual fibres. This arrangement not only ensures a better opening of the fibres but also considerably improves the fibre flow. A laminar air stream, generated by a patented transversal blower(in an open system , not separated from its surroundings), transports the fibres to a sieve conveyor and forms a random web.

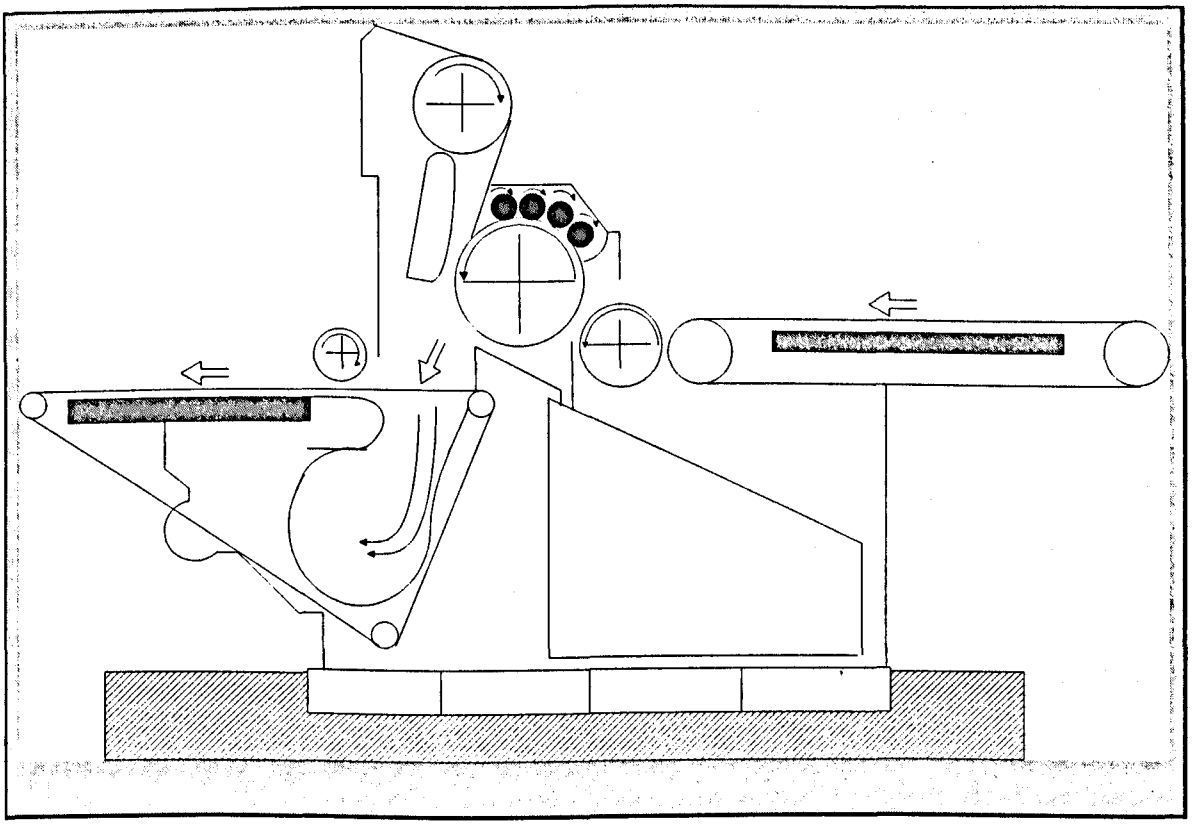

Figure (2.8) Fehrer K12 air-laid random card

The webs from the K12 have a uniform MD/CD (Machine direction / Cross directin) strength ratio and possess fibre orientation in the third dimensions at weights above 50 g/m^2 giving them a bulky structure. Webs of weights 20-2000 g/m^2 can be produced by this system.

Depending on the fineness and type of fibre, the production of the K12 is up to 250 kg/h per metre working width. The output diagram (see Fig. 2.9) of the Fehrer K12 shows clearly that high production rates may only be obtained with coarser fibres of 10-100 deniers.

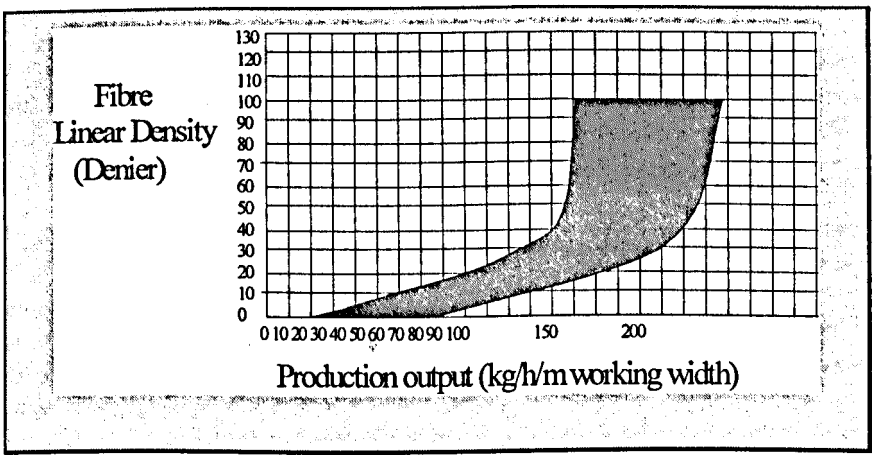

Figure (2.9) Fehrer K12 output diagram

2.4 Bonding options for air-aid webs

The most commercial bonding methods for air laid webs are thermally bonded air laid (TBAL) and latex bonded air laid (LBAL). TBAL webs provide the loft, softness, absorbent capacity required by customers, but dust levels are high and tensile strength may be relatively low. In contrast, LBAL webs offer low web dust levels, but absorbency, and loft are relatively poor. Therefore, alternative method was developed to produce a low dust level, and a high strength TBAL like product. This method is called Multi-bonded air laid (MBAL) which is simply a combination of synthetic fibre and cellulose fluff pulp, like TBAL, plus the addition of latex solids to the web. This combination will create a finished web that has high loft, low density, superior absorbent capacity, good tensile strength and a very low lint or dust level [Westphal 1997]

2.5 Air -laid web characteristics

A unique characteristic of air-laid webs is the possibility of producing a three dimensional fibre arrangement which generally results in a web with isotropic strength . This kind of structure can not be produced by any other method of web

formation process. Air-laid fabrics offer an excellent combination of physical properties such as high loft , softness and drape, good wet strength and rubbing resistance and superior absorbency. The variety of products in which air-laid fabrics have found application is shown in figure (2.10).

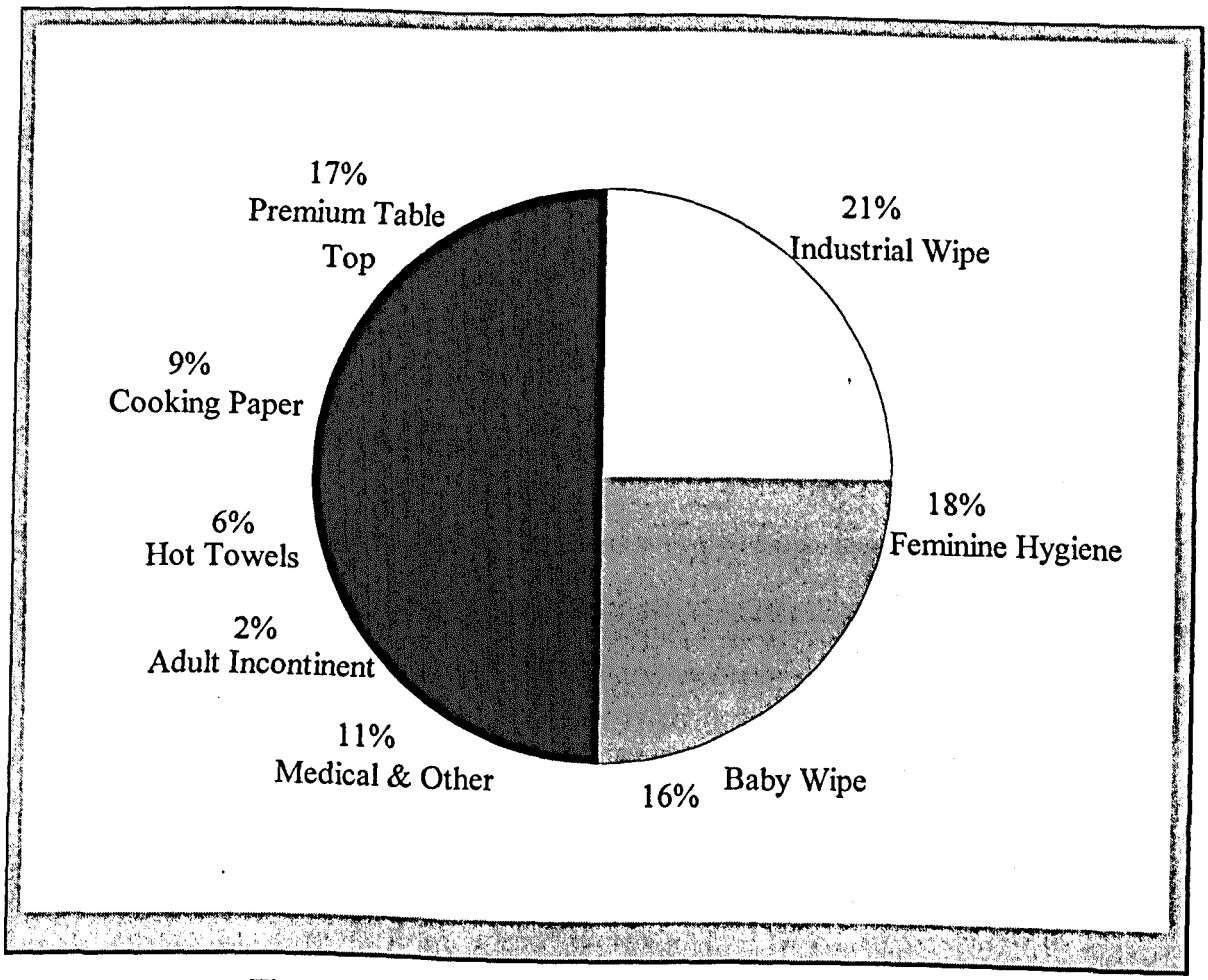

Figure(2.10) World air laid fabric usage by product

As we aim to study the fibre dynamic behaviour in the air-laid technology, particularly in the fibre transport zone it is beneficial to review the relevant published literature in any branch of textile such as carding process, open-end spinning, friction spinning that involve fibre travelling in the air flow medium. This section of literature review is considered under three categories:

I) fibre separation from saw toothed clothing of a rotating cylinder

II) fibre flow in an air stream

III) fibre deposition or landing on a perforated screen or conveyor belt

2.6 Fibre separation from saw toothed clothing of a rotating cylinder

This is a common section of a variety of textile processes and a lot of work has already been done in this area concerning, the effect of saw tooth on the fibres and how the fibres behave during their movement in this region.

In the air-laid process depending on the type of the machine the number of acting surfaces (i.e. clothed rollers) varies. It is believed that the fibres should preferably be aligned before supplying them into the air-laid machine[Krcma 1971].

A very fundamental work in this area has been done by Rohlena[Rohlena 1975]. He pointed out the condition in which fibres can come off the teeth of the drum. This condition is given by the following inequality ;

$$\beta_v < \frac{\pi}{2} - \varphi_v - \alpha_s$$

Where β_V is the front angle of saw-tooth clothing , φ_V is $\tan^{-1}\mu_f$ (where μ_f is coefficient of friction) and α_S is the direction of resultant forces acting on the tooth.

A theoretical analysis of the conditions for fibre shedding from the surface of the cylinder was carried out by Kaster and Emanuel [1964]. They found that the following condition must be satisfied for the fibres leaving the wires :

$$\frac{R}{f_a} > \frac{cos\beta + \mu \sin\beta}{sin\beta - \mu \cos\beta}$$

Where R and f_a are the resultant forces perpendicular to the card clothing base and air drag respectively. This expression shows that the condition for fibre shedding depends on the angle of inclination β of the wire to the base and on the coefficient of friction μ of the fibre on the wire.

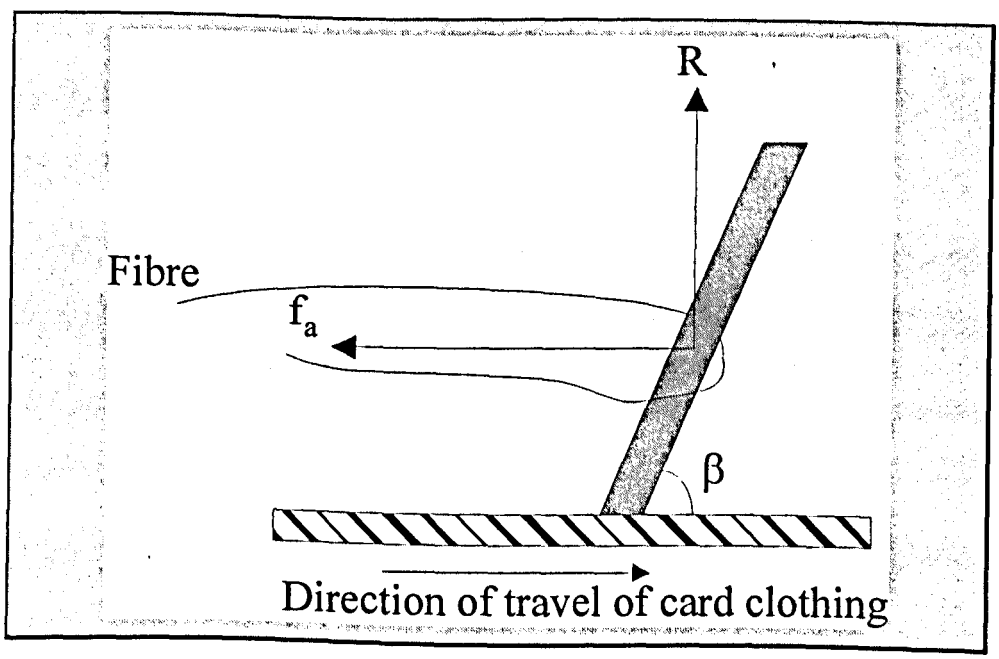

Figure(2.11) Forces acting on the fibre during its shedding from the cylinder

Chen [1988] in his work considered the behaviour of fibres between the opening roller and the housing in the OE spinning process. He assumed that the boundary air layer speed rotating with the opening roller is only fractionally lower than that of the teeth. Then the distribution of the air flow from the roller base to the housing would be similar to that shown in figure (2.11). He also used Bernoulli's equation and found the distribution of the air pressure as shown in figure(2.12). According to that figure the pressure is at its minimum at the tip of the pin, thus the fibres move up the length of the pins towards the tips.

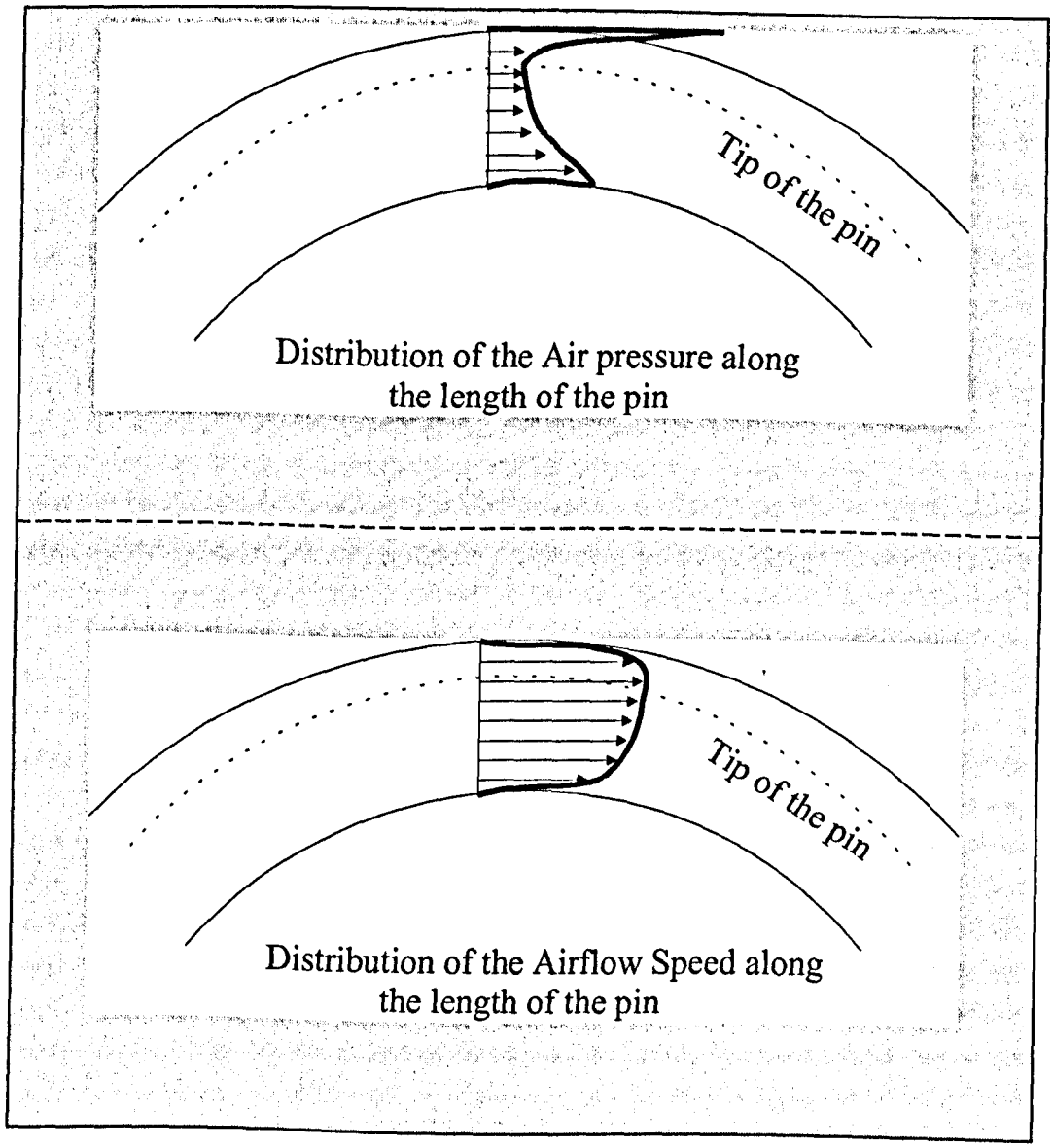

Figure(2.12) The distribution of air speed and pressure along the length of the pin

2.7 Fibre Flow in an Air Stream

In any air-laid web formation system it is extremely important that the machine be able to achieve good fibre separation in the air stream otherwise fibre reaccumulation will occur , as the fibres move towards the landing section. There are several works in fibre dynamics in this region.

In 1948 a patent issued by F.M. Buresh explained that static charges which are presumably generated in the air stream by the friction between air and fibres during

the pulling out and the doffing action at the licker-in cause the fibres to attract each other and accumulate.

Wood [1980] carried out a theory to explain two important factors affecting fibre reaccumulation in the air stream . These are ;

1) the residence time of the fibre in the conveying zone

2) the ratio of the fibre to air in the conveying zone

Based on his theory the ideal amount of fluid required for air-laid web formation is dependent on the two major factors:

- To be able to individualise each fibre from its neighbour
- To completely encapsulate each fibre in its own fluid volume.

He assumed that the maximum volume which one fibre can take for rotating in any direction without linear motion is a sphere having a diameter equal to the fibre length, then, this volume of fluid would be that for complete encapsulation of that fibre. The following equation gives the quantity of fluid required to maintain fibre separation.

$$Q_t = \frac{k.p.l^2}{d}$$

Where p is machine production rate per unit of time, l is fibre length, d is fibre denier and k is a constant.

The behaviour of fibres in airflow have been studied by H.Stalder [1968]and B.Edberg [1974]. They investigated the effect of the type of flow (laminar or turbulent) on the fibre orientation and fibre transport. Edberg continued his research

to determine the forces acting on a fibre as a function of the fibre length and air velocity. It was shown that the level of orientation and parallalization which can be achieved with laminar flow is very low because of the low flow rate. On the other hand, significantly better result can be obtained with high air velocities despite the turbulent flow.

Lunenschloss, et al [1976] also in their work, regarded the effect of fibre velocity, opening roller speed and negative pressure in fibre orientation at the exit from the fibre duct in OE spinning, showed that at low fibre velocity (V_f=40 m/s) the number of unstraightened fibres are considerably greater than that of high fibre velocity. He also stressed that the fibre orientation decreases significantly at extremely high opening roller speed (11,500 RPM).

In another work Lunenschloss [1980] used high speed cinematography to show how fibres leave the opening roller and move in the air flow. He emphasised the decisive effect of centrifugal force, air drag and friction force in the fibre movement. The fibre velocity profile, obtained from his work, along the fibre path indicates that the mean fibre velocity in the opening roller housing is only 30-50% of the opening roller peripheral speed (see Fig. 2.13)

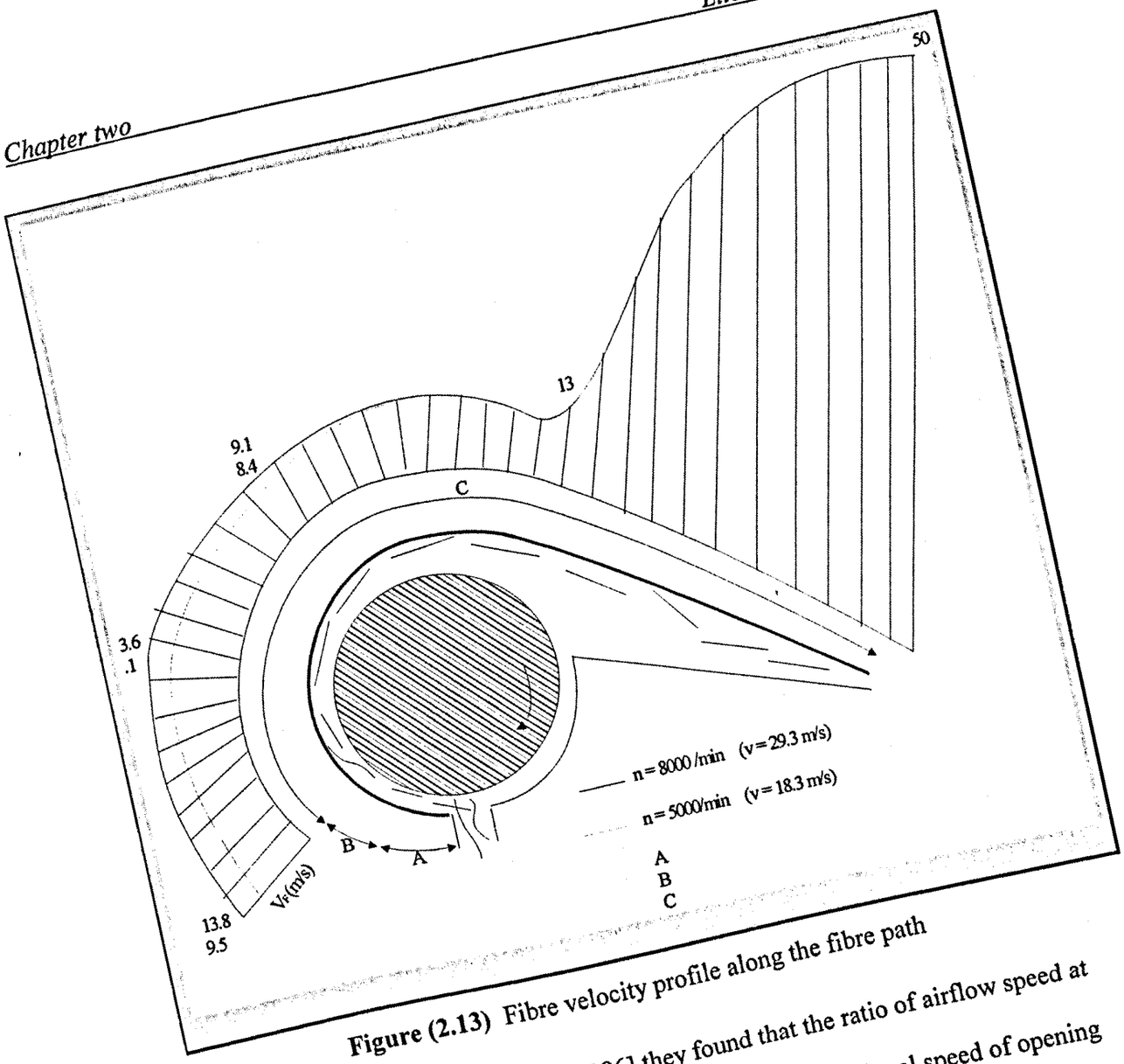

Figure (2.13) Fibre velocity profile along the fibre path

In a work by Lawrence and Chen [1986] they found that the ratio of airflow speed at the inlet of the transfer channel in a Rotor spinner to the peripheral speed of opening roller ($\frac{V_{air}}{V_{OR}}$) has dominant effect on fibre configuration during transport from the opening roller to the rotor. They expressed that the higher the ratio ($\frac{V_{air}}{V_{OR}}$) the greater the chance of having straightened fibres along the line of flow. Theoretically, it can be assumed that for the fibre to leave the opening roller, the airflow speed must be greater than the peripheral speed of the opening roller. They

also established a numerical method for evaluating fibre configuration in the transfer zone. According to their theoretical analysis the profile of the average airflow velocity along the axis of the transfer channel can be shown in figure (2.14).

This profile has been plotted based on continuity equation $U_x = \frac{\text{Airflow rate}}{A_n}$.

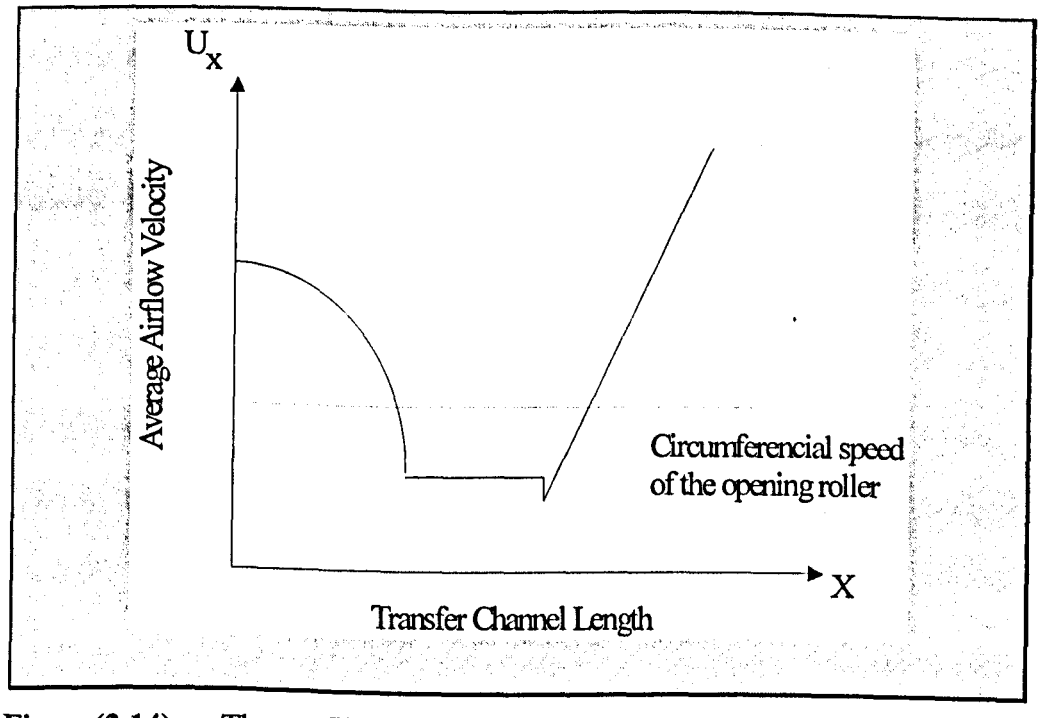

Figure(2.14) The profile of the average airflow speed in the transfer channel

The diagram shows that regardless of the value of the airflow rate, the airflow will not continuously accelerate the fibres along the axis of the channel. Ideally for fibres to be carried in a straightened form by an airflow the leading end of the fibre must be continuously accelerated to a higher speed than the trailing end.

Rohlena [1975] in his study stressed the behaviour of a fibre ejected from the saw teeth by analysis of the movement of fibres in a stationary medium, and also obtained a realistic picture by adding the effect of the air current. He made the following assumptions:

- The fibre taken as a point mass (centre of gravity of the fibre)

- The medium surrounding the opening roller is stationary (the velocity of the air is equal to zero)

- The fibre leaves the cover at a known velocity and its centre of gravity moves along a straight path (e.g. at the velocity of the opening roller v_1)

- The resistance of the medium is proportional to the square of the relative velocity of the fibre and the air and the coefficient of the medium resistance does not depend on the velocity.

- The fibre weight is negligible compared to the resistance of the medium.

He used the change of momentum theory and expressed the fibre velocity by the following equation :

$$v = v_1 e^{-Cx}$$

where v_1 is the velocity of the opening roller, C is the coefficient of the relative resistance of the media against the fibre and x is the path length.. This expresses the rapid exponential decrease of fibre velocity with the path length.

Considering that the fibres are acted on by an air current and applying the law of the change of momentum, we can write the equations for the fibre velocity and movement:

$$v_y = \frac{v_{1y}}{1 + C.v_{1y}.t} \qquad v_x = v_v - \frac{v_v - v_{1x}}{1 + C(v_v - v_{1x}).t}$$

Where v_v is air stream velocity and v_{1x} and v_{1y} are entering velocity of fibre in x and y direction respectively. By integrating the above equations we can get the expressions for fibre trajectory.

We should notice that the above equations are based on the assumption of the fibres entering into a parallel air stream with the speed of V_V.

A method for simulating the dynamic behaviour of rigid and flexible fibres in a flow field was proposed, regarding the fibre as made up of spheres that are lined up and bonded to each neighbour[Ymamoto, Matsuoka 1993]. The fibre model can stretch, bend, and twist, by changing bond distance, bond angle, and torsion angle between spheres, respectively. The motion of the fibre model in a flow field is determined by solving the translational and rotational equations for individual spheres under the hydrodynamic forces and torques exerted on them. The proposed method was applied for simulating a rigid and a flexible fibre in a shear flow under the conditions of infinitely dilute system, no hydrodynamic interaction, and low Reynolds number of a particle. It was shown that the results are similar to experimental ones described by Forgacs and Mason[1959]. The advantage points of this particle simulation method are i) treatability of an arbitrary shaped particle, ii) alterability of the particle stiffness, and iii) simplicity of simulation procedure.

A simple approach to the alignment of short fibres using fluid dynamic forces was explored [Bangert 1977]. This approach consists of conveying fibres in an essentially irrotational air stream and then causing this stream to undergo a rather rapid contraction, followed by a rather slow divergence. The resulting velocity gradients in the irrotational flow produce moments on a fibre that in most cases tend to align it parallel to the flow direction. The desired degree of air-stream contraction and divergence can be easily controlled by using transversely-blowing air jets. An approximate analysis was developed for the effects of aerodynamic forces on fibre motion and was combined with a theory for the influence of

transverse air jets on the main flow. In this analysis the fibre was represented by a rigid cylinder and the motion of the fibre was assumed to be two-dimensional. The equations of motion of the fibre are set based on Conservation of X and Y momentum and Conservation of Z-angular momentum about the fibre centre of gravity.

The theory was in qualitative agreement with the experimental results. These results showed that fibre alignment parallel to the main stream can be achieved for a wide range of initial fibre angles. Further, this alignment can be performed with low-speed air flows, which may facilitate fibre handling in many applications.

Ulku *et al* [1993] studied fibre alignment and straightening in open-end spinning. They used high speed photographic technique to observe the degree of fibre alignment in the transfer channel. To indicate the degree of fibre straightness, they counted the number of intersection points of the fibre images with three straight lines drawn parallel to the nominal flow direction. It was concluded that at constant air flow speed, as the speed of the opening roller is increased, fibre straightness and degree of alignment along the axis of flow deteriorate. At constant opening roller speed, as the air flow speed increases, fibre straightness and degree of alignment along the axis of flow improve.

A computational modelling was presented by Smith and Roberts [1994] for straightening of crimped and hooked fibres in converging transport ducts. A two dimensional dynamic model for the motion of fibres in an accelerating laminar air flow is reported. There are several simplifying assumptions in this model such as the laminar flow assumption for neglecting turbulence and wall effects, the assumption of fibres to be composed of both spherical and cylindrical elements, and

neglecting fibre to fibre interactions. While they made no direct comparison with experiments, the results show the tendency for crimped and hooked fibres to be straightened in convergent flow with sufficient acceleration. They hope that this model may be useful in designing an apparatus to straighten fibres.

A two-dimensional computational fluid dynamics (CFD) model was developed by Kong and Platfoot [1996] to simulate the flow patterns inside the transfer zone of a rotor spinning machine. They used CFD analysis (FIDAP code) to view the likely relationship between the machine set-up and design, and the quality of the yarn produced. In particular the behaviour of the known recirculation zone within the channel was evaluated because of its high potential to bend individual fibres. They have studied the dimensions of the inlet of the transfer channel and the changes in the ratio of the opening roller velocity to the mean flow velocity. Three principal conclusions have been made by their work: First, there is a trade-off in the degree of fibre opening in the transfer channel with regard to the free cross section through which fibres may travel by a strong forward-directed flow. If the channel becomes narrow, then there is a physical obstruction to the flow and if it becomes too wide, then a strengthening recirculation zone acts to block part of the cross section. Second, the distribution of the flow stream does not vary dramatically with increasing Reynolds number, provided the ratio of the opening roller circumferential velocity to the air mean flow velocity is the same. Third, there is a substantial variation in the location of the recirculation zone with increased opening roller speed. It can be postulated that an optimum range of opening roller speed settings exists, outside of which large recirculation zones occur on either side of the transfer channel.

Kong and Platfoot [1997] extended their studies to develop a two phase air/fibre flow model to simulate fibre movement in the transfer channel of a rotor spinning machine. The conveyance of fibres in the transport zone by carrier air is a two phase flow problem because the fibre, as one of the phases, is a flexible material and any part of the fibre may be moved, rotated, or bent relative to the other sections due to the influence of a velocity gradient in the air conveying the whole strand. They indicated that the initial fibre position and the underlying air flow pattern are critical to the final fibre configuration at the exit of the channel. Fibre opening and fibre detachment from the opening roller are identified as the two critical factors in obtaining straight fibres at the channel inlet and their transport to the spinning zone.

2.8 Fibre landing on a perforated screen or conveyor belt

Krause *et al* [1989], established a theoretical model for fibre landing in friction spinning . They derived an equation to describe the effect of various factors such as fibre landing angle γ , transition channel angle φ and the speed ratio n (the ratio of fibre velocity V_f to surface speed of suction drum V_{sd} , $n = \frac{V_f}{Vsd}$). The obtained equation is as follows :

$$\frac{3n^2+1}{2n} = \frac{\cos\gamma.\cos\phi+2}{\sin\gamma}$$

They found the strong effect of speed ratio n, on the fibre landing angle γ. (by increasing n, the fibre landing angle (γ) in a given channel angle (ϕ) decreases, see figure (2.15). They also explained that during fibre landing the fibre leading end is caught by the drum surface whilst the tail continues its travel in the original

direction with the same velocity. Because of decelerating effect upon landing and due to prevailing air flow condition, the fibre will perform a "somersault" and finally deposited in reversed direction at an angle γ.

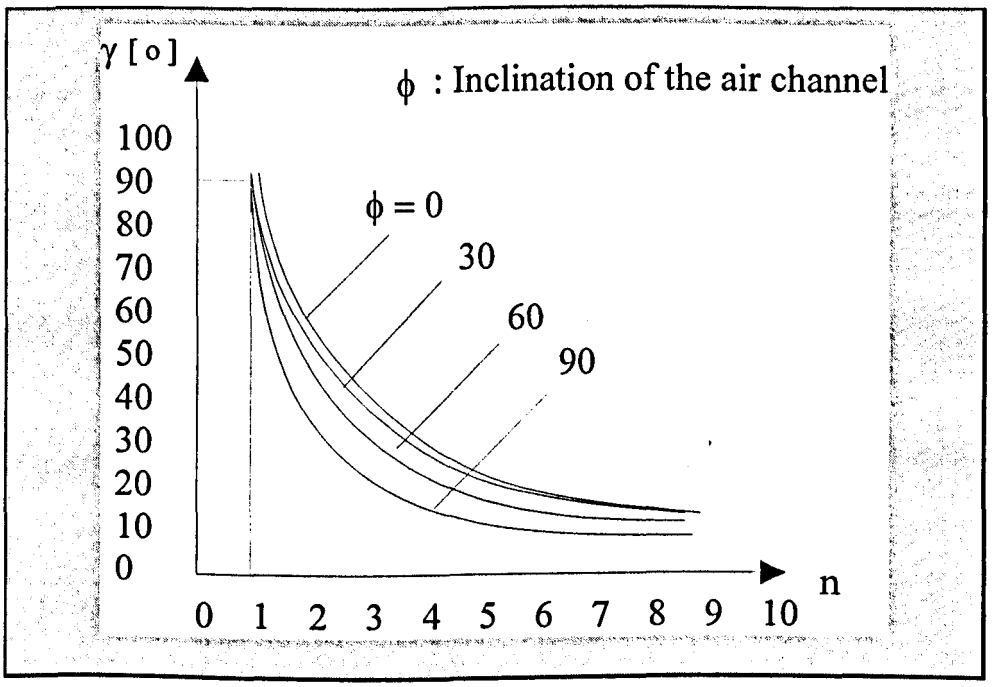

Figure (2.15) Fibre landing angle , theoretical

A simplified model of the behaviour of fibre landing in the twisting zone of a friction spinner has been made by Zhu *et al* [1993]. This theoretical analysis of the fibre landing process showed that there are several different parameters affecting the fibre landing which resulted in different fibre configuration in the final yarn. These parameters include air force (magnitude and direction), fibre landing angle, fibre bending rigidity and the initial fibre configuration.

The angle that fibre makes with the air stream seems to be an important parameter, and the best result (i. e. undesirable loop) are obtained when the fibre makes a large positive angle with the air stream, see figure (2.16). The angle that the landing fibre makes with the "embryo" yarn is also important, since small angle lead to undesirable loops being formed in the fibre.

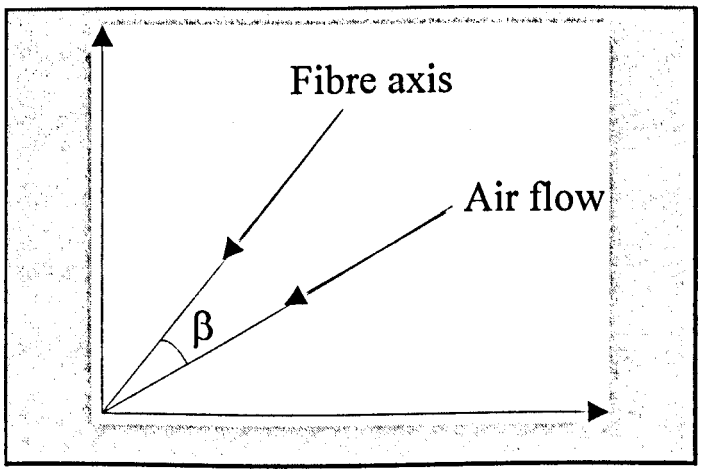

Figure (2.16) The angle between Fibre Axis and Airflow Direction in Friction Spinning

Fine fibres, with a low flexural rigidity, tend to buckle and crimp more than coarser fibres on landing, and high air speeds lead to similar behaviour (i.e. by increasing the air-force the fibres crimp and bend severely). This creates a difficult problem in designing a reasonable airflow to help the fibre transit and landing. This is because during fibre transit it will be necessary to use a high air flow velocity to maintain the fibre movement, or even to improve the fibre configuration, but in the fibre landing stage it is better to use a low airflow velocity. In respect to initial fibre configuration it can be said that a highly crimped fibre might lead to undesirable final configuration.

Lawrence and Jiang[1996] made an attempt to find out the effect of the angle and velocity at which the fibres approach the collecting surface on the final alignment of fibres in the yarn and its structure. Based on a theoretical work they found that the following three parameters are fundamental to determining the final fibre deposition in the yarn:

- Fibre approach angle
- Fibre velocity angle

⊕ Fibre velocity

They pointed out that the closeness of the fibre approach angle with the velocity angle is the principal reason for low fibre length utilisation (i.e. as these angles become close the fibres do not lie in the yarn axis) .

2.9 Summary

The literature review shows that most of the studies in fibre dynamic behaviour in the air flow medium are related to yarn spinning processes, which are basically looking at straightening the orientation of the fibres that have escaped from the opening roller. This allows a satisfactory configuration of fibres in the final product. It was reported that the ratio of air speed to the peripheral speed of opening roller ($\frac{V_{air}}{V_{OR}}$) has the dominant effect on fibre configuration during transport from the opening roller to the rotor. The higher the ratio ($\frac{V_{air}}{V_{OR}}$) the greater the chance of having straightened fibres along the airflow axis. The dimension of the inlet of the transport channel has also been indicated as a crucial factor. If the channel inlet narrows, then there is a physical obstruction to the flow. If it becomes wide, then a recirculation zone is created which blocks part of the channel cross-section.

Currently, the Computational Fluid Dynamics (CFD) has been introduced to the textile problems, particularly open-end yarn spinning. They have reached some interesting results in simulating the fibre transport zone and identified the critical

factors which are: ($\frac{V_{air}}{V_{OR}}$), initial fibre speed and position, geometry of the transport channel.

The theoretical and experimental studies of fibre landing revealed that number of parameters namely, airflow, fibre landing angle, fibre rigidity and initial fibre configuration are attributed to the fibre configuration in the final yarn.

The air laid web formation technology, however, is seeking for three dimensional fibre arrangement (i.e. random fibre orientation) which is different from yarn processes that are aimed to make the fibre orientation in the yarn axis. This technology as described earlier (see fig.2.7) is a well growing in use in the nonwoven industry and still there are further improvements which can be done to reach a better final product in terms of quality and cost. In order to be able to make these improvements a fundamental understanding of the system is essential. This work is the first attempt (or a simple basic approach) to make this understanding and to model this complex process of making web, theoretically. This work provides a sound foundation for developments in creating a complete modelling algorithm for the air-laid web formation system. With regard to this modelling it is now possible to numerically describe the movement of fibres during transport. Such predictions can provide the fundamental support for optimisation machine design and can also minimise the experimental effort in fibre processability with a fixed machine design.

Chapter Three

Theoretical Work

3.1 Introduction

Since most problems concerned with textile systems are extremely complex, when analysing the situation it is useful to set up a theoretical model of the system concerned. A model is a system which has some similarities with the real problem, but introduces simplifications, i.e. it eliminates certain properties of the real structure which make the problem too complicated and which are not of immediate interest. As long as the properties of the model are similar to those of the real structure it is legitimate to compare the behaviour of the two, and it is anticipated that the relationships between variables in the model will be similar to the relationships existing in the real problem.

3.2 Description of the mathematical model

The current model is concerned with determining the way in which fibres move along a tooth in a tooth-covered rotating cylinder in the stripping section of an air-laid nonwoven system.

This system is based on using airflow and suction to disperse and land the individual fibres on a perforated conveyor belt (see Fig 4.1). The in put material is a pre-sheet web which is passed through a pair of feed rollers (3) and then through a lickerin roller (4); finally, the main drum (5) picks them up. The fibres are carried by the teeth of the clothing elements of the drum and at the stripping zone (8), with the help of airflow and suction, they are removed from the teeth. The theoretical model considers the stripping section, which is the area in which the fibres come off the teeth.

3.2 1 Assumptions

To be able to derive a mathematical model the following assumptions are made:

1) The fibre is assumed to be a rigid body.

2) The fibre is taken as a connected pair of rods hooked around the tooth, as shown in figure (3.1)

3) The opening roller generates negligible air flow which can be neglected compared to the high speed air coming from the blower.

3.2.1.1 Justifications of the Assumptions

The rigid body assumption of a fibre has been made by the other researchers (Bangert 77, Yamamoto 93, Smith 94). A real fibre is, of course, flexible and although it would be possible to analyse the motion of such a flexible fibre the mathematics would be highly complex. Therefore it seems worthwhile as a starting point to develop a more simplified model, in which fibres are assumed to be rigid. There is some photographic evidence (Lunenschloss 80 and also fig.5.9) that fibres remain straight during their motion in the vicinity of the opening roller, so that this assumption may produce results that are in reasonable agreement with the experiment. The object of the study is to model the trajectory of a fibre from the saw tooth roller and the rigid body assumption should give acceptable results.

2) The hooked configuration of fibre around the tooth of the opening roller has been reported by Ghosh and Bhaduri [1968]. The photographic observations by Lawrence [1988] showed that the hooked fibres escape from the pins by sliding to the tip of the pin and then are ejected from the opening roller surface

3) The opening roller due to its rotation generates air flow which can be approximated by the equation $u = \frac{A}{R + r}$ (Acheson 96) where r is the distance from the roller surface,

R is the radius of the roller and A is a constant. If the radius of the opening roller is R=170 mm and it rotates at angular velocity ω=11.52 rad/sec, then the boundary condition (i.e. no slip situation) at the opening roller surface may be applied to obtain: $A = 0.33\ m^2 / sec$. Substituting the value of A into the airflow equation, the velocity at any distance from the opening roller surface can be obtained, for example at $r = 10$ mm, $u = 1.8\ m / sec$. This airflow can be neglected compare to the airflow due to the blower which is about 40m/sec.

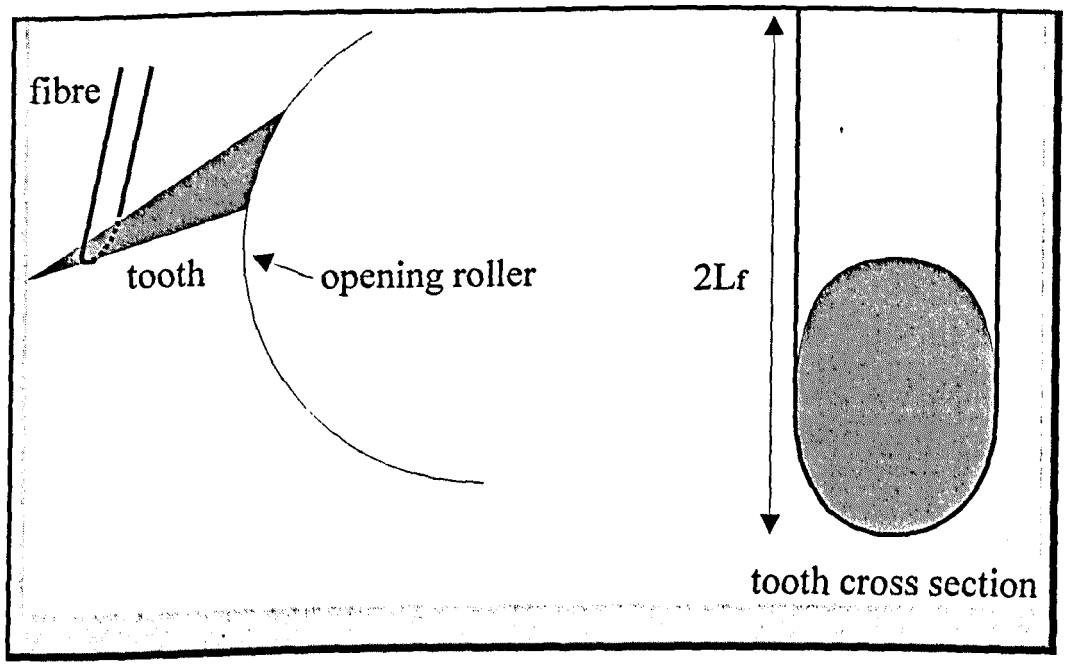

Figure (3.1) Fibre configuration on the tooth of the cylinder

3.2.2 Geometrical considerations

Figure(3.2) shows the fibre position at two instants of time. The upper position is the initial situation when the fibre is just coming to the stripping zone and starting its movement down the tooth. In this initial position the radius of the drum to the base of the tooth makes an angle θ_0 with the fixed horizontal axis (i.e. OX), the fibre is inclined at an angle ϕ_0 to the tooth and the trailing end(or loop centre) of the fibre is at a distance r_0 from the tooth base.

At time 't' the radius of the drum to the tooth makes an angle 'θ' with the horizontal axis, the trailing end of the fibre is at a distance 'r' from the tooth base and the fibre makes an angle 'ϕ' with the tooth , as shown. Let the total length of the fibre be $4L_f$. We assume that there is a length $2L_f$ on each side of the tooth (i.e. the fibre is symmetrical about the contact point, see Fig.3.1). Let 'R' be the radius of the drum and take origin of axes at the centre of the drum with OX horizontal and OY vertical.

The co-ordinates of the centre of gravity of the fibre at time 't' can be expressed as follows:

$$\begin{aligned} X_G &= OC''' + C'''C'' + C''G' \\ &= R\cos\theta + r\sin(\gamma - \theta) + L_f \sin(\phi - \gamma + \theta) \end{aligned} \quad , \qquad (3.1)$$

and

$$\begin{aligned} Y_G &= OH + HH'' - H'H'' \\ &= R\sin\theta + r\cos(\gamma - \theta) - L\cos(\phi - \gamma + \theta) \end{aligned} \quad , \qquad (3.2)$$

where:

θ is the angle between OX and the radius of the drum to the base of the tooth; if ω is the angular velocity of the drum then $\theta = \omega.t$,

ϕ is the angle between fibre and tooth at time 't',

r is the distance of the fibre from the base of the tooth,

γ is the working angle of the tooth,

L_f is one-fourth of the fibre length,

R is the radius of the drum.

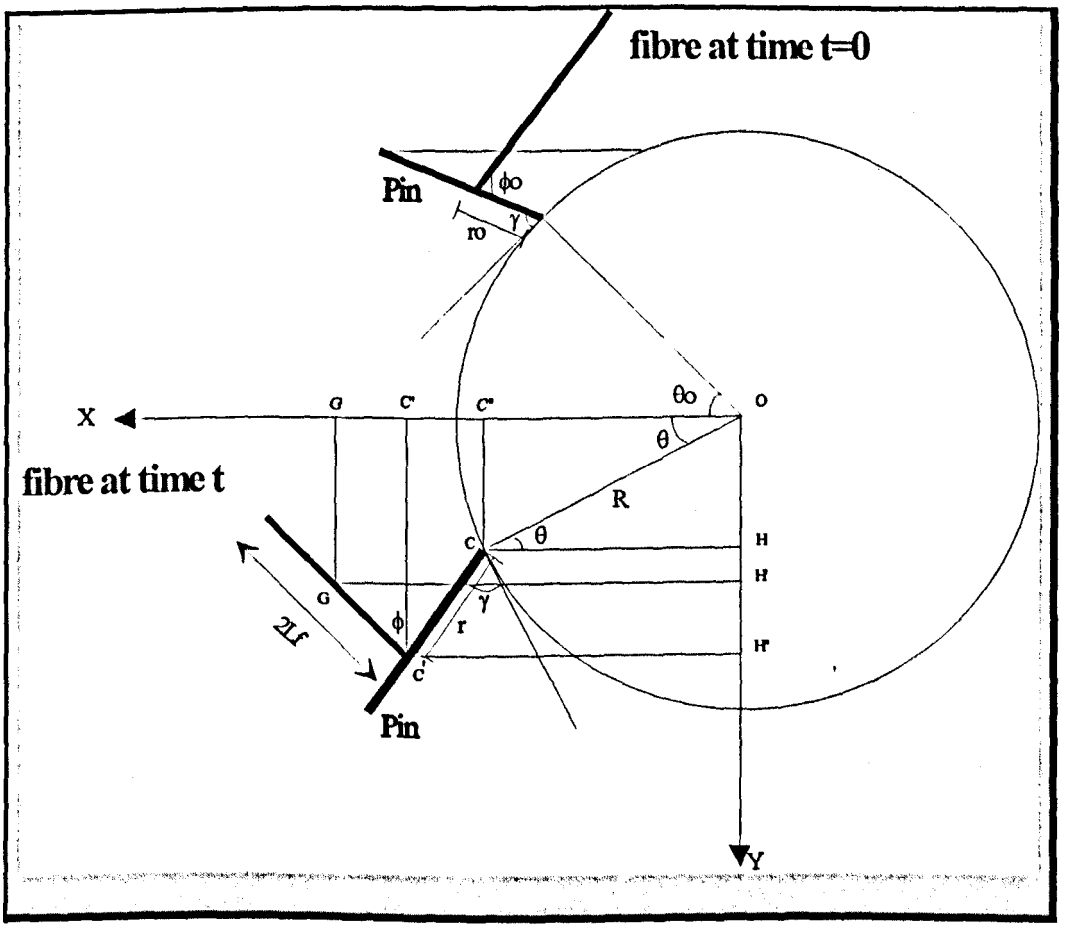

Figure (3.2) Geometrical description of the model

3.2.3 Forces acting upon the fibre

The following forces act on the fibre:

1) Air Drag, which has two components, normal and tangential to the fibre line.

2) Fibre weight.

3) Normal reaction between the fibre and the tooth.

4) Friction between fibre and tooth.

Of these forces, the air drag component is dependent on the relative velocity of the fibre and the ambient air, and consequently varies along the fibre. Let the normal and tangential components of the air drag force, per unit length of fibre, be F_n and F_t respectively. Then the forces acting on the fibre are as shown in figure(3.3).

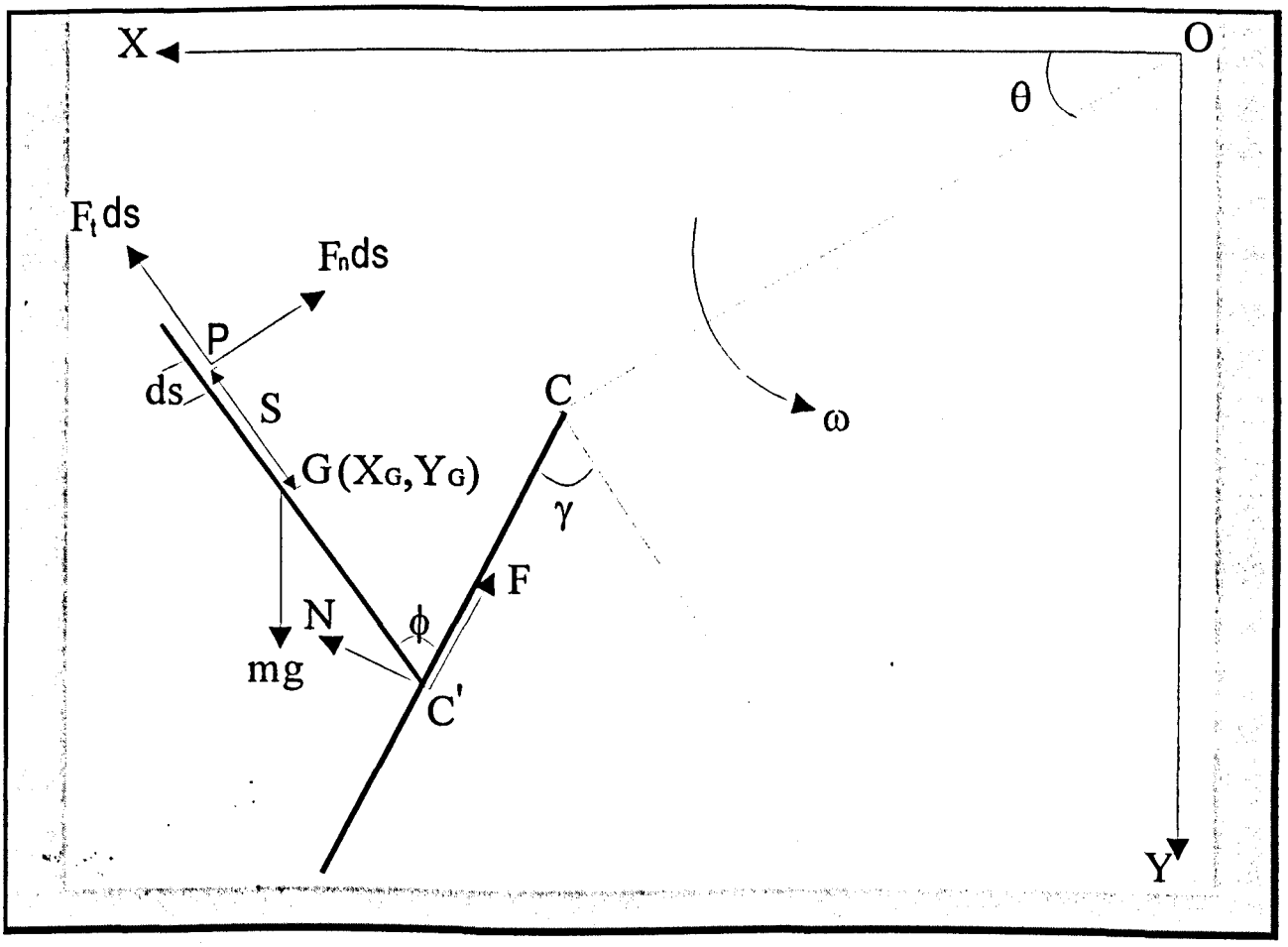

Figure (3.3) Forces acting on the fibre

3.2.4 Derivation of equations of motion of fibre on the teeth

Considering an element of length dS at a distance S from G. The equation of motion in the horizontal direction is

$$m\frac{d^2X_G}{dt^2} = N\cos(\gamma-\theta) - F\sin(\gamma-\theta) + 2\int_{-L_f}^{L_f} F_t dS \sin(\phi-\gamma+\theta) - 2\int_{-L_f}^{L_f} F_n dS \cos(\phi-\gamma+\theta)$$

$$= N\cos(\gamma-\theta) - F\sin(\gamma-\theta) + A_t\sin(\phi-\gamma+\theta) - A_n\cos(\phi-\gamma+\theta) \qquad (3.3)$$

Where $A_n = 2\int_{-L_f}^{L_f} F_n dS$, $A_t = 2\int_{-L_f}^{L_f} F_t dS$

In the vertical direction we similarly obtain

$$m\frac{d^2Y_G}{dt^2} = m.g - N\sin(\gamma-\theta) - F\cos(\gamma-\theta) - A_t\cos(\phi-\gamma+\theta) - A_n\sin(\phi-\gamma+\theta) \qquad (3.4)$$

Moments about 'G'

Let the ψ be the angle between the fibre and the fixed vertical axis, then $\psi = \phi - \gamma + \theta$ and hence

$$\text{Angular acceleration} = \frac{d^2}{dt^2}\psi = \frac{d^2}{dt^2}(\phi - \gamma + \theta) = \frac{d^2\phi}{dt^2} + \frac{d^2\theta}{dt^2}$$

Also, $\theta = \omega.t$, therefore $\frac{d^2\theta}{dt^2} = 0$ and we get, taking moments about the centre of gravity G,

$$I_G \frac{d^2\psi}{dt^2} = I_G \frac{d^2\phi}{dt^2} = F.L_f \sin\phi - N.L_f \cos\phi + 2\int_{-L_f}^{L_f} S.F_n dS \qquad (3.5)$$

where I_G is the moment of Inertia of the fibre about its centre of gravity, given by $I_G = \frac{mL^2_f}{3}$ where $(m = 4\rho_f L_f)$ is the total fibre mass.

We have now three main equations (3.3, 3.4, 3.5) and we need one more to be able to find the four variables ($\dot{r}$, $\dot{\phi}$, F, N). This equation can be found from the assumption of whether or not slipping is occurring.

In the case of slippage we have: $F = \mu N$, and when there is no slippage $r = \text{constant}$.

3.2.5 Derivation of equations of motion of fibre off the tooth

The above analysis applies when the fibre is on the tooth. In the case of fibre motion off the tooth the equation of motion can be simplified by eliminating the friction and normal forces. Then the equations of motion will be:

$$m\ddot{X}_G = A_t \sin(\psi) - A_n \cos(\psi) \qquad (3.6)$$

$$m\ddot{Y}_G = mg - A_t \cos(\psi) - A_n \sin(\psi) \qquad (3.7)$$

$$I_G \ddot{\psi} = 2\int F_n S dS \qquad (3.8)$$

In all of the equations of fibre motion we have terms related to the air drag forces. In order to solve these equations it is necessary to find a proper description for the air drag force. The following section discusses this force in more detail.

3.2.6 Air Drag

The calculation of air drag is greatly simplified if aerodynamic theory is used. It is common practice in this theory [Goldstein 1938] to present formulae for air drag on cylinders in the form

$$F_d = \frac{1}{2}\rho V^2 dC_d \qquad (3.9)$$

where F_d is the air drag per unit length, ρ is the air density, V is the air speed relative to the cylinder, d is the cylinder diameter and C_d is a quantity known as the drag coefficient which is a function of the Reynolds number. The above expression can be written in the form $F_d = P_d . V^2$, where P_d is a constant which depends on the flow characteristics and the dimensions of the objects to which the air drag forces are applied, i.e.

$$P_d = \frac{1}{2}\rho C_d d \qquad (3.10)$$

3.2.6.1 Derivation of the equation of the air drag force

Let the angle between the fibre and the Y axis be ψ , when the fibre is still on the tooth, as in figure (3.4) then

$$\psi = \phi - \gamma + \theta$$

Let also the tangential velocity of the fibre be V_t , which is the same at all points of the fibre length.

The normal velocity at a typical point P of the fibre is V_n ,which varies along the length of fibre. V_n has the values V_a, V_b at the ends and V_G at the centre . If PG = S then,

$$V_n = V_G + S\dot{\psi} \qquad (3.11)$$

where $V_G = \dot{X}_G \cos\psi + \dot{Y}_G \sin\psi$

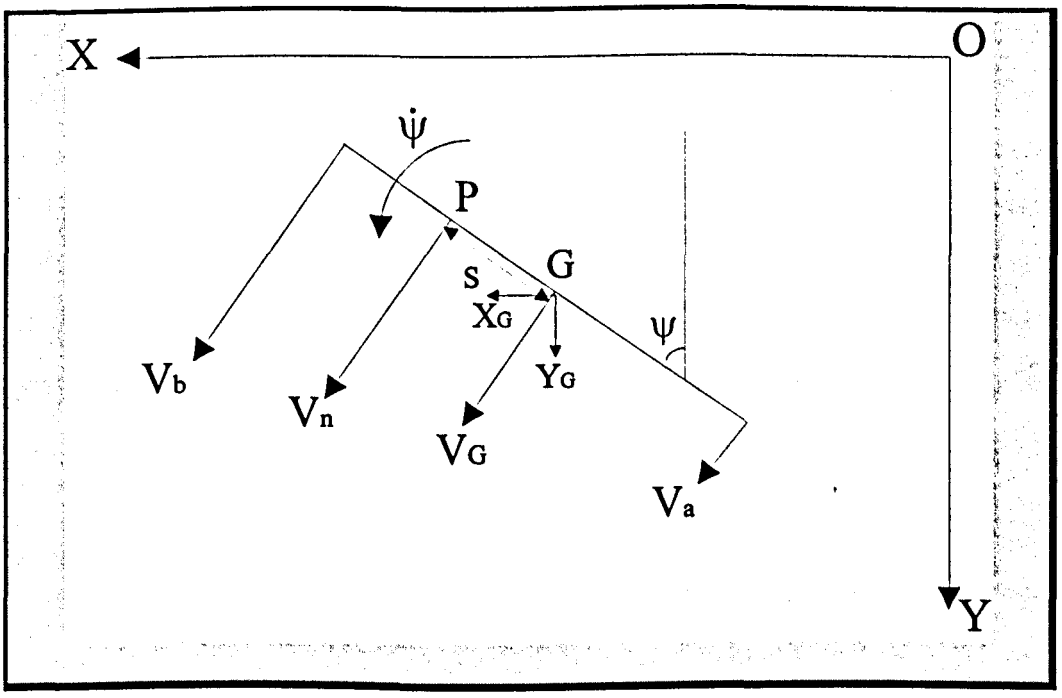

Figure (3.4) Normal and rotational velocities of fibre

We will calculate the total resistance force in terms of V_t , V_a , and V_b. These velocities may be positive or negative but are considered positive if they are in the senses shown in figure(3.4).

Note the special cases of equation (3.11):

$$V_a = V_G - L_f\dot{\psi} \qquad (3.11a)$$

$$V_b = V_G + L_f\dot{\psi} \qquad (3.11b)$$

so that

$$V_G = \frac{1}{2}(V_a + V_b) \qquad (3.11c)$$

Let the air drag forces on a fibre element of length dS be $F_n\,dS$ and $F_t\,dS$ where F_n and F_t are the normal and tangential drag forces per unit length respectively. They may be positive or negative but are considered positive if they are in the senses shown in

figure(3.3).

The equations for F_n and F_t are :

$$F_n = p_n V_n^2 \text{sign}(V_n) \quad (3.12)$$

$$F_t = P_t V_t^2 \text{sign}(V_t) \quad (3.13)$$

where $P_n = \frac{1}{2}\rho C_n d$, $P_t = \frac{1}{2}\rho C t d$ (refer to equ. 3.10.C_n and C_t are drag coefficients that will be discussed in more detail in section 3.2.6.2) and sign (X) is

$$= \begin{cases} 1 & \text{if} \quad X \rangle 0 \\ 0 & \text{if} \quad X = 0 \\ -1 & \text{if} \quad X \langle 0 \end{cases}$$

Then the total normal and tangential forces are :

$$A_n = 2 \int_{-L_f}^{L_f} F_n ds \quad (3.14)$$

$$A_t = 2 \int_{-L_f}^{L_f} F_t ds \quad (3.15)$$

Total Tangential Air Drag

$$A_t = 2 \int_{-L_f}^{L_f} P_t V_t^2 \text{sign}(V_t) ds$$

Using (3.15) and (3.13), this leads to

$$A_t = 4 P_t L_f V_t^2 \text{sign}(V_t) \quad (3.16)$$

where

$$V_t = \dot{Y}_G \cos\psi - \dot{X}_G \sin\psi$$

Total Normal Air Drag

From (3.14), (3.12), and (3.11) we have

$$A_n = 2\int_{-L_f}^{L_f} F_n dS$$

$$= 2\int_{-L_f}^{L_f} P_n V_n^2 \text{sign}(V_n) ds$$

$$= 2\int_{-L_f}^{L_f} P_n (V_G + S\dot{\psi})^2 \text{sign}(V_n) ds \qquad (3.17)$$

There are two cases:

Case 1 Sign (V_a) = Sign (V_b)

This case also applies if one of sign (V_a) or sign (V_b) is zero(i.e V_a or $V_b = 0$).

In this case sign (V_n) is constant and therefore from (3.11a, 3.11b, 3.17):

$$A_n = \frac{2P_n \text{sign}(V_a)}{3\dot{\psi}} \left[V_b^3 - V_a^3\right]$$

Substituting for $\dot{\psi}$ from (3.11a, 3.11b) we get

$$\dot{\psi} = \frac{V_b - V_a}{2L_f} \qquad (3.18)$$

and

$$A_n = \frac{4}{3}[P_n L_f \text{sign}(V_a)]\,[V_b^2 + V_a V_b + V_a^2] \qquad (3.19)$$

Case 2 Sign $(V_a) \neq$ Sign (V_b)

Case 2a Sign $(V_a) < 0$, Sign $(V_b) > 0$

There is a point C (where S = C) at which $V_C = 0$.

Then from (3.17) :

$$A_n = 2\int_{-L_f}^{L_f} P_n (V_G + S\dot{\psi})^2 \text{sign}(V_n) ds$$

$$= -2\int_{-L_f}^{c} P_n(V_G + S\dot{\psi})^2 \text{sign}(V_n)ds + 2\int_{c}^{L_f} P_n(V_G + S\dot{\psi})^2 \text{sign}(V_n)ds$$

which after some algebra leads to

$$A_n = \frac{4P_nL_f}{3}\left[\frac{V^3{}_a + V^3{}_b}{V_b - V_a}\right]$$

Case 2b $\text{Sign}(V_a) > 0$, $\text{Sign}(V_b) < 0$

Clearly in this case we would get the same result as in 2a with $V_a - V_b$ instead of $V_b - V_a$

Therefore the overall result for case 2 is :

$$A_n = \frac{4P_nL_f(V^3{}_a + V^3{}_b)}{3|V_b - V_a|} \qquad (3.20)$$

Air drag contribution in the moment about G

The contribution of air drag in the overall moment about 'G' is the last term of equation (3.5) that has to be considered in different cases, i.e.

$$Z = 2\int_{-L_f}^{L_f} S \times F_n d_s$$

$$= 2P_n \int_{-L_f}^{L_f} (V_G + S\dot{\psi})^2 \, \text{sign}(V_n) S dS \qquad (3.21)$$

after using (3.11) and (3.12).

There are two cases as before :

Case 1 $\text{Sign}(V_a) = \text{Sign}(V_b)$

In this case,

$$Z = 2P_n \text{sign}(V_a) \int_{-L_f}^{L_f} (V_G + S\dot{\psi})^2 S dS$$

which leads to

$$Z = \frac{2P_n L_f \text{sign}(V_a)(V^2{}_b - V^2{}_a)}{3} \qquad (3.22)$$

Case 2 $\text{Sign}(V_a) \neq \text{Sign}(V_b)$

We still have equation (3.14) but sign (V_n) changes in the interval and there is a point C (S = C) where $V_c = V_G + C\dot{\psi} = 0$

Therefore ;

$$Z = 2P_n \int_{-L_f}^{C} (V_G + S\dot{\psi})^2 \, \text{sign}(V_n) S dS + 2P_n \int_{C}^{L_f} (V_G + S\dot{\psi})^2 \, \text{sign}(V_n) S dS$$

Case 2a $\text{Sign}(V_a) < 0$, $\text{Sign}(V_b) > 0$

Here,

$$Z = -2P_n \int_{-L_f}^{C} (V_G + S\dot{\psi})^2 SdS + 2P_n \int_{C}^{L_f} (V_G + S\dot{\psi})^2 SdS$$

which eventually gives

$$Z = \frac{2P_n L^2_f (V^4_a - 2V^3_a V_b - 2V_a V^3_b + V^4_b)}{3(V_a - V_b)^2} \qquad (3.23)$$

case 2b $\text{Sign}(V_a) > 0$, $\text{Sign}(V_b) < 0$

This case also leads to equation (3.23).

3.2.6.2 Evaluation of air drag parameter

The air drag parameters are

$$P_n = \frac{1}{2} C_n d\rho \quad , \quad P_t = \frac{1}{2} C_n d\rho \quad ,$$

where ρ is the air density ($1.2 \times Kg.m^{-3}$) , d is the effective fibre diameter and C_n and C_t are drag coefficients associated with the normal and tangential air resistance respectively.

For smooth cylinders C_n varies with the Reynolds number [Schlichting 79].

Reynolds Number

The nature of a flow (laminar or turbulent) is determined by the value of a dimensionless parameter which is called the Reynolds number, the name of a British engineer who pioneered its use. For a fluid flow through a pipe or tube , it is defined as the ratio of the inertia forces to the viscous forces acting on the fluid, i.e.

$$R_{ef} = \frac{\rho V_f d_t}{\eta} \quad ,$$

where R_{ef} = fluid Reynolds number

ρ = density of the fluid

V_f = relative velocity of the fluid in the pipe

d_t = pipe diameter (in general it is a characteristic length descriptive of the flow field geometry)

η = dynamic viscosity of the fluid

It has been found that[Hinds 82]

$$\text{if} \quad \begin{cases} R_{ef} < 2000 & \text{the flow is laminar} \\ R_{ef} > 4000 & \text{the flow is turbulent} \end{cases}$$

By substituting the velocity of a particle for the relative velocity of the fluid and particle diameter for pipe diameter, the above equation gives the Reynolds number for freely settling particles

$$R_{ep} = \frac{\rho V_p d_p}{\eta}$$

where R_{ep} = particle Reynolds number

V_p = particle velocity

d_p = particle diameter

The flow around a particle is laminar if $R_{ep} < 1$ and is turbulent if $R_{ep} > 1$ [Hinds 1982].

In the present work the air speed in the stripping zone was set to 40 $m.s^{-1}$ and the other values for calculating Reynolds number are :

Channel diameter 15 cm

Fibre diameter 4.6×10^{-5} m

Kinematic viscosity 15×10^{-6} $m^2.s^{-1}$

Thus the fluid Reynolds number is 4×10^5 and the particle Reynolds number is 122.8 .

Based on the calculated Reynolds number the flow in the transfer channel is classified

as turbulent.

Figure (3.5) shows the relationship between C_n and Reynolds number. From the graph the C_n value corresponding to Re = 122.8 is about 1.75; therefore the value of P_n is 4.83×10^{-5} kg.m^2. The value of the tangential air drag parameter P_t is more difficult to obtain. However, it may be deduced from some data given by Popov et al.[Popov 1962] namely that the tangential air drag parameter will generally be less than 1/10 the value of the normal air drag parameter and usually near 1/20 of that value; therefore P_t will be taken as 0.484×10^{-5} kg.m^2.

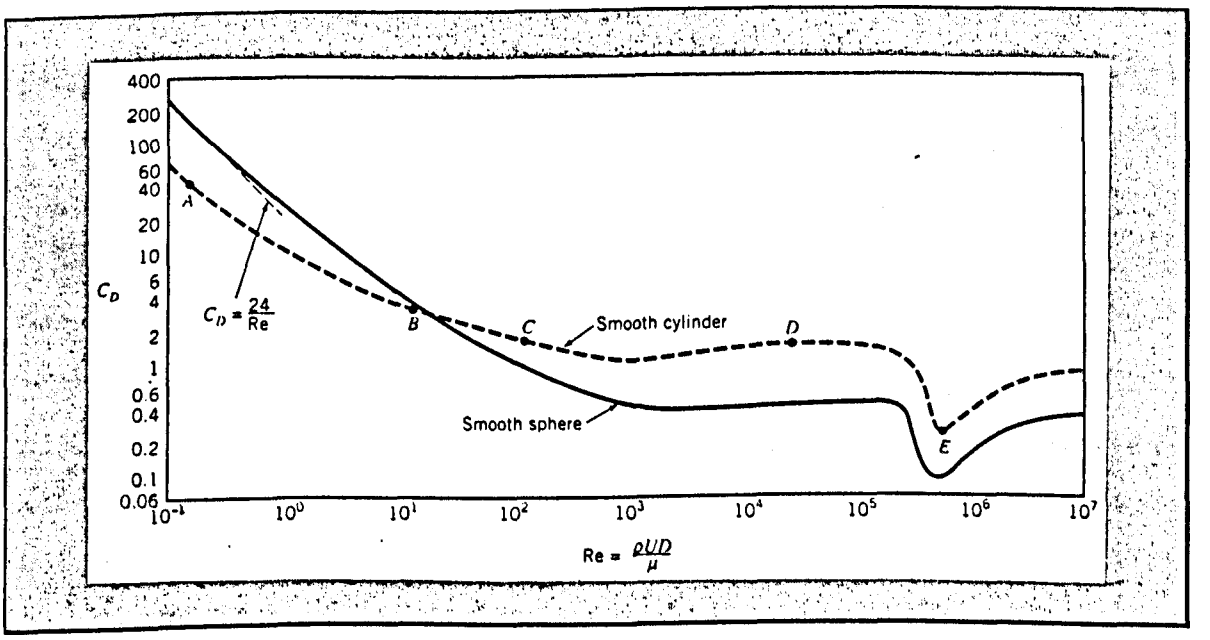

Figure(3.5) Drag coefficient as a function of Reynolds number for a smooth circular cylinder and a smooth sphere

3.3 Theoretical considerations of the airflow pattern in the transport channel

The phenomenon of fibre movement in the transport channel mainly depends on the airflow behaviour in the channel, which is a very complex problem. In this study an extreme simplification was made to be able to model the air flow behaviour through the channel. The approach, which is used to discover the velocity profile, is to apply the

continuity equation and assume that the flow pattern across the channel will be either parabolic or uniformly distributed across the channel.

Figure(3.6) shows a schematic view of the air-laid transfer channel

3.3.1 Assumptions for airflow pattern

Parabolic air velocity distribution

First, we assume that the air velocity distribution is a parabola. This assumption is based on the fact that the flow along the transfer channel can be modelled as a flow between parallel plates, which has a parabolic profile.[Munson 1998]

It was found that the calculation would be made easier if we rotate XY axes, about the origin 'O', to create a new set of UV axes, which are parallel and perpendicular to the channel sides (figure3.6). Figure(3.6) shows a schematic view of the air-laid transfer channel with a parabolic air velocity distribution.

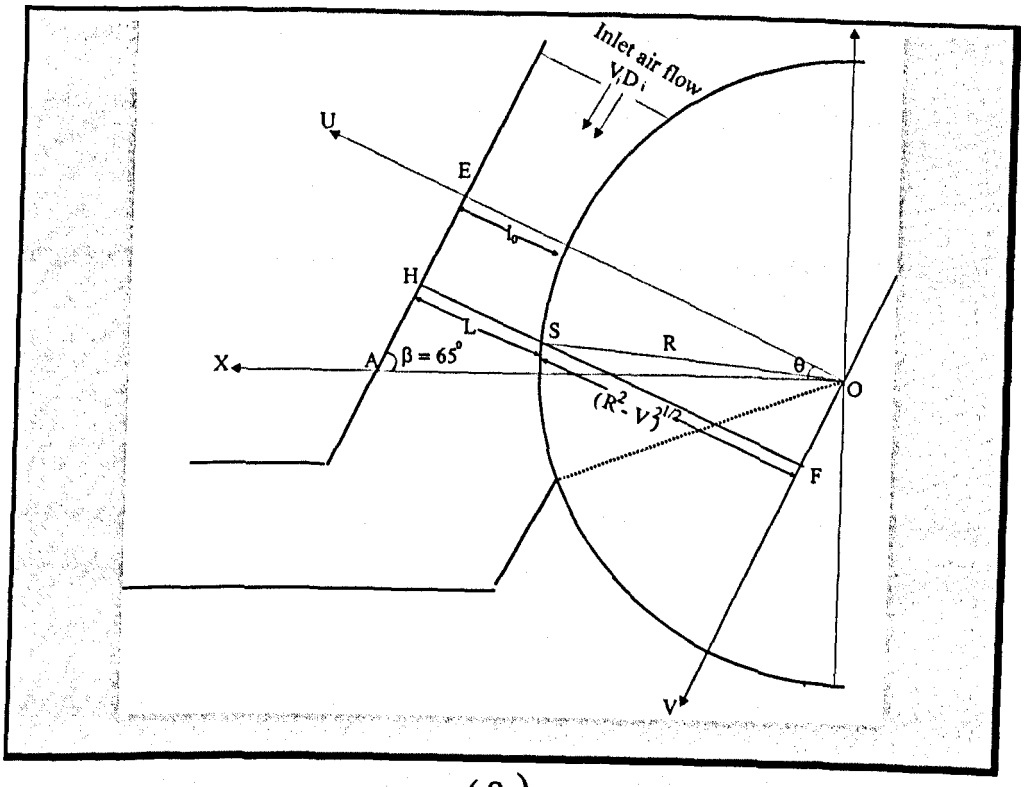

(a)

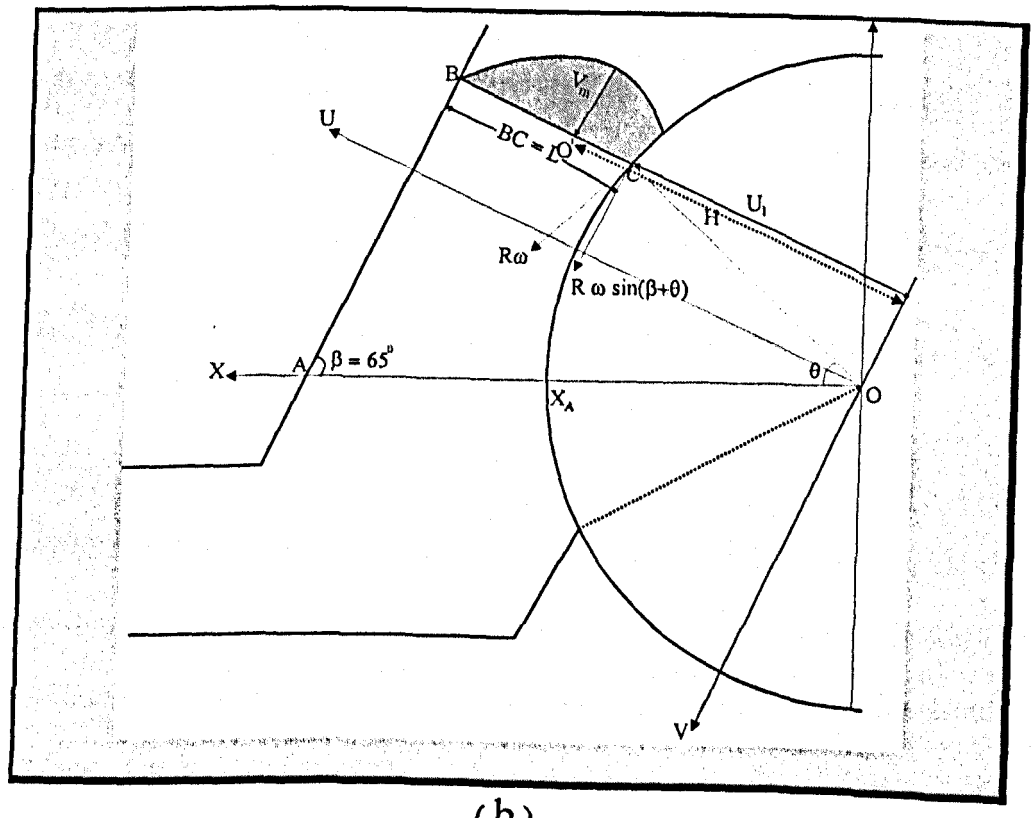

(b)

Figure (3. 6) Schematic view of the transfer channel of the air-laid machine

Continuity equation : The application of the principle of conservation of mass (matter can neither be created nor destroyed) to a steady flow results in the continuity equation which expresses the fact that in steady flow the mass flow rate $A\rho V$,where A is area of cross section of channel, passing all sections of channel is constant. Applying the continuity equation for the flow through the channel, gives

$$V_i D_i = \overline{V}.L = \int_a^b V.dU \qquad (3.24)$$

where V_i , D_i , $\overline{V}$,V and L are inlet air velocity, inlet channel width, average air velocity, air velocity at any point across the channel cross section and width of channel respectively. The boundary conditions of this integral, a and b, are -O'C and O'B that can be substituted by -[H-U_l] and [U_l+L-H] relative to origin O' as shown in figure(3.6b).

The parabolic air velocity distribution can be expressed by the following equation (taking UV axes with origin O) :

$$V = V_m - K(U-H)^2 \qquad (3.25)$$

where V_m is the maximum value of 'V' and K is a constant . H is the length OO' which can be found from the geometry of the system (see Fig 3.6a)

$$H = R\sin(\beta + \theta)$$

Considering the boundary condition

Referring to figure 3.6, at point C where the air is in direct contact with the drum surface, it is assumed that it has the same velocity as the drum itself, i.e. there is no slip at the boundary [Munson 1998]. At this point we assume that the air velocity is equal to the component of the surface speed of the drum in the direction of V (the component of the drum surface speed in the direction of U is negligible), therefore;

At point C where $U = U_1$ then $V = R\omega\sin(\beta+\theta)$ (3.26)

Point B where $U = U_1 + L$ then $V = 0$ (3.27)

Solving the integral(3.24) results in an expression for $\overline{V}$ in the form

$$\overline{V} = V_m - \frac{k}{3}[3(U_1 - R\sin(\beta+\theta))^2 + 3(U_1 - R\sin(\beta+\theta))L + L^2] \quad (3.28)$$

We have now three equations namely 3.26, 3.27, 3.28 in order to find three unknowns (K, V_{mo}, u_1). The results of solving the above equations are

$$K = 3\frac{(2L-1)R\omega\sin(\beta+\theta) - 2V_iD_i}{L^2(2L-3)}$$

$$U = \frac{-1}{3}[\frac{3R^2\omega\sin^2(\beta+\theta)(1-2L) + 6V_iD_iR\omega\sin(\beta+\theta) + 2L^2R\omega\sin(\beta+\theta) - 3LV_iD_i}{(2L-1)R\omega\sin(\beta+\theta) - 2V_iD_i}]$$

$$V_m = \frac{1}{3}[\frac{6V_iD_i(3-4L)R\omega\sin(\beta+\theta) + (9+16L^2-24L)R^2\omega^2\sin^2(\beta+\theta) + 9V_i^2D_i^2}{(2L-3)[(2L-1)R\omega\sin(\beta+\theta) - 2V_iD_i]}]$$

In the above equations L is the channel width which from the geometry of the system (fig3.6a) can be expressed as follows

$$L + SF = OE$$

$$L + \sqrt{R^2 - V^2} = R + l_0$$

Therefore,

$$L = R + l_0 - \sqrt{R^2 - V^2}$$

where l_0 is the shortest channel width which is expressed by

$$l_0 = X_A \sin\beta - R$$

X_A and β are the length of OA and the inclination ot the channel which depend on the machine design and R is the radius of the drum. In the machine used for this research X_A, β, and R are 317.9mm, 65°and 170mm respectively; thus l_0 is about 118.1mm

Uniform air velocity distribution

The second assumption for the airflow pattern through the transfer channel was a uniform airflow distribution across the channel. The same system of axes as the previous one (i.e. VU) was used in this calculation.

Again applying the continuity equation we obtain

$$V_i D_i = V.L \qquad \text{or} \qquad V = \frac{V_i D_i}{L}$$

Here V is the air velocity at any point across the channel, which has a different constant value at each channel cross section.

In the air-laid machine, because the air viscosity is very small (15×10^{-6} $m^2.s^{-1}$), it can be neglected and flow is considered to be inviscid . In an inviscid flow the viscous forces are negligible and hence the boundary layer will no longer exist.

3.4 Nondimensional version of the equation

When we are involved with a multi-variable physical problem it is often beneficial to recognise the dimensionless groups to analyse the problem instead of struggling with numerous independent variables. One of the very well known dimensionless parameters is the Reynolds number, which indicates the nature of a fluid flow inside a pipe by the magnitude of the dimensionless term $R_e = \frac{DV\rho}{\eta}$ (where D, V, ρ, and η refer to the diameter , velocity, density and viscosity , respectively). In this section a dimensionless version of the equations is presented. If 'R', 'ω', and 'm' are the diameter of the cylinder, the angular velocity of the cylinder and the mass per unit length of the fibre respectively, then we define the dimensionless groups

$$X'_G = \frac{X_G}{R}, \quad Y'_G = \frac{Y_G}{R}, \quad L'_f = \frac{L_f}{R}, \quad r' = \frac{r}{R}, \quad \dot{r}' = \frac{\dot{r}}{R\omega}, \quad \ddot{r}' = \frac{\ddot{r}}{R\omega^2},$$

$$\dot{\phi}' = \frac{\dot{\phi}}{\omega}, \quad \ddot{\phi}' = \frac{\ddot{\phi}}{\omega^2}, \quad A'_n = \frac{A_n}{mR\omega^2}, \quad A'_t = \frac{A_t}{mR\omega^2}, \quad N' = \frac{N}{mR\omega^2}, \quad F' = \frac{F}{mR\omega^2},$$

$$Z' = \frac{Z}{mR^2\omega^2}, \quad t' = \frac{t}{2\pi/\omega}$$ (where $2\pi/\omega$ is the time needed for one revolution of the cylinder).

The equations of motion then become:

$$N'\cos(\gamma - \theta) - F'\sin(\gamma - \theta) + A'_t \sin\psi - A'_n \cos\psi = \frac{d^2X'_G}{d\theta^2} \qquad (3.3)'$$

$$g' - N'\sin(\gamma - \theta) - F'\cos(\gamma - \theta) + A'_t \cos\psi - A'_n \sin\psi = \frac{d^2Y'_G}{d\theta^2} \qquad (3.4)'$$

$$\frac{1}{3}L'^2_f \ddot{\phi}' = F'L'_f \sin\phi - N'L'_f \cos\phi + Z' \qquad (3.5)'$$

By doing some algebra we can get three equations of the form:

$aN' + bF' + c\ddot{r}' + d\ddot{\phi}' = e$ where a, b , c, d and e are functions of $\theta, r', \dot{r}', \phi', \dot{\phi}'$

the other equation is either:

$$\dot{r}' = 0$$

or

$$F' = -\mu N'$$

depending whether or not there is slipping.

Thus, we have four equations which are linear in $F', N', \ddot{r}', \ddot{\phi}'$, and can be solved by using a proper subroutine (for any given set of initial values of $\theta, r', \dot{r}', \phi', \dot{\phi}'$) in the main computer program.

3.5 Method of solving the equations

In order to solve the equations of fibre motion a numerical method was applied. There is no single numerical method which is applicable to every differential equation, or even to every ordinary differential equation. This field is very large, and for the most effective use of the computer, coupled with the necessity for producing accurate results, we need a variety of methods, each appropriate for particular problem. The most useful and flexible technique for solving first-order ordinary differential equation (i.e. $\frac{dy}{dx} = f(x,y)$) is a method which was first introduced by C.Runge and subsequently modified and improved by W.Kutta.

The fourth-order Runge-Kutta method is the most popular. It is a good choice for most purposes because it is accurate and simple to use, and it allows adjustment of the length of the integration step from point to point without modification of the method [Jeffery 1985].

3.5.1 Selecting a suitable routine for the present problem

In the present problem all the equations of fibre motion can be expressed by a system of ordinary differential equations in the form

$$y_2' = f_1(t, y_1, y_2, y_3, y_4)$$

$$y_4' = f_2(t, y_1, y_2, y_3, y_4)$$

Where $y_1 = r, y_2 = \dot{r}$, $y_3 = \phi$, $y_4 = \dot{\phi}$

The initial values of the independent variables $(r, \dot{r}, \phi, \dot{\phi})$ must be supplied at a given point (t = 0). Also a point, $t = t_e$, at which the values of the dependent variables are required, must be specified.

The numerical solution is then obtained by a step-by-step calculation which approximates values of the variables at finite intervals over the required range [$t = t_0$, $t = t_e$]. The routine adjusts the step-length automatically to meet specified accuracy tolerances.

For simple first-order problems with low accuracy requirements, that is problems with a short range of integration, with derivative functions that are inexpensive to calculate, the best routines to use are likely to be Runge-Kutta Merson (RKM) routines. These routines are available in the Computer system of the University and named DO2BxF (where x is A, B, D, G or H).

For larger problems, over long ranges or with high accuracy requirements the variable-order, variable-step Adams routines should usually be preferred. These routines are also available in the Computer system of the university and named DO2CxF (where x is A,

B, G, H or J).

At first because we could not classify the problem, we performed some preliminary calculations with DO2BDF (RKM) and we also did some trial calculations with DO2CJF (Adams), before deciding to use DO2CJF for solving the equations of fibre motion.

3.5.2 Computing Technique

We know that

$$\theta = \theta_0 + \omega t \quad , \quad \dot{\theta} = \omega \quad \text{and} \quad \ddot{\theta} = 0$$

and also that

$$\psi = \phi - \gamma + \theta \quad \dot{\psi} = \dot{\phi} + \omega \quad \ddot{\psi} = \ddot{\phi}$$

The geometrical equations are;

$$X_G = R\cos\theta + r\sin(\gamma - \theta) + L_f \sin\psi$$

$$Y_G = R\sin\theta + r\cos(\gamma - \theta) - L_f \cos\psi$$

Differentiating the above equations (with respect to 't') and using the second Newton's law for horizontal and vertical forces give us the following equations:

$$N\cos(\gamma - \theta) - F\sin(\gamma - \theta) + A_t \sin\psi - A_n \cos\psi = m\frac{dX^2}{d^2t} \qquad (3.3)$$

$$mg - N\sin(\gamma - \theta) - F\cos(\gamma - \theta) - A_t \cos\psi - A_n \sin\psi = m\frac{dX^2}{d^2t} \qquad (3.4)$$

Taking moments about the centre of gravity 'G' and using the fact that $I_G = \frac{mL_f^2}{3}$ gives:

$$I_G \ddot{\psi} = \frac{mL_f^2}{3}\ddot{\phi} = F \times L_f \sin\phi - N \times L_f \cos\phi + 2\int_{-L_f}^{L_f} S \times F_n dS \qquad (3.5)$$

The last three equations can be used for the subsequent argument, but it simplified the

calculations to form two new equations from (3.3), (3.4) and use them in place of (3.3), (3.4).

Multiply (3.3) by cos(γ-θ) and (3.4) by -sin(γ-θ) and add them together , simplifying the sines and cosines that result. Finally, rearrange them to put terms containing $F, N, \ddot{r}, \ddot{\phi}$ on the left and everything else on the right.

$$N - (mL_f\cos\phi)\ddot{\phi} = mg\sin(\gamma-\theta) - mR\omega^2\cos\gamma - 2m\omega\dot{r} + A_n\cos\phi - [A_t + mL_f(\dot{\phi}+\omega)^2]\sin\phi \quad (3.29)$$

$$F + m\ddot{r} + (mL_f\sin\phi)\dot{\phi} = mg\cos(\gamma-\theta) + mR\omega^2\sin\gamma + m\omega^2 r - A_n\sin\phi - [A_t + mL_f(\dot{\phi}+\omega)^2]\cos\phi \quad (3.30)$$

The NAG routine chosen assumes that equations to be solved are of the form

$$\ddot{r} = f_1(r, \phi, \dot{r}, \dot{\phi}, t)$$

$$\ddot{\phi} = f_2(r, \phi, \dot{r}, \dot{\phi}, t)$$

What we have is three equations in the form

$$aN + bF + c\ddot{r} + d\ddot{\phi} = e$$

Where a, b, c, d, and e are functions of $r, \phi, \dot{r}, \dot{\phi}, t$ [namely (3.5), (3.29), (3.30)]. The extra equation is either: $\dot{r} = 0$ if there is no slipping

$F = \mu|N|$ if slipping is in direction r^+

$F = -\mu|N|$ if slipping is in direction r^-

Therefore at any time we have equations (3.5), (3.29), (3.30) and one of the last three equations. All four equations are linear in $F, N, \ddot{r}, \ddot{\phi}$, thus a linear subroutine can be applied to find $\ddot{r}, \ddot{\phi}$ and incidentally F and N for any given set of value of $(t, r, \phi, \dot{r}, \dot{\phi})$.

It was found that the easiest way, from the computer programming point of view, to solve these simultaneous equations is to use a matrix equation. Therefore we denote X

as a column vector containing $(N, F, \ddot{r}, \ddot{\phi})$, then we have the following matrix equation:

$$A \times X = B$$

Where A and B are two matrixes that can be defined as follows:

1	0	0	$-mL_f\cos\phi$	N		equ.29
0	1	m	$mL_f\sin\phi$	F	=	equ.30
$L_f\cos\phi$	$-L_f\sin\phi$	0	$mL_f^2/3$	$\ddot{r}$		-Z
no slipping 0	0	1	0			0
slipping r^+ μ	1	0	0	$\ddot{\phi}$		0
slipping r^- $-\mu$	1	0	0			0

Chapter Four

Experimental Air-laid machine

In order to be able to carry out experimental studies, the existing rig needed to be modified due to the poor design of some components, especially the feeding unit, so that a fairly uniform web could be achieved.

4.1 Description of the available air-laid machine

The existing air-laid machine consists of a feeding conveyor(1) ,a weighing plate(2) , a pair of feed rollers(3) , a licker-in roller(4) , a saw-tooth cylinder(5) and an exit conveyor(6). In addition , there are six stationary carding plates(7), clothed with metallic wire, placed around the front top of the cylinder to provide additional carding. An air knife with the aid of a suction system is used to doff the fibres from the cylinder. The cylinder diameter is 340 mm , with a working width of 480 mm. In operation, feed rollers (3) hold the fibres which are fed by an infeed conveyor and then subjected to an initial carding between feed rollers and lickerin. Because of the high speed of the saw-toothed cylinder, the fibres are then taken by the saw-teeth of the cylinder in a very thin stream. The fibres are carried by the teeth of the cylinder and then with the aid of airflow and suction , they are removed and deposited on the exiting conveyor. A schematic view of the existing air-laid machine is shown in figure(4.1).

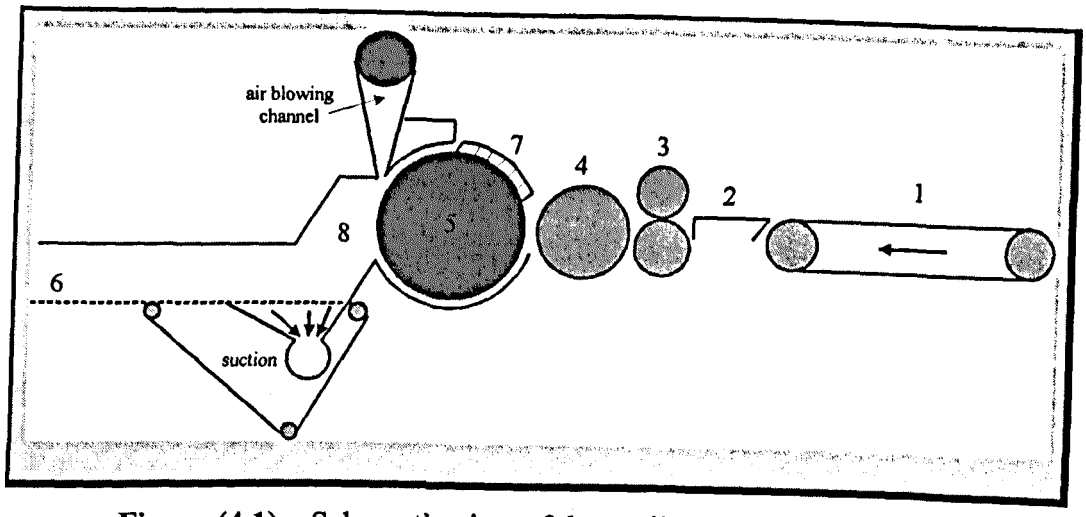

Figure (4.1) Schematic view of the available air-laid machine

4.1.1 Description of the machine components

The specifications of the different units of the machine, i.e. feeding unit, opening unit, blower and suction system, are explained below.

4.1.1.1 Feeding unit

The feeding unit comprises a conveyor belt and a pair of rollers, a metallic tooth-clothed one at the bottom and a fluted one at the top. A weighing plate is placed between the conveyor belt and the feeding rollers in order to control the input fibre weight.

4.1.1.2. opening unit

The opening unit includes a licker-in roller, main cylinder and six stationary flats. Use of the stationary flats gives more carding action and consequently better fibre opening during the process. The distance between the cylinder and the lickerin and also the cylinder and the stationary flats are adjustable so as to have flexibility in using different input materials.

The details of the rollers are listed in the Table (4.1).

Rollers	Diameter (mm)	Width (mm)	Wire Type	Wire density points/in^2	Working angle	Height (mm)
Top feed roller	72	480	fluted			
Bottom feed roller	77	480	saw-tooth	47	120	4
Lickerin	124	480	saw-tooth	55	104	5
Cylinder	340	480	saw-tooth	161	82	2

Table (4.1) Characteristic features of the rollers

4.1.1.3 Aerodynamic system

The aerodynamic system plays an important role in making a uniform web. It is extremely important to provide a uniform air stream velocity distribution in the fibre transport section. It has been pointed out [Fehrer 93, US Patent 76] that if the turbulence intensities are large , large eddies or vortices are in the fibre transport section and the velocity profile becomes unstable and this causes streaks (lines of different fibre density which are caused by local variations in air stream velocity) or blotchiness (small nonuniformities which are formed by depositing clumps of fibres) in the web. In order to avoid such turbulence the air knife has to create a laminar flow.

Air knife unit

In the present air-laid machine the air knife unit creates an air stream for doffing the fibres from the cylinder and transferring them to the exit conveyor. The air stream created by a powerful fan, blowing air into the air chamber (C) via the pipe (A) and the air duct (B), see Fig 4.2. The air duct has a cylindrical shape with a slot along its side;

the air passes through the slot into the air chamber. The air chamber is a converging section which causes the air stream to speed up as it flows downstream towards the outlet of the chamber. There is a series of screws at the end of the chamber to adjust the dimensions of the outlet which in turn alters the air stream velocity (due to the continuity equation $V_{out} = \frac{V_{in} \times A_{in}}{A_{out}}$ where V_{in}, V_{out}, A_{in} ,A_{out}, are the velocity of inlet air , the velocity of outlet air , the cross section of the inlet area and cross section of the outlet area respectively). Figure (4.2) shows a schematic diagram of the air knife unit.

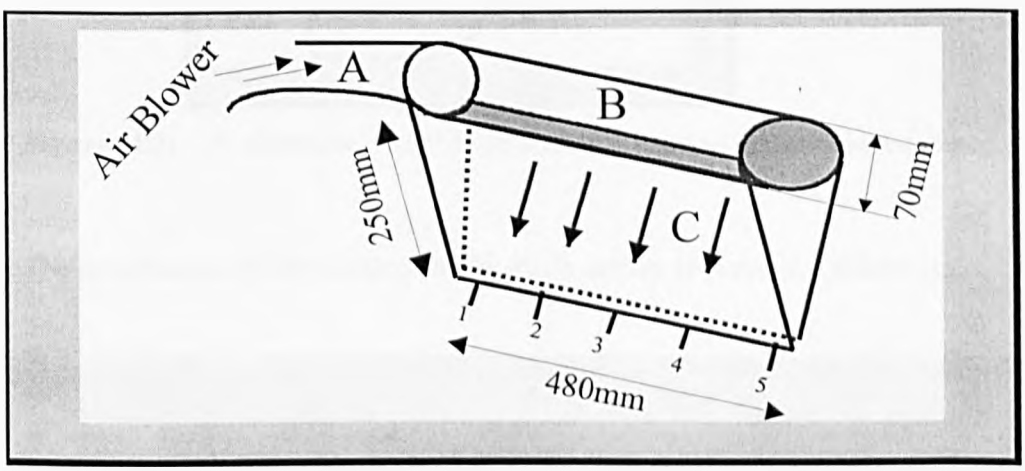

Figure (4.2) Air knife system of the air-laid machine

It is extremely important to provide a uniform air stream distribution across the air chamber.

Suction system

In order to land the fibres on the exiting conveyor a suction system was provided. Figure (4.3) shows the details of this suction unit.

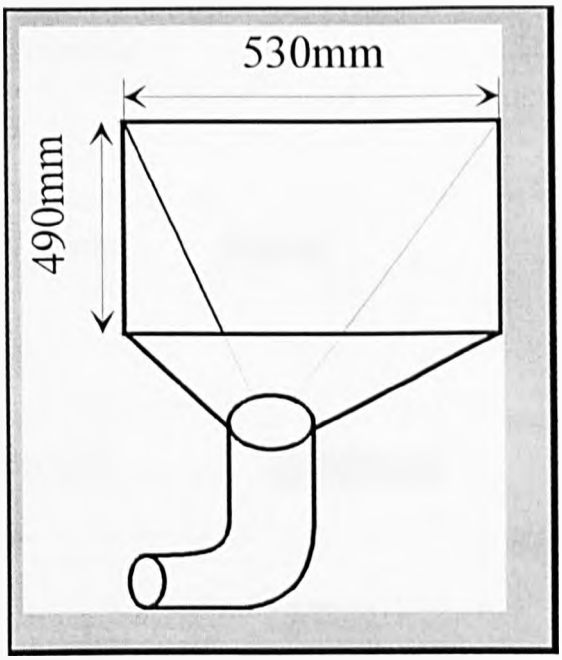

Figure (4.3) A schematic view of the suction system in the air-laid machine

The specification of the suction and air knife motors is given in Table(4.2).

Items	Power (KW)	Speed (Revs/min)	Volts	Amps	Freq.
Airknife	1.5	2850	220-240	5.5-5.9	50
Suction	2.2	2850	220-240	7.8-7.9	50

Table (4.2) Specification of the suction and airknife motors

4.1.1.5 Driving system

Figure (4.4) shows the driving system of the machine. There are four motors to drive the machine components. The main cylinder and lickerin are driven by two individual motors and the other two motors are used for driving the feed and exit units.

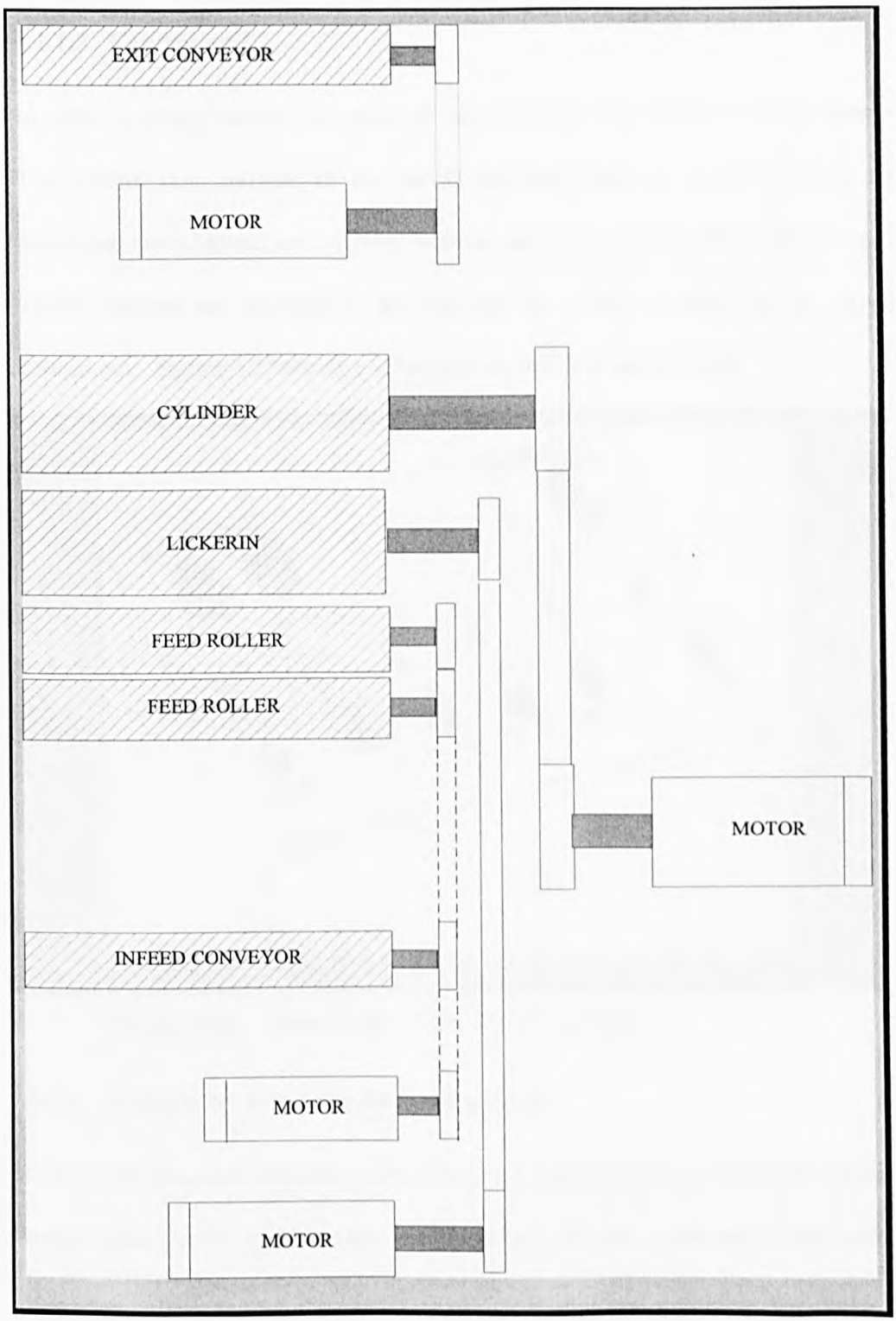

Figure (4.4) Schematic view of the driving system of the air-laid machine

4.1.1.5 Control unit

In order to easily control the speed of the machine components a control unit is used. The control unit consists of six on/off switches with six speed variators for each individual components, i.e. cylinder, lickerin, air knife, suction, feed and exit conveyors. These switches are arranged so that the start up of the machine can be conveniently carried out. Figure(4.5) shows a schematic view of the control unit.

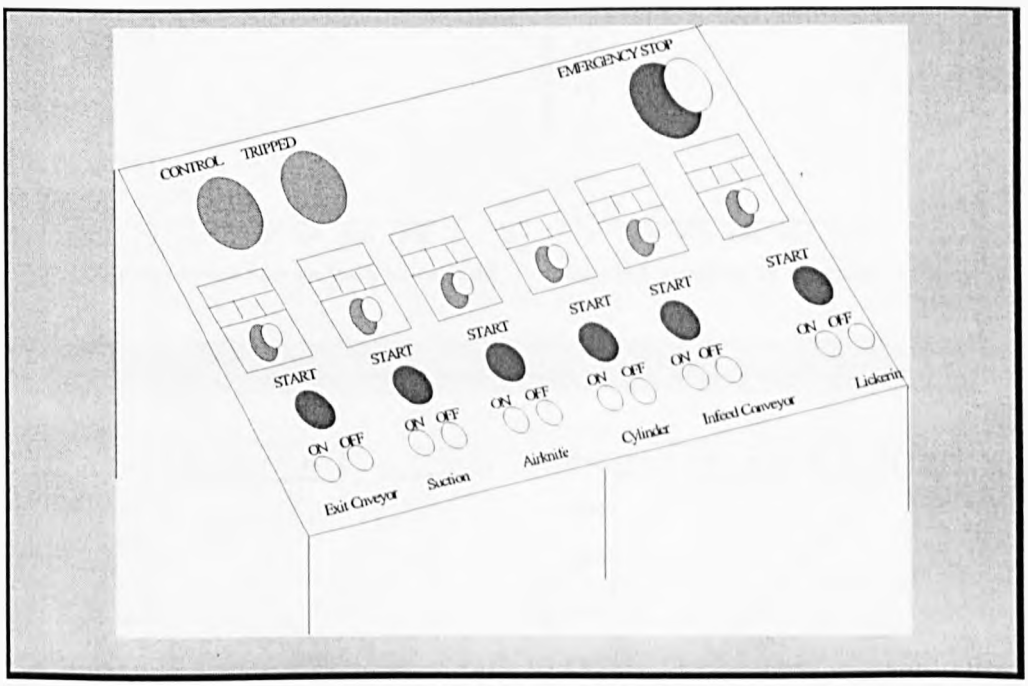

Figure (4.5) Control unit of the air-laid machine

4.1.2 Calibration of the machine components

In order to determine the relationship between the displays in the speed variators and the actual roller speeds and air velocity due to the air knife, calibration tests were carried out.

For the rotating components, i.e. the cylinder, lickerin, infeed and exit rollers, a digital tachometer was used. The speed variators were increased in steps of 50 units at a time and the roller's speed were measured. This test was carried out until the maximum

number of 999 on the speed variators was reached, then the machine numbers were plotted against the measured values of the rollers speed (revs/min). The results are shown in figure (4.6) along with the fitted curves and the equations which enabled the determination of each component's speed.

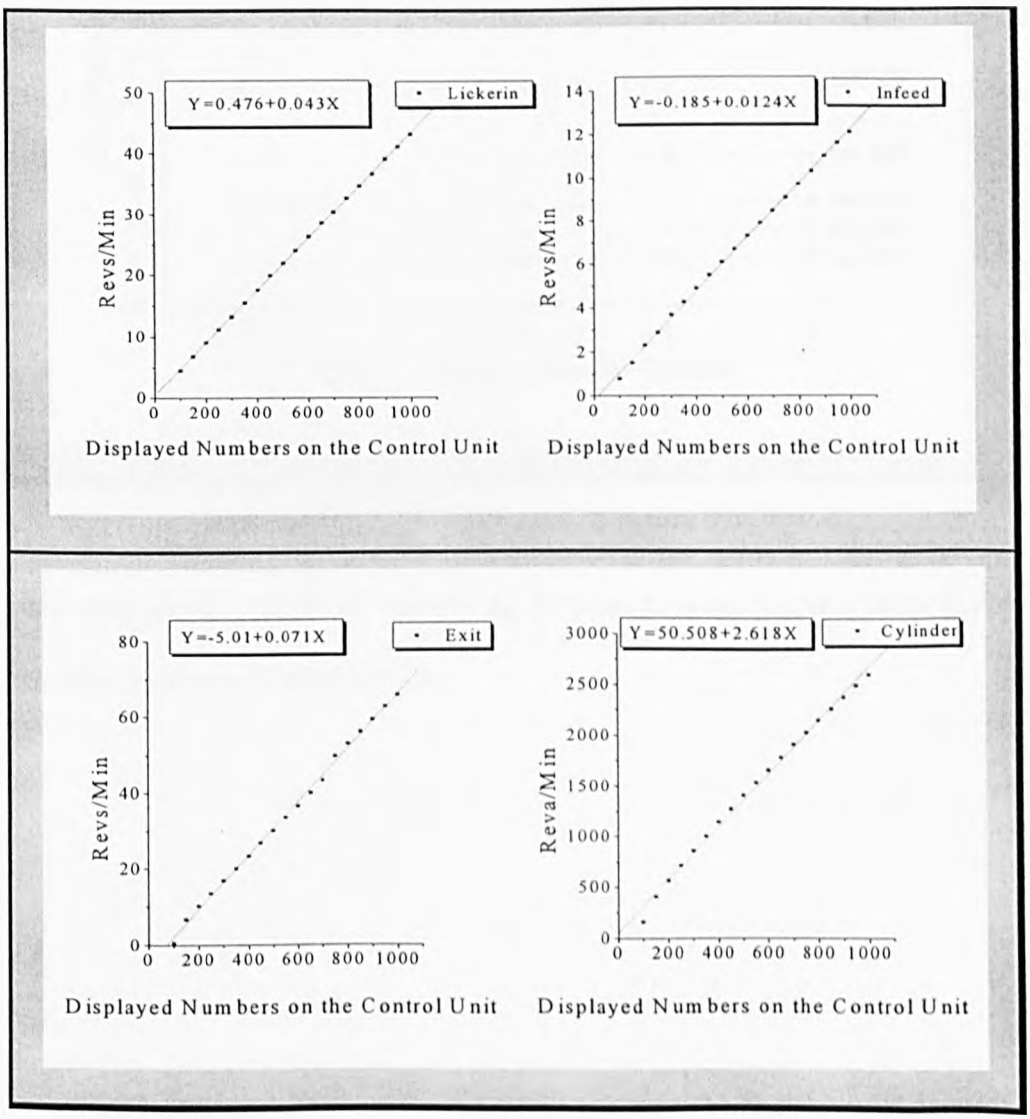

Figure(4.6) Calibration graphs for rotating components of the air-laid machine

To determine the relationship between the air knife speed and numbers in the speed variator a Pitot static tube was employed. The Airknife variator was altered in steps of 50 and the air velocity was measured at five different points across the air chamber (see Fig.4.2). Figure(4.7) shows the results with the fitted curves.

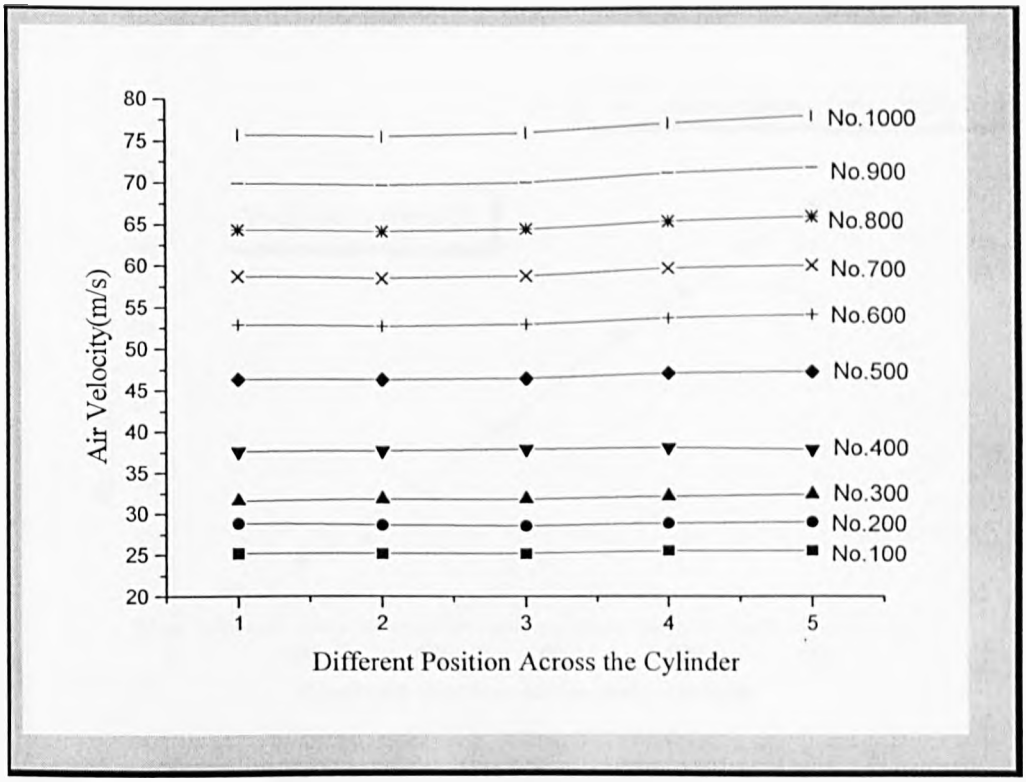

Figure (4.7) Air knife velocity across the channel

The average value of the air velocity for each machine number was taken to plot against the displayed numbers(figure 4.8).

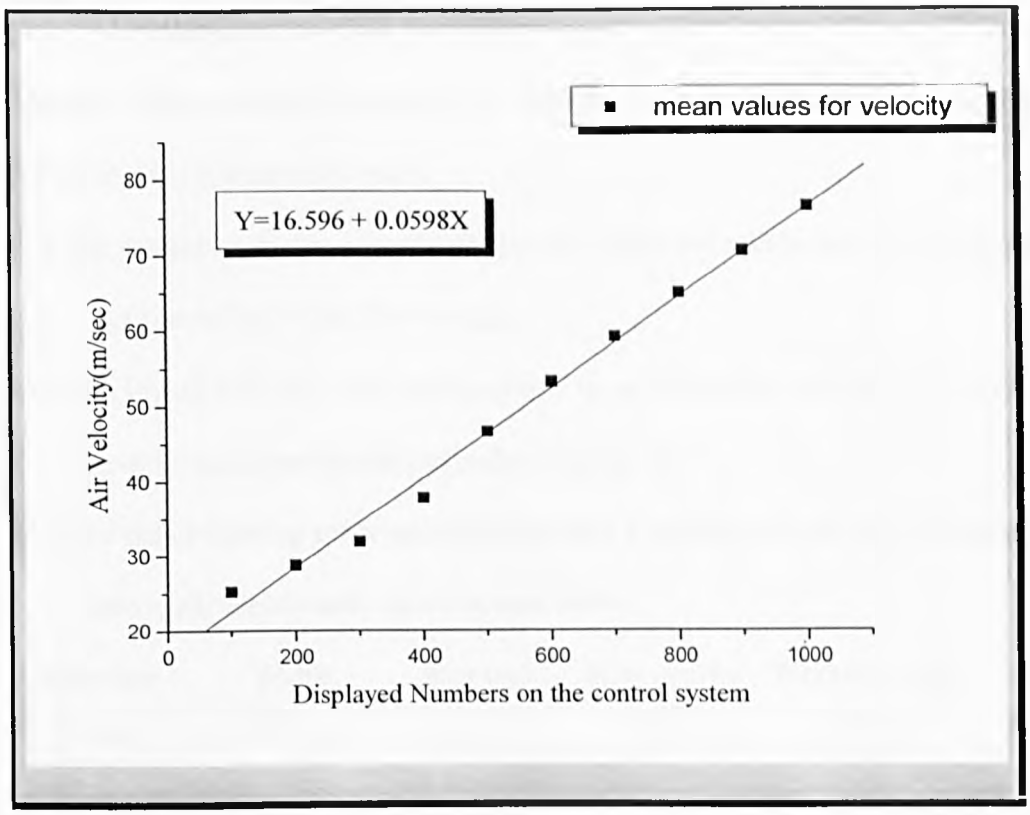

Figure(4.8) Calibration graph for airknife velocity

4.1.3 Problem incurring with running the machine

As explained in section 4.1.1 the available air-laid machine has a feeding unit consisting of a pair of feed rollers namely a clothed roller at the bottom and a fluted one at the top. It was found that this arrangement led to inadequate holding of the fibres, causing poor control of the fibre feed. Clearly, this affects the regularity of the final product. Apart from the feeding roller problem the weigh plate was not satisfactory due to the fact that there was no effective contact of fibres with the plate which is the essential point for measuring and controlling the fibre weight.

4.2 Reconstruction of the air-laid machine

Because of the problems incurring with running the machine the following changes to the feeding system were made.

1) The weighing plate was removed because it was not satisfactory for the purpose of controlling of the fibre weight.

2) The infeed conveyor belt was extended to an adjustable distance of a range of about 10 mm from the feeding rollers 3 in fig. 4.9.

3) The fluted opening roller was replaced with a metallic clothed roller having the same tooth specification as the bottom roller:

Diameter	Width	Wire type	Wire density	Working angle	Height
77 mm	480 m	saw-tooth	40/in^2	82 deg.	3.5 mm

After several trial runs it was also found that in the exit section, the suction area was too large so that the web could not be formed; therefore this area was reduced from (490×530) to (490×200) mm^2. Figure(4.9) shows a diagram of the modified air-laid machine used in this work.

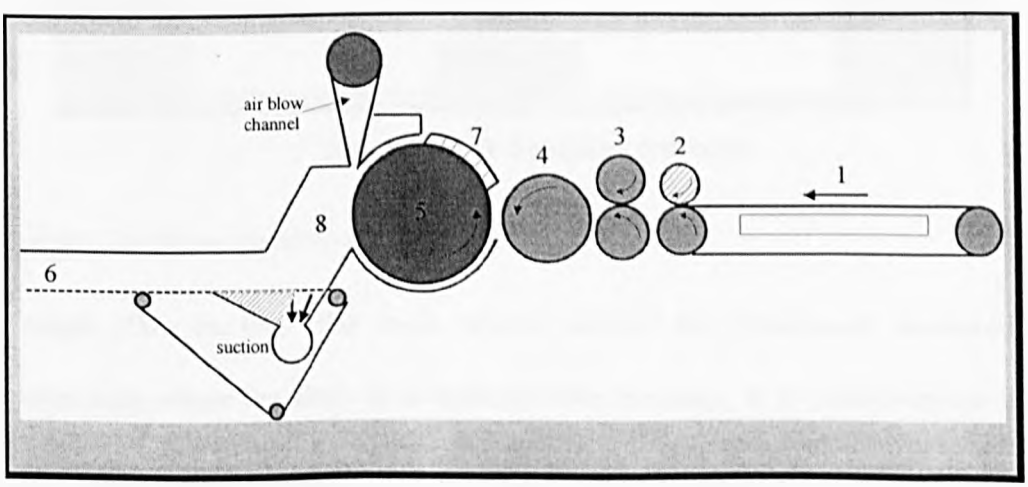

Figure(4.9) Schematic view of the modified air-laid machine

4.2.1 Fibre Breakage

Since the feeding system of the air-laid machine was reconstructed, it was necessary to investigate the fibre breakage due to the increased fibre holding power between the rollers; therefore, tests for fibre breakage were carried out.

-Sampling Method

A suitable sampling procedure for man-made staple fibres is indicated as follows. The initial sample is divided into sixteen tufts and by a process of doubling ,drawing , halving , and discarding , they are reduced to the representative sample for measurement as shown in figure(4.10).

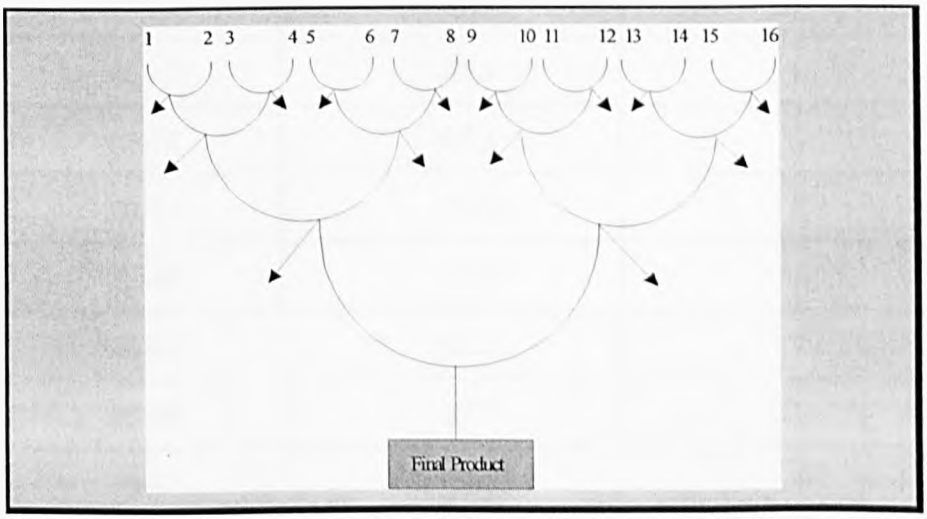

Figure (4.10) Sampling procedure

-Fibre length measurement

Single fibre method- The most reliable method for fibre-length measurement, especially where the study is to estimate fibre breakage, is to straighten the fibres from the sample , one by one, over a suitable scale and measure their lengths directly. This method was used to measure the actual fibre breakage during the process.

The results are shown in tables (4.3) and (4.4). It can be seen that the fibre length before and after the operation is the same and we can conclude that there is little or no fibre breakage during the air-laid web production.

class value	mid value	frequency
35-40	37.5	3
40-45	42.5	1
45-50	47.5	0
50-55	52.5	2
55-60	57.5	3
60-65	62.5	1
65-70	67.5	3
70-75	72.5	6
75-80	77.5	1
80-85	82.5	3
85-90	87.5	1
90-95	92.5	4
95-100	97.5	7
100-105	102.5	181
105-110	107.5	112
110-115	112.5	15
Summation		343

Table (4.3) Fibre length before process

$$\text{Mean Value} = \frac{\sum x_i f_i}{\sum f_i} = 101.7mm \qquad \text{Variance} = \frac{\sum f_i (x_i - \bar{x})^2}{\sum f_i} = 58$$

S.D.=7.62

S.E.of the mean = 0.4

class value	mid value	frequency
35-40	37.5	1
40-45	42.5	6
45-50	47.5	1
50-55	52.5	2
55-60	57.5	2
60-65	62.5	6
65-70	67.5	4
70-75	72.5	1
75-80	77.5	2
80-85	82.5	5
85-90	87.5	4
90-95	92.5	1
95-100	97.5	47
100-105	102.5	243
105-110	107.5	182
110-115	112.5	20
Summation		527

Table (4.4) Fibre length after process

$$\text{Mean Value} = \frac{\sum x_i f_i}{\sum f_i} = 101.7mm \qquad \text{Variance} = \frac{\sum f_i (x_i - \bar{x})^2}{\sum f_i} = 37.8$$

S.D.=6.15

S.E.of the mean = 0.27

Chapter Five

High Speed Photography

5.1 Introduction

We use photography in our every day life to create a permanent record of our visual experiments, and to help us share those experiences with others. In showing a photograph, we avoid the need for any tedious and ambiguous verbal description of what was seen. We usually rely on our eyes for most of the information we receive concerning our surroundings, and our brains are particularly adept at visual data processing. There is thus a scientific basis for the well-known saying that 'a picture is worth a thousand words'. However, in the study of the world around us, we have constantly been faced with the problem of events which are of short duration or move so fast that they have been unable to be observed with the naked eye.

In order to understand these fast events, a fundamental requirement is to measure, quantify and record them. The introduction of high speed photography began to offer a new and powerful means of making such measurements. Thus, high speed photography was initially developed and improved to serve primarily as a measurement tool. In modern times its use has been extended into the field of art, communication and modern films, so that advertisement or drama make much use of high speed photography in order to produce slow motion effects.

High speed photography provides two major benefits. Firstly, it enables the observation and recording of events in which the movement is normally too rapid to be followed by the naked eye. Secondly, it gives the power to manipulate time; events can be speeded up or slowed down from their natural occurrence rate when the record is reproduced.

This is a major advantage as the event can be repeatedly played back at a rate which can be followed by the naked eye, until all the information required has been obtained either by simple observation or by detailed analysis.

The aim of this chapter is to describe and introduce some of the specific technical aspects of high speed photography and also to provide general background in the subject.

5.2 High speed photography

What is high speed photography? It is the general term given to the photographic record of rapidly moving subjects, or of events too fast for the eye to follow and analyse intelligently. The eye is an extremely poor analyser of rapid movements. Events occurring at over 3 or 4 times per second, i.e. shorter than about 1/4 second, begin to blur or become unintelligible.

5.2.1 Applications of high speed photography

The uses and applications of high speed photography are extremely wide and grow steadily as exposure times become shorter, framing rates become faster and resolution and image quality improve. Some of the areas in which high speed photography is used are listed in table(5.1).

Fluid flow and combustion research
Aero and armament research
Machining and tool design
Manufacturing processes
Physical and chemical processes
Sporting and physiological studies
Behaviour and movement of animals, birds and insects
Lighting and electrical engineering research
Medical research
Astrophysics research
Accident research
Racing timing
Transport and vehicle research
Materials research
Atomic energy research
Educational studies
Advertising and entertainment

Table(5.1) List of field of application of high speed photography

5.2.2 Advantages and disadvantages of high speed photography

The first high speed photographic experiments were conducted nearly 150 years ago. Since that time light sources and cameras have developed through an amazing variety of systems, usually with the aim of providing higher and higher framing rates.

As the subjects and events selected for study have grown more exotic and tended towards shorter duration, mechanical cameras have reached their limits and electro-mechanical and purely electronic systems have evolved to cope with the extremely short exposures and high framing rates required. In fact, for some time it has been possible to proceed from image capture to hard copy printout via electronic camera and computers without the use of film at all. In addition, the steady increase in performance of video cameras and recording systems has opened up a new area of opportunity for photographers.

A comparison of the major advantages and disadvantages of film and video is given in table(5.2).

The growth in ability of electronic cameras systems does not mean that film is becoming obsolete. This is far from the case and it is likely that the two systems will proceed not as rivals but as complementary systems, each with their own special merits.

Film	Video
Advantages	
Very wide range of framing rate	Instant reply
High spatial resolution	Reusable recording medium
Colour/black and white	Direct computer interfacing
Relatively low equipment cost relative to exposure capacity	Ease of use
Well established laboratory services	Ease of multiple camera synchronisation
Storage depreciation characteristics well known	Colour/black and white
Wide range of film speed	On screen photometric adjustment and analysis
Large format	Synchronised sound
Traditional technology	Long recording times
	Low running costs
	Fast information transfer
	Relatively easy to operate
	Low environmental impact
Disadvantages	
High running costs(film and chemicals)	High capital cost
Relatively difficult to operate	Lower resolution
Short recording times	Complex maintenance
Slow processing of results	Media storage characteristics not well known
Complex maintenance for high performance cameras	Smaller format of recording element
Relatively tedious analysis	Lower range of framing rates
Slow information transfer	Lower light sensitivity range, but this is constantly improving
Logarithmic recording of intensity	
Film processing and analysis equipment	
Additional requirement to camera	
Chemical handling involved in environmental impact	

Table(5.2) The advantages and disadvantages of film and video systems for high speed photography

5.3 High speed rotating prism

The high speed rotating prism principle was first introduced in 1932 by F.J. Tuttle[Ray 1997]. He designed a system which used a two sided rotating prism located between the incoming image and a continuously moving film wheel. The prism, the rotation rate of which is synchronised with shutter and rate of film movement, moves the focused image onto the film so that they are stationary relative to each other. This gives a still image on the film, even though it moves continuously through the camera.

Figure(5.1) shows an arrangement of components using the rotating prism system. As the film moves around the sprocket wheel the image forming light for one frame, having entered through face 1 of the prism, follows the film as it passes the rear of the prism. This is followed rapidly by the next frame, supplied by the light entering from the other face of the prism. This system was used in the Eastman 3, and Fastax T cameras.

Following Tuttles's development in 1932, camera design remained largely unchanged over the next 25 years. In 1960 Shoberg developed the Hycam, a revolutionary optical relayed rotating prism camera. In this new design the rotating prism and film sprocket shared a common drive spindle (see Fig 5.2), and therefore image resolution and stability was improved. The long optical path from prime lens to film path lowered the effective aperture of the system to two stops less than the Fastax.

Less than a decade later Shoberg built the Photec camera to embody the wide aperture optics of the Tuttle system with the high quality image of the Hycam. In this camera, further redesign allowed a reduction of the number of relay prisms and lenses in the light path and regained the lost image intensity of the Hycam.

In the present work the Photec high speed rotating prism camera was used. A more detailed explanation of this camera is given in the following section.

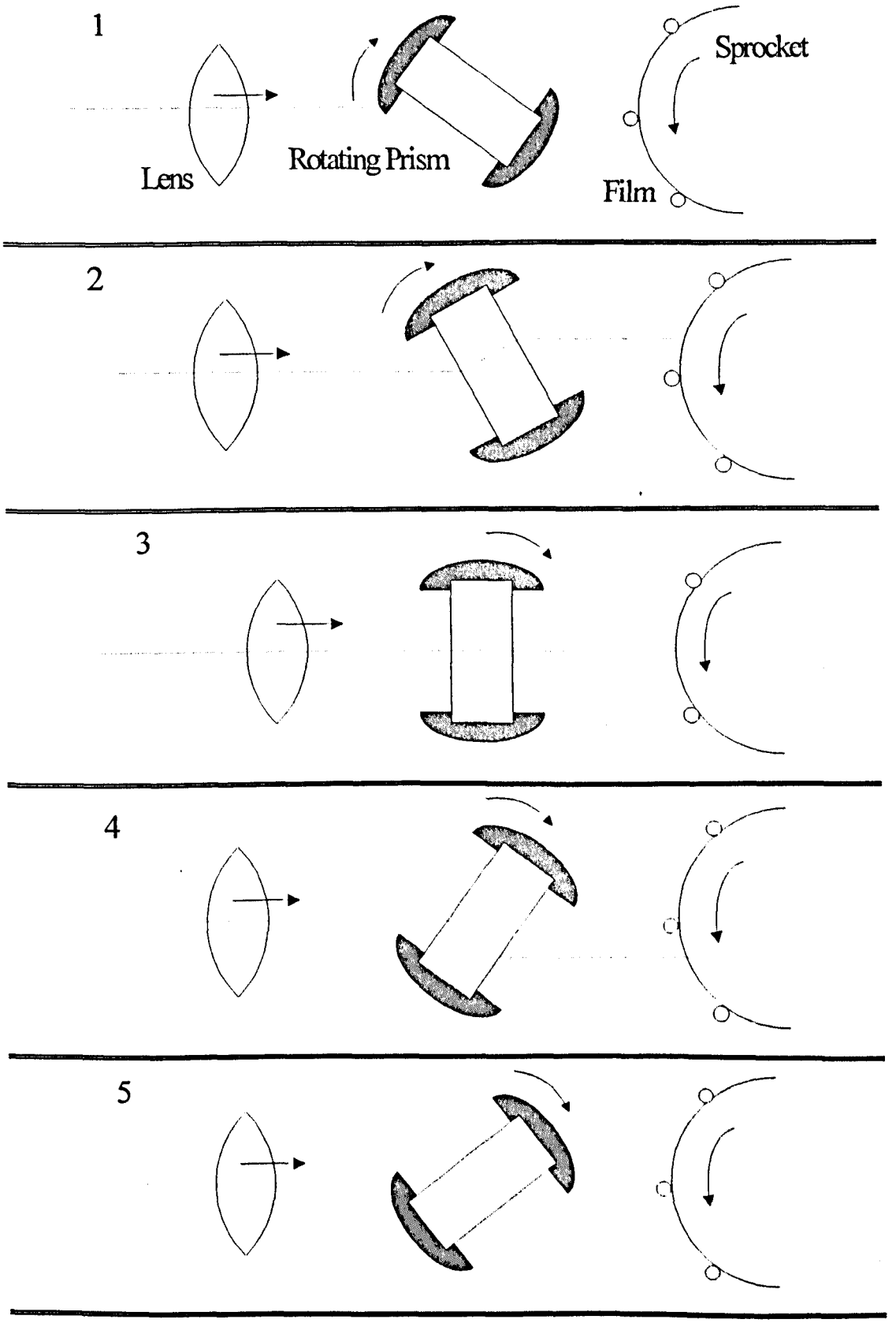

Figure(5.1) Principle of the Tuttle system using a two sided rotating prism

5.4 Photec high speed rotating prism camera

The Photec is a 16-mm rotating prism camera capable of recording up to 10000 pictures per second (PPS). In the following section the 00601-0115A Photec high speed rotating prism camera is described.

5.4.1 Camera description

The camera consists of the following main assemblies and components:

- Control panel
- Motor
- AC main circuit card assembly
- Timing light block
- Optics components
- Film path components

Control panel, The control panel is the primary operator interface for the camera system. It consists of controls, indicators, fuses, and connectors. Input connectors on the control panel are for power input, remote switch, event synch, and external timing light generator. Output connectors are for frame rate output and timing light output. Fuses protect the power input and event synch circuits.

Motor, The motor turns the take-up reel that pulls film through the camera. The motor speed is determined by the PPS thumb wheel setting. The motor is rated at 2 horsepower.

AC main circuit card assembly, The ac main circuit card assembly (CCA) contains the control and monitor circuits of the camera system, and includes one small toggle switch. The toggle switch position is used to select the correct motor acceleration and deceleration rates for ESTAR(the trademark of polyester based film) and acetate film.

Table(5.3) shows the acceleration time for two different film lengths. In this work the ILFORD HP5 400 Motion Film, an acetate film, was used; therefore the toggle switch was set for acetate film.

Picture per second	1000	2000	3000	4000	5000	6000	7000	8000	9000	10000

◆ 125 feet/38.1 meters

elapsed time (seconds)	0.5	0.6	0.7	0.8	1.0
elapsed film(meters)	1.8	3.9	6.4	9.7	15.5
ecording time(seconds)	5.2	2.8	2.1	1.7	1.5

◆ 450 feet/137.1 meters

elapsed time (seconds)	0.7	0.7	0.8	0.9	1.0	1.2	1.4	1.5	1.7	1.8
elapsed film(meters)	4.2	5.1	7.0	9.7	15.5	21.9	31.7	45.1	53.3	73.7
ecording time(seconds)	18.0	9.3	6.5	5.0	4.0	3.7	3.4	3.0	3.0	2.9

Table(5.3) Acceleration time of the film in camera system

Timing light block, Timing lights provide a visible reference mark on the developed film. This mark gives the film viewer an accurate time base. For low range, light is pulsed at 100 HZ and for high range light is pulsed at 1000 HZ with a 100 overlay.

Optics components, the optics components focus the target image onto the film and consist of:

- Rotating prism
- First prism
- Second prism
- Shuttle
- Film gate
- View finder
- Focus gate
- Aperture mask
- View prism

Figure(5.2) shows the optical path of the camera system. As shown the full frame rotating prism is mounted on the same shaft as the film sprocket. The first prism, which is a stationary glass prism, bends the image from the rotating prism at a right angle through the shutter to the second prism. The shutter size determines the exposure time. As shorter exposure time means that more action can be stopped. Exposure time can be calculated by using the formula:

$$E = \frac{1}{B \times (PPS)}$$

where E is exposure time, B is the denominator of the shutter ratio, and PPS is the number of picture per second. An example of exposure time is as follows:

$$E = \frac{1}{2.5 \times 5000} = 80 \text{ microsecond}$$

The installed shutter with the available camera has the standard shutter ratio of 1:2.5.

The second prism bends the image from the first prism at a right angle on to the film, and finally the film gate masks the focused image to the standard 16-mm format film (7.6mm H ×10.2 mm W).

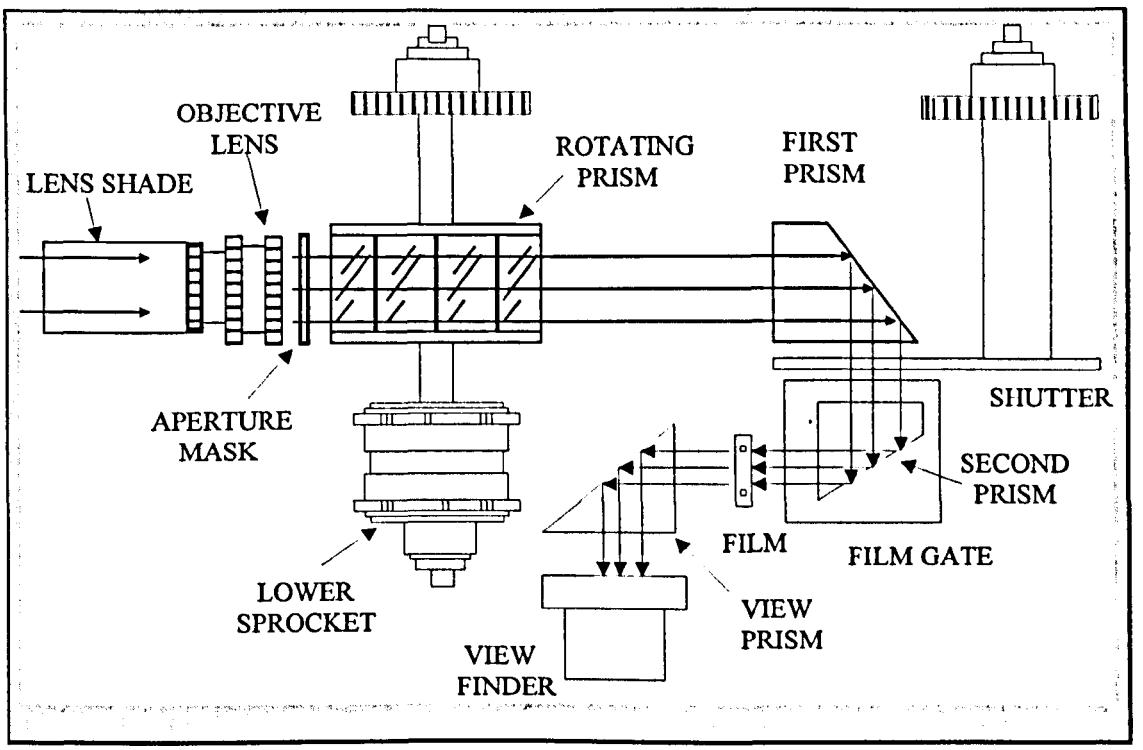

Figure(5.2) Optical path components of the Photec high speed rotating prism camera

Film path components, Film path components guide the film from the supply reel to the take-up reel while maintaining precise optical alignment. Picture quality highly depends on the smooth flow of film through the camera.

5.4.2 Lenses

Various lenses may be used on the camera system. The camera system is limited by the light transmission at the film to f2.8. No additional exposure will be seen on the film if a lens is opened beyond f2.8. Lenses must have a minimum back focal length of 65mm [Photec manual 1991].

The available lenses with the camera were the Mamyia-Sekor C 80 mm f/2.8 N and Mamyia-Sekor Zoom C 55-110 mm f/4.5 and also an Auto Extension Ring No.3-S. In most cases the 80 mm f/2.8 Mamyia lens was used.

5.4.3 Focusing comments

In order to have a proper focus the following steps must carried out [Jantzen 96]:

✷Set the lens aperture setting at the lowest setting so that the lens is wide open. A lens shade must be used to prevent lens flare.

✷Place the focusing gate in the film gate position on the second prism and make sure that the focusing gate is properly seated.

✷Rotate the sprocket until full aperture appears through the viewing prism.

✷Move the focusing tube in and out until the cross-hair reticule and ground glass are in sharp focus.

✷Place the camera at a proper distance from object. Do not rely on the lens footage scale or aerial the image focus. Always use the focus gate or focus on the film to make sure the picture is clear.

✷Frame the camera properly and focus the objective in a normal manner on the ground glass.

✷Set the f-stop for proper exposure.

✷Remove the focusing gate and return it to its storage position, and install the film gate.

5.5 Lighting for high speed photography

Photography has been described as "painting with light", and the provision of a suitable light source is a fundamental requirement for all photography. It assumes particular importance in high speed photography due to the high framing rates and short exposure times required. These in turn demand very high light intensities to achieve good exposure. Another extremely important function for lighting in high speed photography is to form a very useful alternative to mechanical or electrical shuttering of cameras. Excellent results can be obtained by using an open shutter in darkened ambient conditions and exposing the image by single or multiple short duration light flashes.

5.5.1 Type of light source

The light sources used for high speed photography are either continuous or intermittent, depending upon the application. Table (5.4) shows different light sources in decreasing order of exposure time.

Source	Typical duration(seconds)
Sunlight	Continuous
Tungsten filament lamps of various types	Continuous
Arc sources	Continuous
Flash bulbs	$0.5\text{-}5\times10^{-3}$
Electronic flash	$10^{-3}\text{-}10^{-6}$
Argon bomb	$10^{-6}\text{-}10^{-7}$
Electric spark	$10^{-6}\text{-}10^{-9}$
X-ray flash	$10^{-7}\text{-}10^{-9}$
Pulsed laser	$10^{-6}\text{-}10^{-12}$
Super radiant light sources	10^{-9}

Table(5.4) Types of lighting used for high speed photography

5.5.2 Lighting Techniques

The basic methods of lighting arrangement for high speed photography are shown in figure(5.3), which covers most possibilities.

Front lighting, The front lighting technique is the normal way of lighting and allows the photographer to record exactly what he 'sees'.

Diffused rear illumination, This is a very simple lighting technique in which the subject is silhouetted against a front-lit screen which could be a plain or a retroreflective screen. In this technique the camera is usually positioned perpendicular to the direction of the subject motion, in order to maximise the view of the shadow.

Shadowgraph technique, This is a very effective back-lighting technique and enables illumination of larger areas. Images produced with this technique are very sharp as the depth of field is unlimited, owing to the divergence of the light from a point source such as the end of a small diameter optical fibre.

If using laser light source in this technique, care needs to be taken as the amount of laser light passing through the camera lens system may be sufficient to harm the human eye. This can be overcome by viewing the subject through the camera with film in place.[Oxford Laser 1989]

Lighting with retroreflective material, Retroreflective screens reflect light within a few degrees of its original source axis and use of such material allows back lit photography over a large area. The subject is lit directly from the front and also in shadow graph mode against a retroreflective screen, and the light source is placed as near as possible to the camera viewing axis.

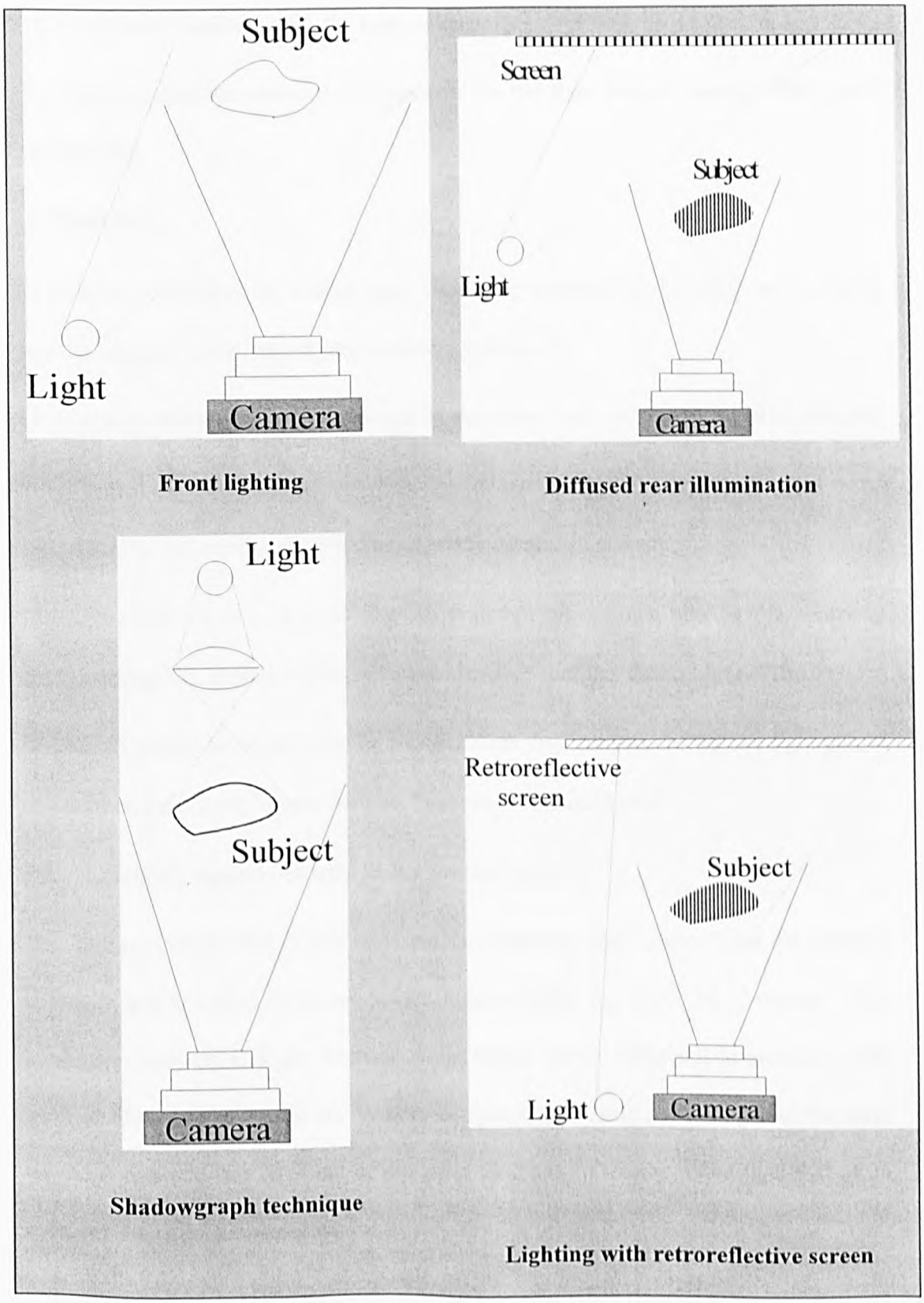

Figure(5.3) Lighting arrangement for high speed photography

5.5.3 General requirements for light sources

The following are the essential requirements for the light sources used in high speed photography.

- Portability
- Sources, or at least the output head, should be compact so that they can be easily positioned close to the subject and/or camera if required.
- It is very useful if light sources can be run from both AC mains supplies and DC current.
- Reliability and minimum maintenance needs are also important.
- Replacement of items such as filament lamps or tube, which may have a relatively short working life, should be simple and not involve complex dismantling of the device.
- Sources should be efficient in the way in which they convert energy into light output so that their local environment does not become unreasonably hot

5.6 Lighting equipment used in the present work

The lighting system used in this work was a continuous light source from the Dedotec company and is called Dedocool, which almost fulfils the above requirements. The lamps are Tungsten Halogen filament lamps which allows Dedocool to provide a high level of illumination at very low ambient temperature. Using Halogen gas in the lamp envelope improves the life time of the lamp to about 200 hours, more than that of an ordinary Tungsten filament lamp.

The lighting system consists of :

- Dedocool Transformer/Control unit
- Two Dedocool light heads, including two 24V, 250W bulbs

Figure (5.4) shows the lighting system used in the present work.

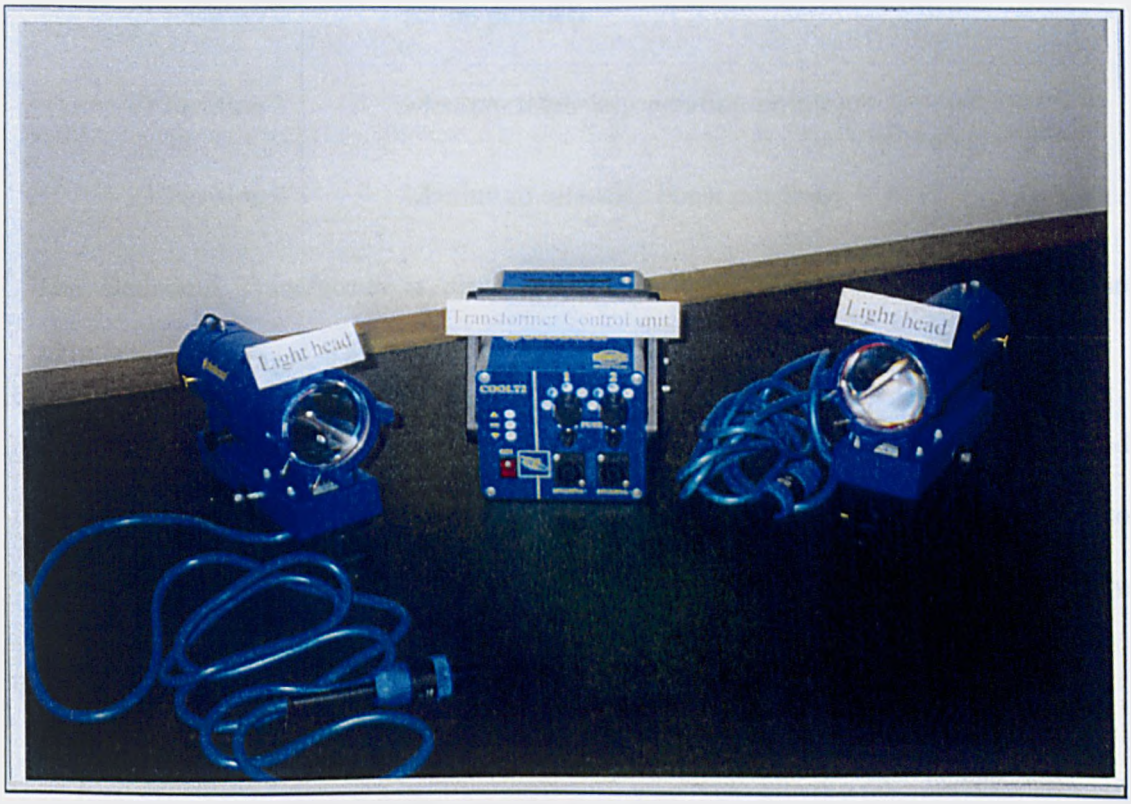

Figure (5.4) The Dedocool lighting system

Dedocool Transformer/Control unit, This unit is designed to power one or two light heads, each with a maximum lamp rating of 250 Watts. Each output may be switched independently for intensity and colour temperature in four different positions which are:

- Position 1 off
- Position 2 set-up position
- Position 3 Medium intensity(operating switch)
- Position 4 Maximum intensity(boost position)

The Dedocool Transformer is also equipped with a voltage selector to select the following six voltages; 110, 120, 130, 220, 230, 240.

Dedocool Light heads, Dedocool light heads contain two cooling fans which are located on the bottom and rear of each head. The optical system in the heads contains two carefully matched heat reflecting filters and a heat transmitting mirror which in combination with two fans, reduces the heat carried by the light beam.

5.6.1 Light intensity

The optical system of the Dedocool light system is designed to provide highly concentrated light. The maximum light intensity is reached at approximately 20 cm from the front lens. Table(5.5) illustrates the light levels which may be reached at various distances with one light head in the Boost position(i.e. position 4).

DISTANCE[1]	20 cm	30 cm	40 cm	50 cm
LUX × 10^6	2.39	1.13	0.58	0.37
FOOT-CANDLE	222,000	105,000	54,000	34,000
LIT AREA Ø	6.5 cm^2	7.0 cm^2	9.0 cm^2	12 cm^2
TEMPERATURE[2]	59°	42°	35°	31°

1) Between front lens of Dedocool and object.
2) Approximate temperature of object after prolonged exposure to light.

Table (5.5) Light intensity of the Dedocool head light

The above figures are based on ONE Dedocool light head in the boost position. Overlapping beam patterns of two Dedocool light heads will double the lux and foot-candle values [Dedocool manual 1991].

5.7 Film processing

When experimental work is being done it is necessary to check progress by developing and viewing each experimental film in order to see what is being recorded and whether alterations need to be made to the recording process or the event set-up. It is usually better to have film processed in a professional processing laboratory to get the best results, but if the equipment is readily available and the photographer is adequately skilled processing can be carried out on site.

In the present work ,because the equipment was available, the film processing was carried out in the Department.

5.7.1 Description of the film processor

The BARY 16/35 Mini processor was used to develop the exposed films. This equipment is a compact, uncomplicated table top film processor which is able to process both acetate and polyester films up to 100 metres in length. It was designed as a processor of simple robust construction, having low power consumption, requiring the minimum of maintenance but retaining the flexibility offered by both variable speed and thermostatically controlled solutions to assure high film production quality.

The processor specifications are :

Transport speed	Variable; 0 to 3 m/min.
Temperature	Variable ± 0.5°C, Ambient to 47°C
Length/Width/Height	85 cm / 31 cm / 58 cm
Weight	27 Kg
Water consumption	5 Litres/min. Maximum
Electrical requirement	240 V , 5 Amp.

The processor mainly consists of a control panel and solution compartments.

Control panel, Control panel is designed to switch functions in logical order (from 1 to 5) to prevent incorrect switch selection so that the correct control sequence take place when film is to be processed. Figure(5.5) shows the control panel with all the switches.

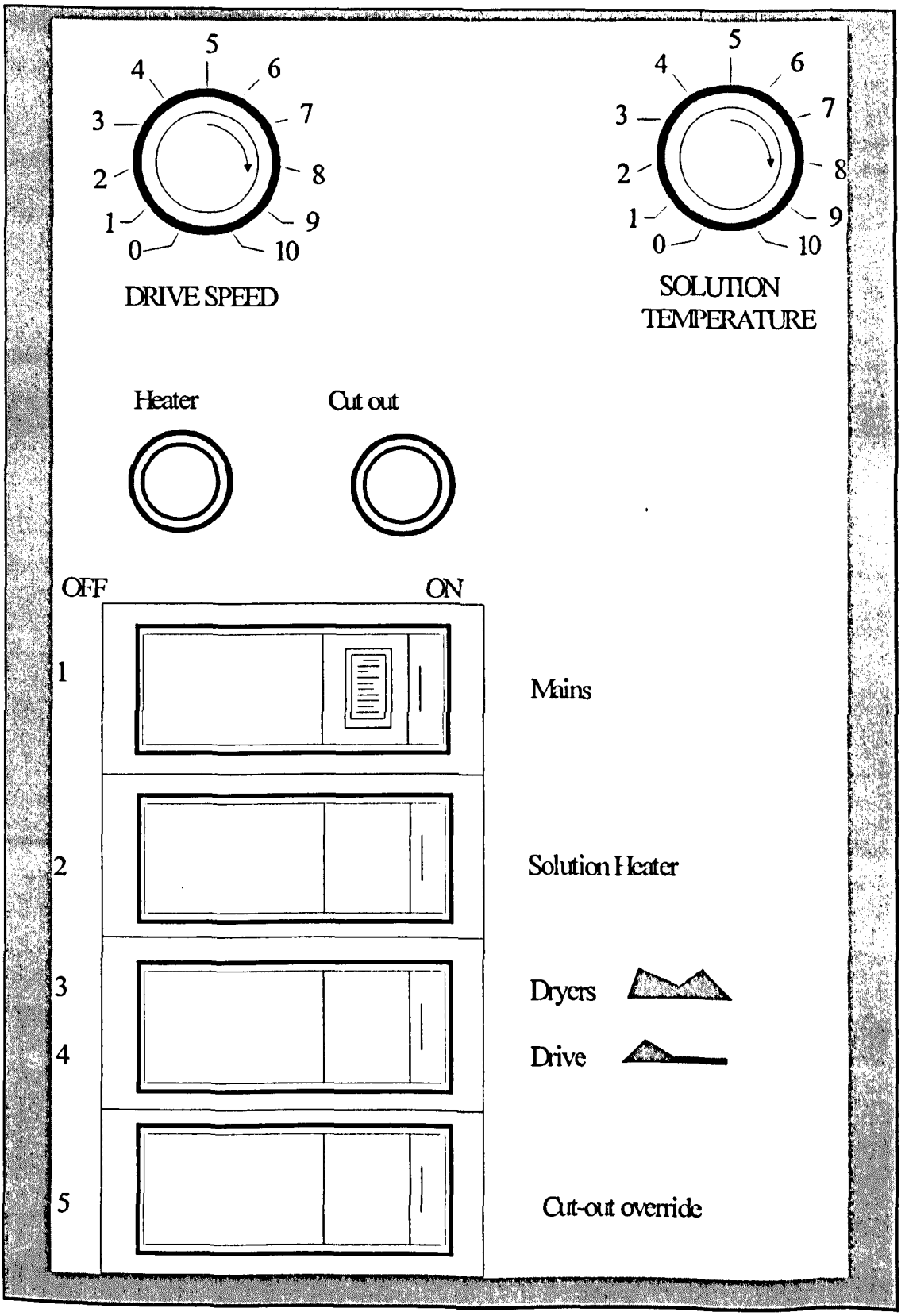

Figure(5.5) The control panel of the BRAY Table -Top Mini processor

Compartments, The compartments are (from left to right):

Tank 1	Developer	2.8 Litres
Tank 2	Fixer	2.8 Litres
Tank 3	Running rinse and spray wash	2.8 Litres
Tank 4	Running rinse/Spray wash/Sponge wipe and squeegee	1.5 Litres
Tank 5	Dry low heat high air volume	
Tank 6		

Figure(5.6) shows the tank arrangement in the BRAY Processor.

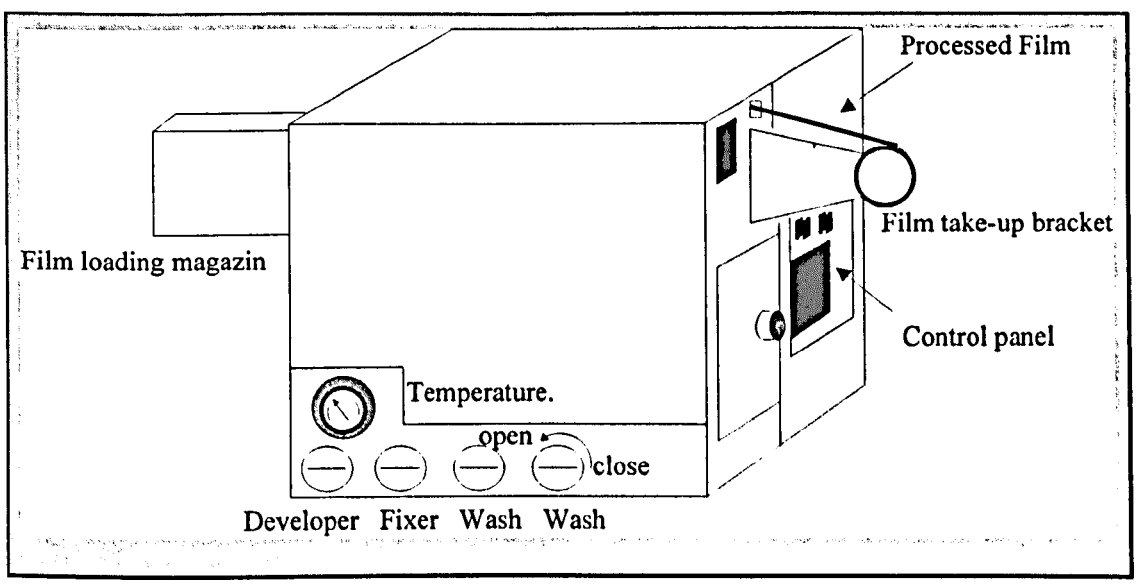

Figure(5.6) The BRAY Table -Top Mini processor

5.7.2 Instruction for filling the tanks

Experience has shown that the following solutions are suitable for processing the photographed films:

Developer	Fixer
1 part Developer	1 part Fixer
6 parts water	2 parts water

The running speed of the film was set to 3 ft/min and the temperature of the solution was kept between 28°c-30°c [Jones 1996].

ILFORD 2000 RT Machine Paper Developer and ILFORD 2000 RT Machine Paper Fixer were used.

5.8 Film analysis and data extraction

The analysis of high speed film recordings is an important part of the overall technology of high seed photography. The need for quantitative rather than qualitative analysis has led to the development of specific designs of film readers and associated software packages that are designed to reduce the time taken to obtain results.

In order to obtain accurate results from the analysis, certain actions must be taken at the image acquisition stage. An accurate time base needs to be made for calculating parameters of the moving object such as velocity, acceleration, momentum, etc. With film systems not only the camera requires time to run up to its operating speed, but also the final run speed may not be exactly as programmed due to tolerances in the camera transport and control system. Therefore, to provide accurate timing data, a timing mark must be inserted on the edge of the film at the time of exposure. Typically this consists of a light emitting diode (LED) fed from a crystal controlled time base at 100 or 1000 HZ depending on the camera speed setting, i.e. framing rate. This is used to calculate the exact framing time rate at the time of exposure.

The camera system also needs to be calibrated. This can be as simple as knowing the exact distance between two points on the object being photographed.

5.8.1 Film analysis system

A film analysis system consists of several components, including a projection head to transport the film, a screen onto which the image can be projected, a cursor for entering the data points, and a computer and software for storing and manipulating the data. The function of the projection head is to transport the film so that the various frames may be viewed either as a sequence or one frame at a time. The transport mechanism should therefore be capable of running in both continuous mode , in both the forward and reverse directions, and frame by frame mode.

The viewing screen should be of an adequate size to ensure the easy identification of the points of interest. For 16 mm film this will require a magnification of the order of 30 times the film negative size.

The data analysis software is the means by which the raw data from the film is processed into usable data.

5.8.2 The film analysis system used in the present work

The film motion analyser used in this work is Film Motion Analyser Mode 160 F, designed and manufactured by NAC, Inc.TOKYO, Japan. This high precision film analyser is specially designed to project 16 mm motion picture film onto a built-in rear screen in slow-motion or at variable speeds for qualitative/quantitative analysis of events recorded on film.

5.8.2.1 Description of the analyser

The film motion analyser consists of a projection head and a measuring case that contains the digitiser and an interface. Figure (5.7) shows a schematic view of the Film Motion Analyser.

Projection head, The projection head contains the film feed and take-up mechanism, their controls and projection optics. The optical system uses a light source consisting of a 120V, 250W Halogen lamp with a dichroic integral mirror and blower cooling. The screen brightness can be adjusted to minimise operator fatigue.

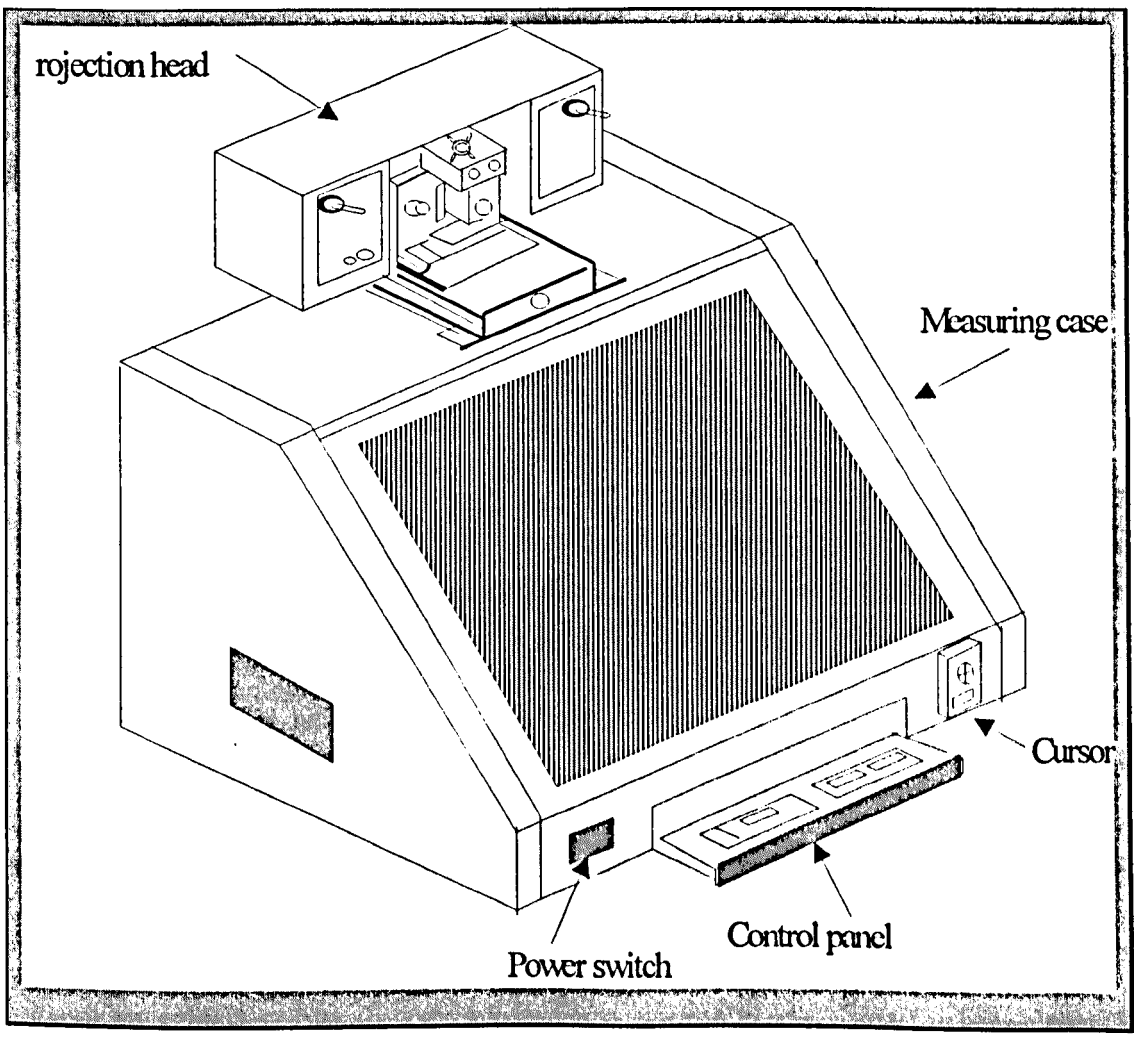

Figure (5.7) Schematic view of the film motion analyser.

Measuring case, The measuring case comprises a large surface-coated mirror, a digitiser tablet integral with rear screen, a control panel, the interface and the cursor.

The digitiser is electromagnetic and an electronic grid is built into the tablet. When the cursor is placed over a point on the screen, the corresponding X and Y co-ordinates are displayed, indicating the position of the cursor on the screen relative to the lower left corner, which is taken as the fixed origin. Pressing a button on the cursor then transfers the data in digital form to a computer.

Control panel, All the controls and indicators are placed in this panel and integrated in three sections as follows:

- *Pre-set* Pre-set of frame count; this is used when a particular film frame is to be assigned a desired number.
- *Film control* Controls for film feed direction, start/stop film advance, film feed speed.
- *Digitiser* Select cursor modes(point digitising, mode 1; digitising continues as the cursor is held pressed, mode 2; digitising starts as the cursor is pressed and continues until the cursor is pressed again)

Interface, The interface is housed in the measuring case and its connector panel is located in the lower-left corner of the rear panel. An interface PCB(either RS-232C or GP-IB) is installed in the interface so that the X and Y co-ordinates data can be sent to an external device such as a computer.

Software, The data analysis software which is used in the present work is the "NAC MOVIAS Film" version 3.0, which has been developed by NAC Incorporated. MOVIAS Film is a motion analysis software capable of producing the results of an analysis of a cine film recorded by a high speed camera such as the position, velocity,

acceleration, centre of gravity, etc. in forms of graphs or tables. The software enables the user to obtain the following parameters for each individual measuring point.

- Position Co-ordinates (location) of a measuring point
- Displacement Displacement of a measuring point
- Velocity Travelling velocity of a measuring point
- Acceleration Acceleration of a measuring point
- Force Force acting on a measuring point
- Momentum Momentum of a measuring point
- Energy Kinetic energy of a measuring point
- Length Length of a line segment passing through two or more measuring points
- Area Area enclosed by line segments passing through three or more measuring points
- Angle Angle determined by three measuring points
- Original Data Raw measuring data

5.8.2.2 Comments for analysing recorded films by photec

As explained in section (5.4.1) the timing light generator in the Photec camera has two possible operating frequencies, 100 HZ and 1000 HZ. If 100 HZ is selected the timing light simply flashes at a rate of 100 HZ, but if 1000 is selected the timing light flashes at 1000 HZ, but also has 100 HZ overlaid (so every 10 marks a double mark will be seen). This method is used so that the frequency used during the shooting of film can be identified after film processing. It implies that when the camera speed is set-up to the high rate (1000 HZ), the 100 HZ identifier must be omitted during collection of timing mark data.

The timing lights on the Photec camera are 5 frames in advance of the image. This means that when using MOVIAS software we should identify the frame from which we

wish to start analysing, reverse the film by 6 frames and forward by 1 and reset the frame counter on the analyser. The timing marks can then be entered over the range of frames to be analysed. Before any measuring points are entered the film must again be positioned at the frame from which analysing is to start (frame 5) and the frame counter reset. When positioning the film for analysis it is important always to reverse beyond the start point and then move the film forwards to the final position. This is so that the correct side of the film perforation is contacting the registration pin [Brown 1996].

5.9 Testing the camera and analyser

In order to test the camera and image analyser a simple experiment was carried out. A small DC motor holding a pulley with a disk stick on it was used (a DC motor was selected in order to maintain a constant speed during the experiment). A straight line was marked on the disk and then the disk speed was measured by a stroboscope. Knowing the disk diameter and rotational speed the surface speed of the disk could be calculated. A cine film was taken from the disk and the surface speed of the disk was determined using the image analyser. This measurement was carried out from two different section of the film, and the results are shown in table (5.6) and compared with the actual speed of the disk, determined by the stroboscope, in figure(5.8). The variation in the results might be due either to the small variation of the timing marks or the thickness of the marked line which made it difficult to input exactly the same point in each frame. It is unlikely to avoid these variation sources and because the SD is not too much we accept these variations.

Table (5.6) Velocity of the rotating disk obtained by photography

	First section of the film	Middle of the film
Average velocity (m/sec)	2.53	2.48
SD	0.242	0.139
SE	0.057	0.034
Number of measured points	18	17

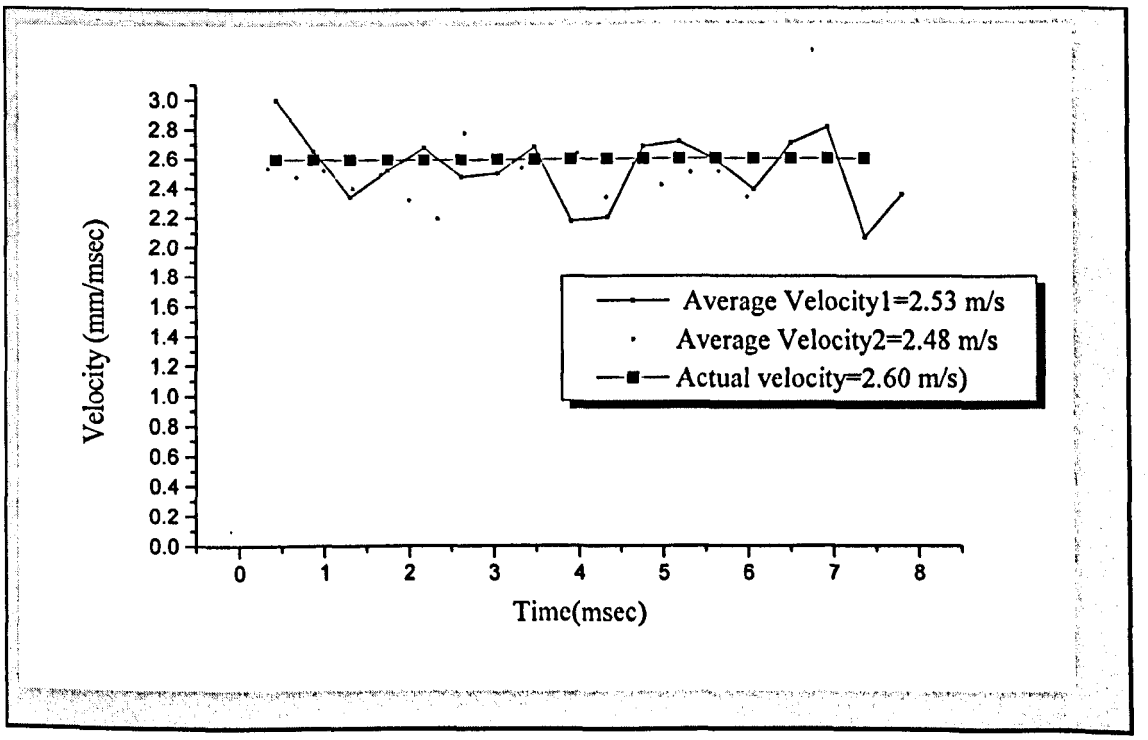

Figure(5.8) Comparison of the disk velocity obtained by filming and actual value by stroboscope

5.10 Preliminary photography

Before starting photography with the high speed camera, in order to get an idea about the fibre arrangement on the cylinder clothing and the feasibility of observing fibres on the cylinder clothing a Nikon camera with a Micro 55 mm f/2.8 lens was used and several pictures were taken. To be able to freeze the fibre motion a high speed flash (Ernert Turner Hs/5) was employed. The flash duration was claimed to be approximately 3 microseconds. The best picture (see Fig 5.9) was taken using a setting of f/2.8 and shutter speed of 125. From the picture it is revealed that the fibres tend to be near the tip of the teeth after leaving the housing and also it indicates that to enable the fibres on the teeth to be observed a very powerful micro lens is needed.

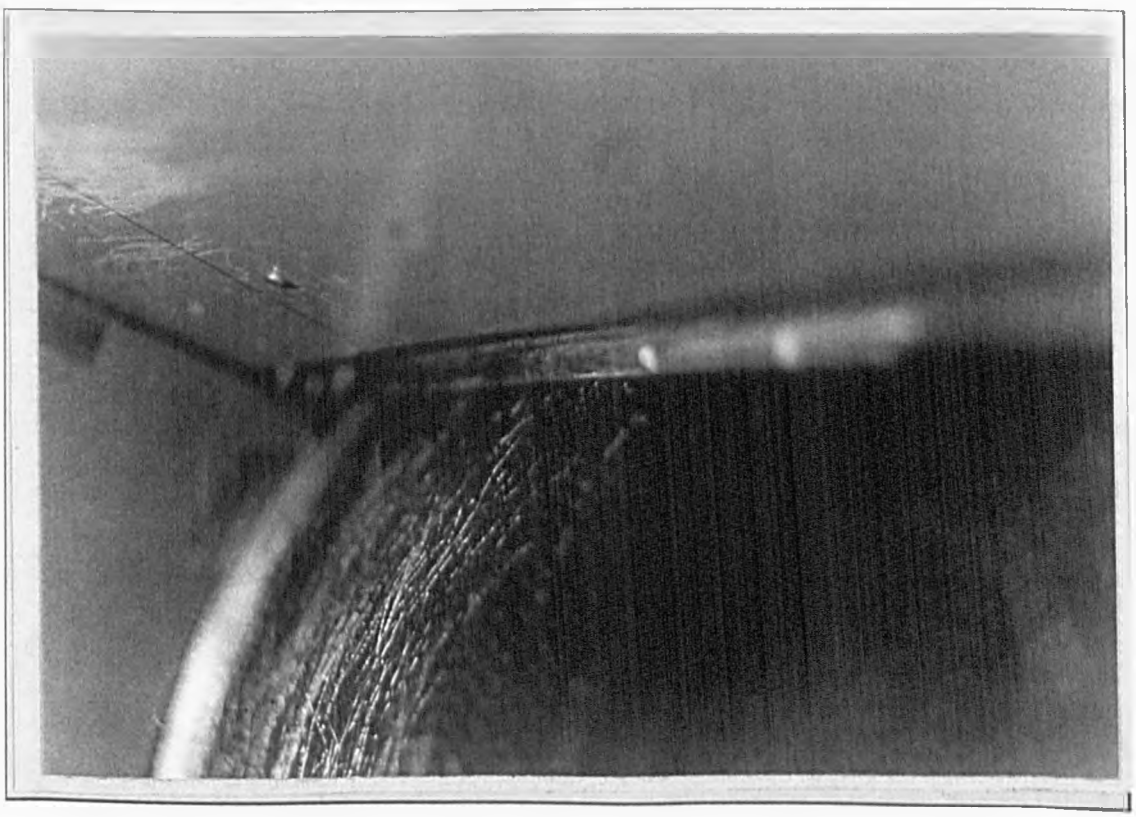

Figure(5.9) Fibre arrangement on the cylinder clothing obtained by still camera

5.11 Flow visualisation

Throughout the history of fluid dynamics there has been great interest in making flow patterns visible. There are three principal methods of flow visualisation:

- Observing changes in refractive index(Density changes)
- Adding particles or tracing elements to the flow
- Introducing energy into the flow.

In the present work the second method was used to visualise the flow details. In this method the added particles may take the form of smoke, vapours or dyes or other large solid particles. The smoke particles must be as small as possible so they closely follow the flow pattern and also large enough to scatter a sufficient amount of light so that photographs of the smoke can be obtained.

Particles with the size of 0.3-1.0 micron are suitable for flow visualisation because they are small enough to follow the flow and they scatter a sufficient amount of light to be readily seen.

5.11.1 Equipment used for flow visualisation

For the present studies, a smoke generator manufactured by NUTEM Ltd. type FVSP102 was employed. In this system of generating smoke the oil is pumped to the nip of the probe, where an electrical coil (called vaporiser) heats it to produce a dense mist.

This system is generally suitable for air flows up to 90 m/s. The recommended oil is Shell 'Ondina EL' or its equivalent because its vapour presents minimum fire and health

risks and has a tolerable odour. Ordinary paraffin oil (Kerosene) can also be used but none of these advantages can be claimed for it.

The general appearance of the smoke generator is shown in figure(5.10).

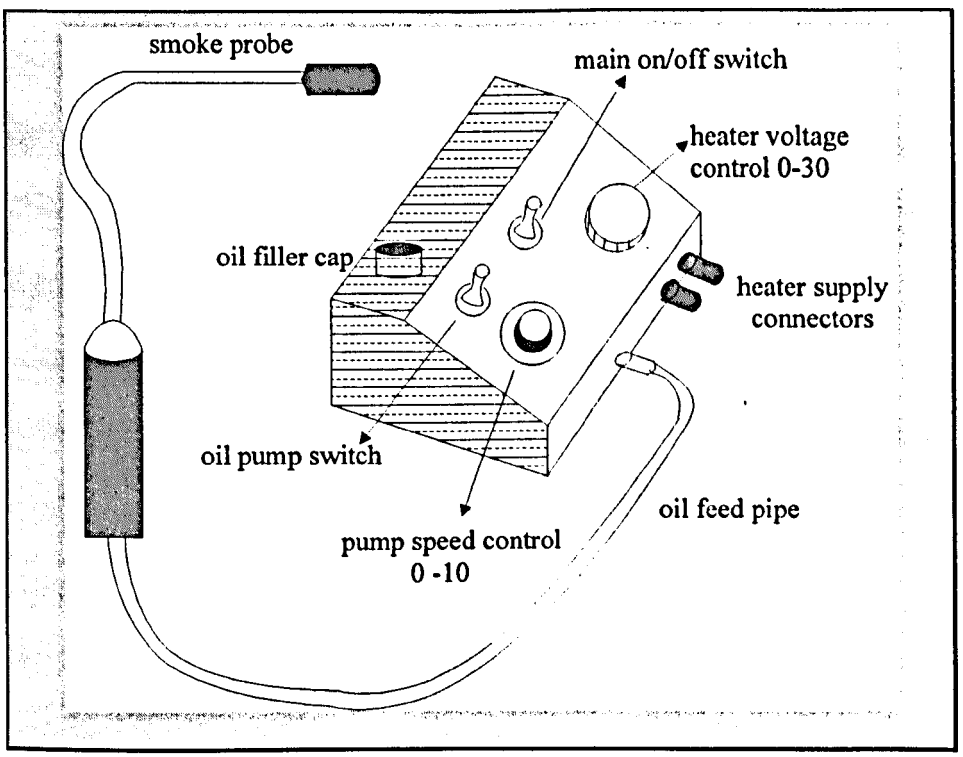

Figure(5.10) Schematic view of smoke generator

In order to be able to visualise the flow pattern using the smoke generator a small channel made of perspex was designed and installed onto the machine. The smoke was inserted sideways to this small channel (see Fig. 5.11).

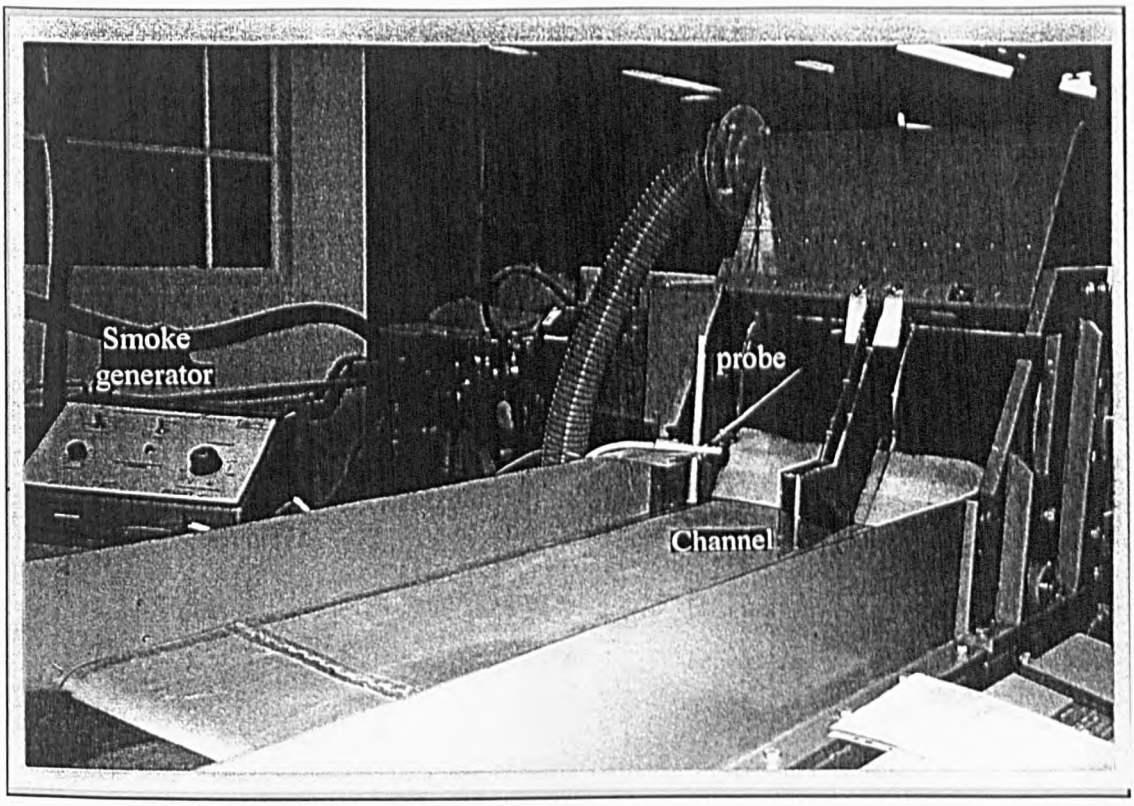

Figure(5.11) The smoke generator and the channel for visualising the flow pattern

With appropriate illumination the smoke flow patterns were recorded by a domestic camcorder (Hi 8 handycam CCDTR780E) and also some photographs were taken using a Nikon camera. The still photographs did not show the pattern of the smoke because the camera speed and flash duration were not fast enough to capture the flow patterns and also the optical contrast between the air and the smoke was not adequate to distinguish the flow patterns. It seems that two types of smoke with different colours should be used to obtain a clear smoke pattern through the photographs. Therefore in order to illustrate the flow patterns the recorded film was reviewed and the flow patterns at different machine settings were drawn. The results are shown in figures (5.12 and 5.14).

For a given air knife speed of 29 m/s the effect of suction speed was investigated at four different settings. In the absence of the suction, distinct turbulent flow extending into the landing zone, was observed and also air exiting the channel, figure (5.12a). As the suction increased the turbulent pattern of the flow became more apparent , figures

(5.12b-5.12d). Figures 5.12e and 5.12f display the flow patterns when the air knife is off and the suction speed is 100 and 250 (the numbers on the control panel of the machine). It is evident that at higher suction the flow becomes more uniform and some air is also being sucked from the ambient. Increasing the suction speed further leads to a hollow region in the vicinity of the opening roller surface and flow presents a uniform distribution all over the channel, figure 5.12g.

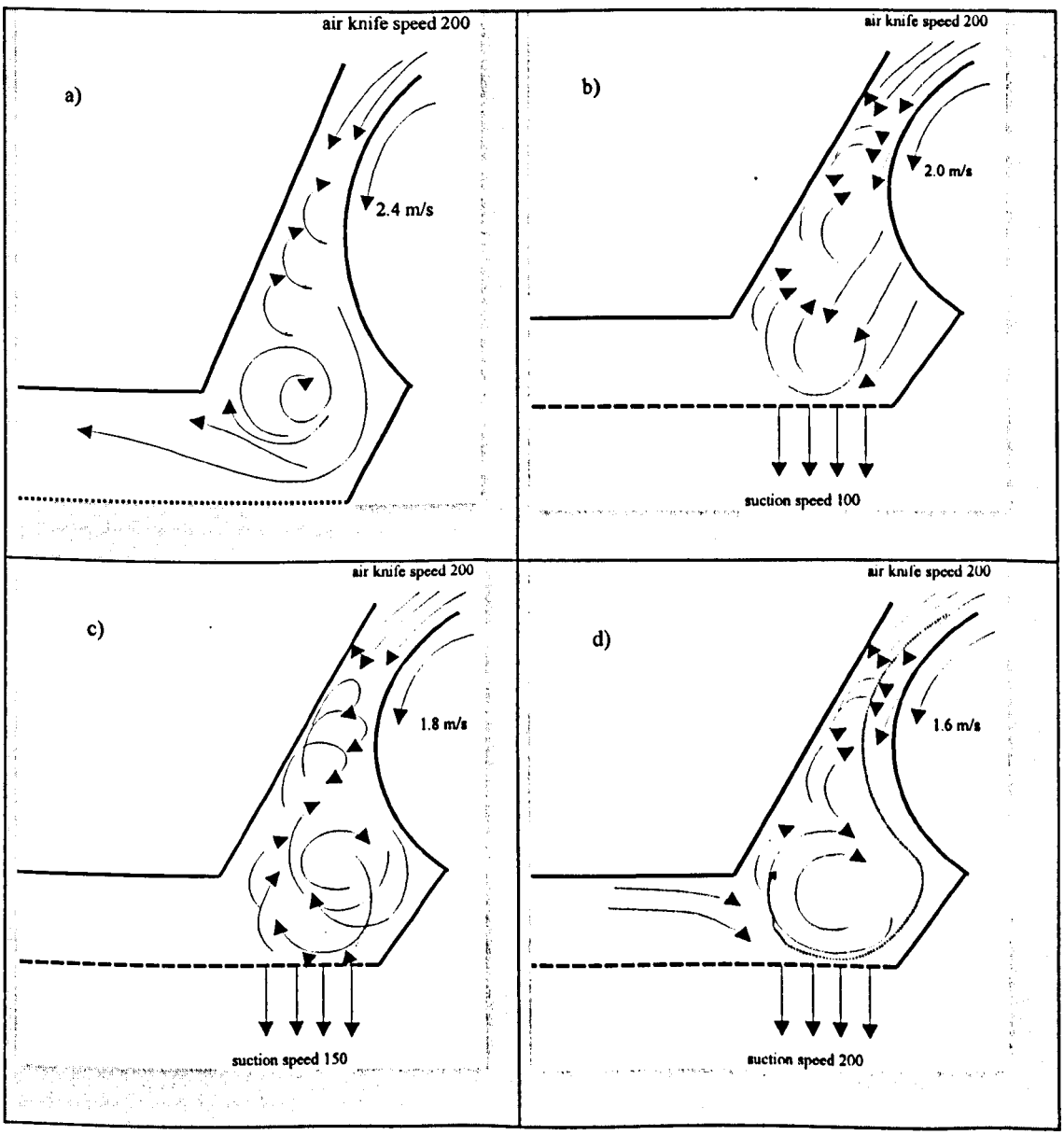

Figure (5.12a-5-12d) The results of the flow visualisation in a closed channel

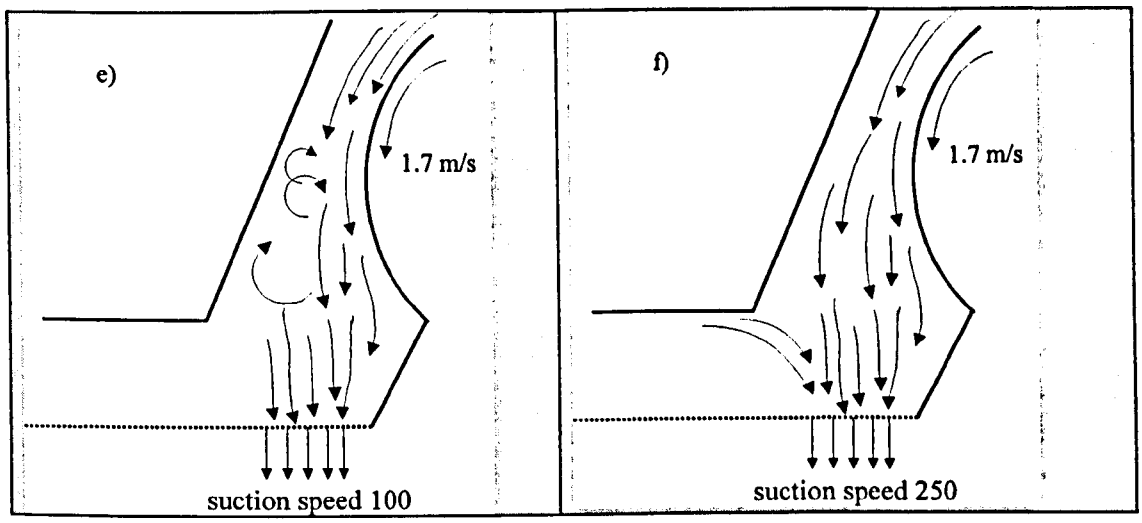

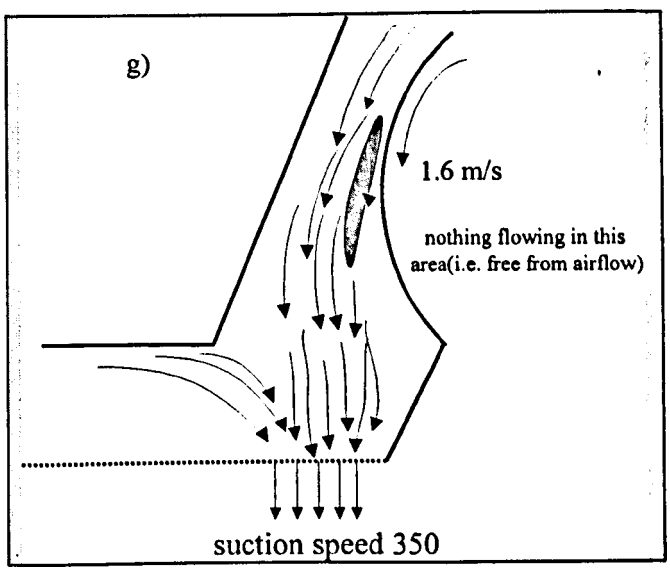

Figure (5.12e-5.12g) The results of the flow visualisation in a closed channel

The flow pattern in the open channel:

The flow pattern in an open channel was also examined. The open channel is the case where the sides of the channel were removed (see Fig. 5.13). The results are shown in figure (5.14). It is shown that in the open channel the flow pattern is much more uniform than in the closed channel. This could be the result of the elimination of the boundary effect in the stationary sides of the channel.

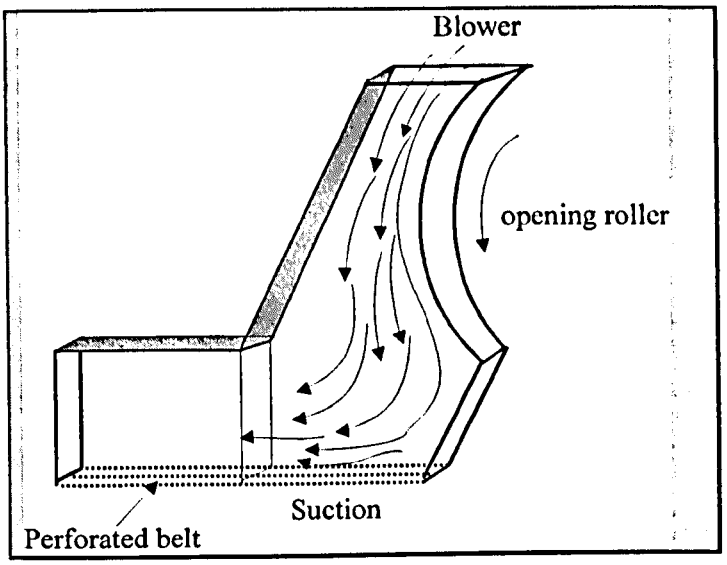

Figure (5.13) The profile of the channel used for flow visualisation

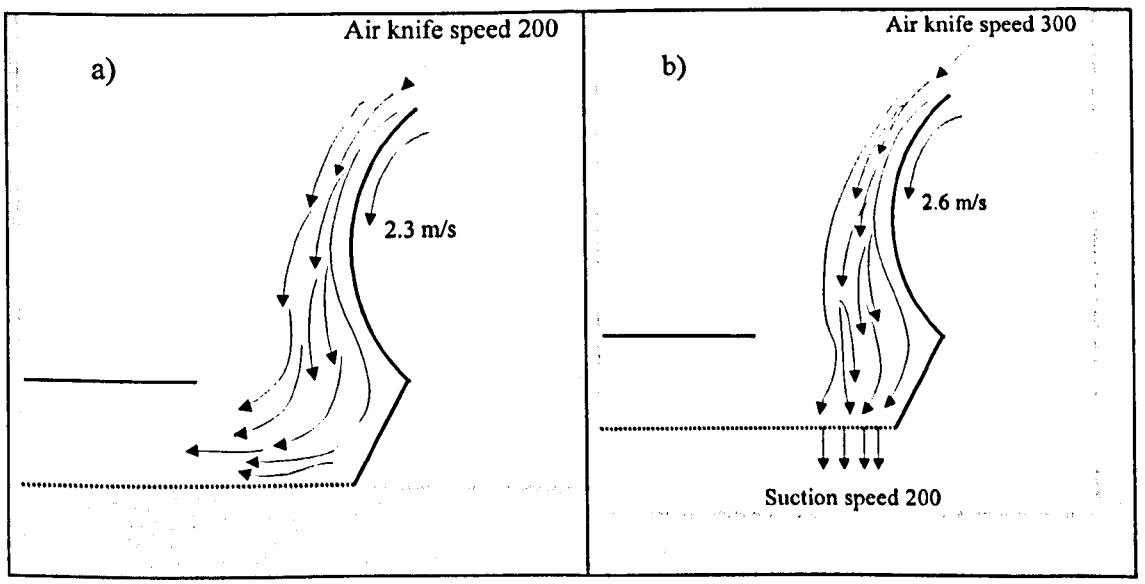

Figure (5.14) The results of the flow visualisation in an open channel

From the above visual understanding it can be concluded that the flow is very complicated for theoretical modelling and it indicates that a separate research work should be carried out to model this complex flow pattern. Since this research is aimed at investigating the fibre trajectory, the average velocity of the air was used for the calculations, therefore, there is no need to take into account the mathematical complexity of the turbulent flow in the channel and it is reasonable to assume that the air flow is uniformly distributed across the channel.

Chapter Six

Experimental and Theoretical Results

In Chapter Three, the theoretical dynamic behaviour of the fibre motion was described. This chapter is concerned with the results of the photographic tests and the comparison of these.

It is difficult to capture the fibre movement along the teeth of the clothing of the opening roller because this needs, as explained in Chapter Five, high light intensity and very powerful lens which were unavailable at time of the work. Therefore, an attempt was made to get acceptable images of the fibre motion after leaving the tooth of the opening roller clothing and to examine the fibre trajectory until fibres are about to land on the perforated screen.

6.1 Fibre selection and preliminary web formation

Generally, the main fibre types which are used in air-laid web formation are polypropylene and polyester fibres.

In the present study polypropylene fibre with the following specification was used:

Fineness	15 denier
Length	60 mm
Crimp	no crimp, almost straight
Colour	white
Finish	Antistatic finish

This particular fineness was chosen because of first, machine limitation and second, the coarser the fibre the easier they can be detected during photography.

Basically, the feed material of any air-laid machine must already be opened by a preliminary opening unit. Therefore, the selected polypropylene fibres were opened on an opener machine, and the opened fibres were then carded and cross-lapped on a laboratory carding machine. To be able to see individual fibres on the film, the amount of feed must be carefully selected. For this reason a narrow band of pre-web with 5 cm width and 50 gr./m^2 weight was fed to the air-laid machine. As a result of this feeding the fibres were transported almost individually in the transport channel, which is a desirable situation for photography.

6.2 Photographic Arrangement and Procedure

A Photec high speed cine camera with the following specification was used to photograph the fibre motion in the transport channel:

Shutter Ratio	1/2.5
Pictures per second(PPS)	3000
Lens	80 mm and f / 8
Film	16 mm, 400 ASA

The standard shutter fitted to the camera is 1/2.5 giving frame exposure of $\frac{1}{2.5 \times PPS}$ second. If the rotational speed of the opening roller (ω) is set to 110 rpm (i.e. a surface speed of 2 m/sec) the surface movement, during the exposure of a frame, of the opening roller is $(2000\ mm/sec) \times \frac{1}{2.5 \times PPS}$ millimetre. By running the camera at 3000 PPS this results in a surface movement of opening roller of 0.27 mm which can be considered as an virtually stationary situation for capturing by camera. Approximately half of the film is used to accelerate the camera to the required speed

[Oxford 1998]. The number of frames and the image size for a 16 mm film that is 30m long are as follows (see Fig. 6.1):

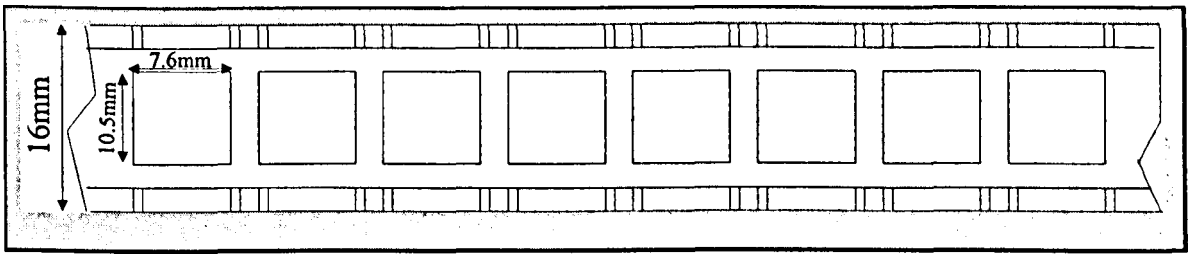

Figure (6.1) 16 mm Film Strip

Image Size : 7.6 × 10.5 mm

Number of frames : 3947

Resolution: 68 lines/mm

The distance from the camera to the object was selected so as to cover the maximum area with a sharp focus on the fibres. It was found by trial and error that the best distance is 35 cm from the object. A black scaled background was positioned in the photographed area to allow us to visualise the fibres more easily and to facilitate the calibration of the film analyser.

A large number of trials were made to photograph the fibre movement along the tooth clothing of the opening roller and in the transport channel. The following problems were encountered in taking satisfactory photographs:

a) The preliminary photography showed that observing the motion of the fibres along the teeth is virtually impossible, with the available equipment, due to the very high speed of motion of the fibres (2 m/sec) and the very short length of the teeth (0.002m). If we assume that fibres are on the middle of the teeth when they arrive in the transport region, then it approximately takes half a millisecond to travel to the tip of the tooth. Although the high speed camera is capable of capturing this very short movement, the other requirements, i.e. a close-up lens and a very powerful light

source, which is basically a pulsed laser, were not available at the time this work was carried out.

b) It is believed that fibres travel three dimensionally and to be able to capture this motion we need to have a three dimensional shot which is not possible with the Photec camera. Therefore, to visualise the fibres we need to have a relatively large depth of field which can be obtained by adjusting the aperture to a high number. Obviously, when the aperture is set to a high number the amount of light passing through the opening is reduced and it requires more illumination to get a sharp picture. This fact indicates that there should be a trade-off between the aperture opening and the light source. The Depth of field (DOF) of photography can be calculated by the following formula (De mare 1970):

$$\text{Nearest distance at which objects give sharp image} = \frac{HD \times X}{HD + X}$$

$$\text{Farthest distance at which objects give sharp image} = \frac{HD \times X}{HD - X}$$

where X is the focused distance and HD is the so called hyperfocal distance, which is the distance between the lens and the nearest object that is sharp when the camera is focused at infinity. The HD can be calculated from the formula:

$$HD = \frac{F^2}{\text{f number} \times \text{diameter of the circle of confusion}}$$

where the F is the focal length of the lens. The diameter of circle of confusion may be taken for general purposes to be F/1000.

Now if we substitute the f number, focal length (F) and X with values f/8, 80 mm and 350 mm ,then the depth of field is about 25 mm which is not sufficient to capture the whole length of fibres and only some part of the fibres which are in the focusing area can be visualised.

c) The transfer channel is too large to be photographed in one shot. Therefore the area was divided in to three different sections and high speed photography was carried out in each of these sections. Each section was about 5 cm in length.

Confronting the above problems, it was decided to take photographs from the transport channel sideways where the fibres are actually off the teeth of the opening roller and travelling through the transport channel. The photography was carried out in two different machine configurations, namely a) when the air-knife is tangential to the surface of the opening roller and b) when the air-knife hits the opening roller surface about line 4, at an angle 15° to the tangential to the surface of the opening roller at point T, see Fig 6.6.

After taking three films, to cover the whole area of the transport channel, for each machine design and processing them, the image analyser was used to analyse the resulting films.

6.3 Film Analysis

In order to analyse the films, each film which contains about 3000 frames was closely studied and the first attempt was to look for the fibres that could be traced in successive frames. It was found that it was almost impossible to capture the whole fibre length and follow a particular fibre in successive frames. This caused difficulty in measuring the positions of the fibre ends in successive frames, because the measuring points in a frame may move in such a way that they can not be recognised in the next frame.

6.3.1 Analysis of individual fibres

However, occasionally a total fibre length could be followed for several frames, and as an example two that could be traced over as many as 10 frames, are shown in figures (6.2 and 6.3). The length of the fibre which appears in each frame for the two samples is given in table (6.1). The results indicate that the fibre remains in the focusing plane over the 10 frames and this allowed measurements to be made of the position of two points along the fibre length, namely the leading and trailing ends.

Table (6.1) The fibre length as it appears in successive frames (mm)

Frame no.	1	2	3	4	5	6	7	8	9	10	Mean
Sample one	32.2	32.4	31.4	31.0	31.5	31.6	32.0	31.7	32.3	31.7	31.8
Sample two	37.2	37.7	38.0	37.8	38.0	38.0	36.9	36.6	36.4	36.0	37.3

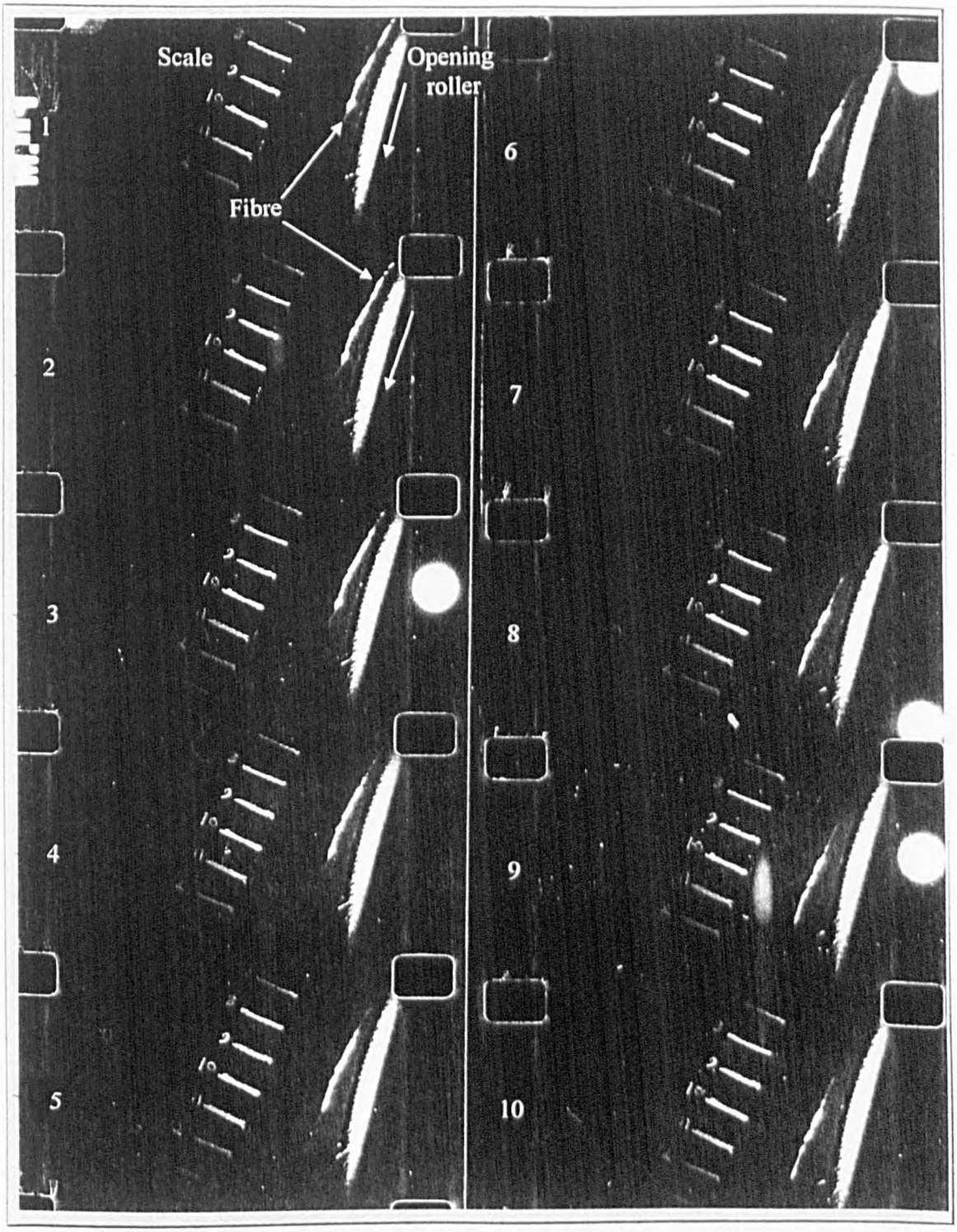

Figure(6.2) Photographs of the sequence of the fibre motion in the transport channel (sample No.1)

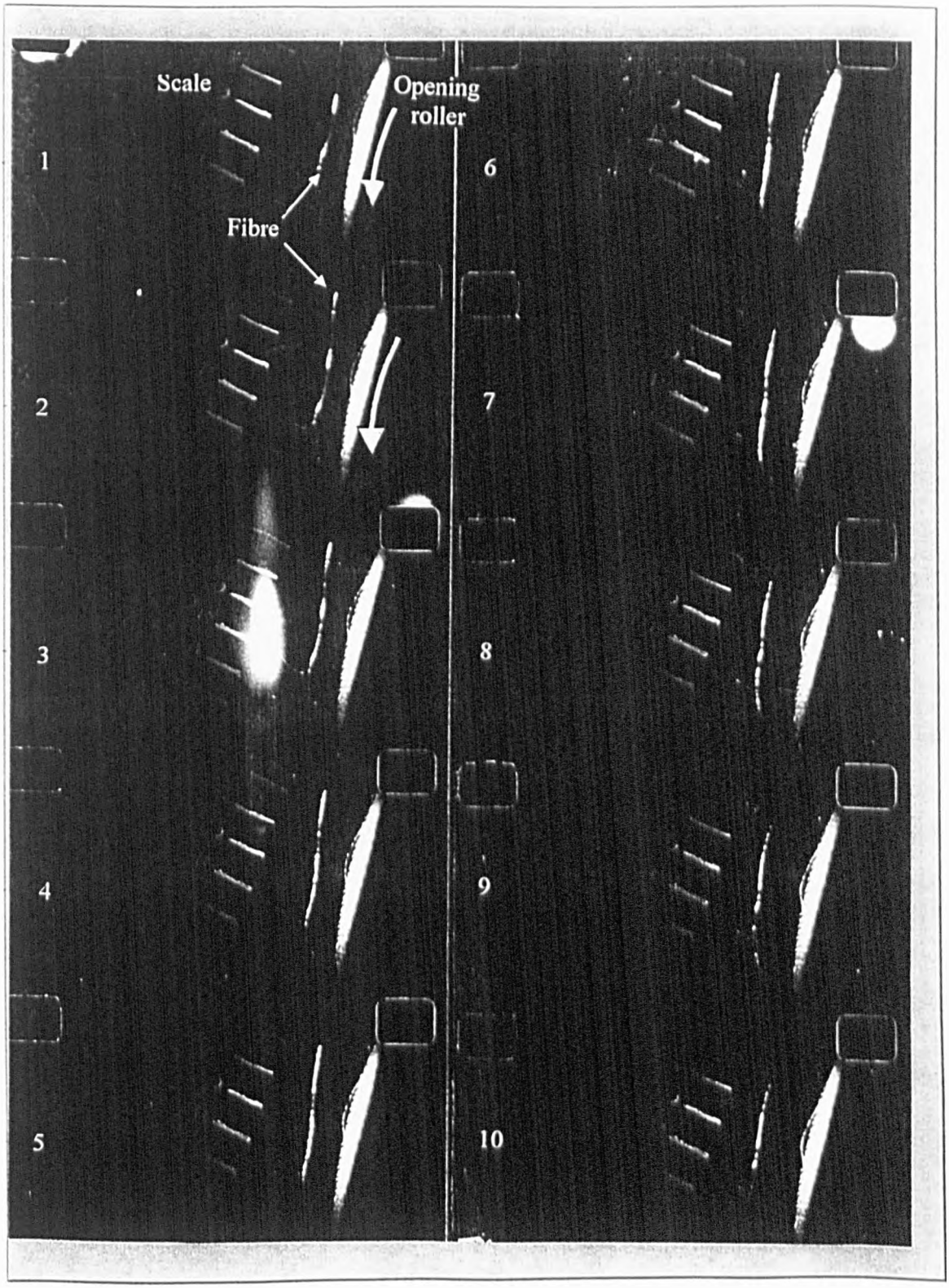

Figure(6.3) Photographs of the sequence of the fibre motion in the transport channel (sample No.2)

The results of these measurements are shown in figures (6.4 and 6.5). The axes shown in these diagrams are OX horizontal and OY vertical with origin at the centre of the opening roller, see Fig. 5. While these findings may be interesting they are too few data to yield any satisfactory conclusions about possible fibre trajectories. The experimental difficulties involved in obtaining such data are great; consequently an alternative approach was devised.

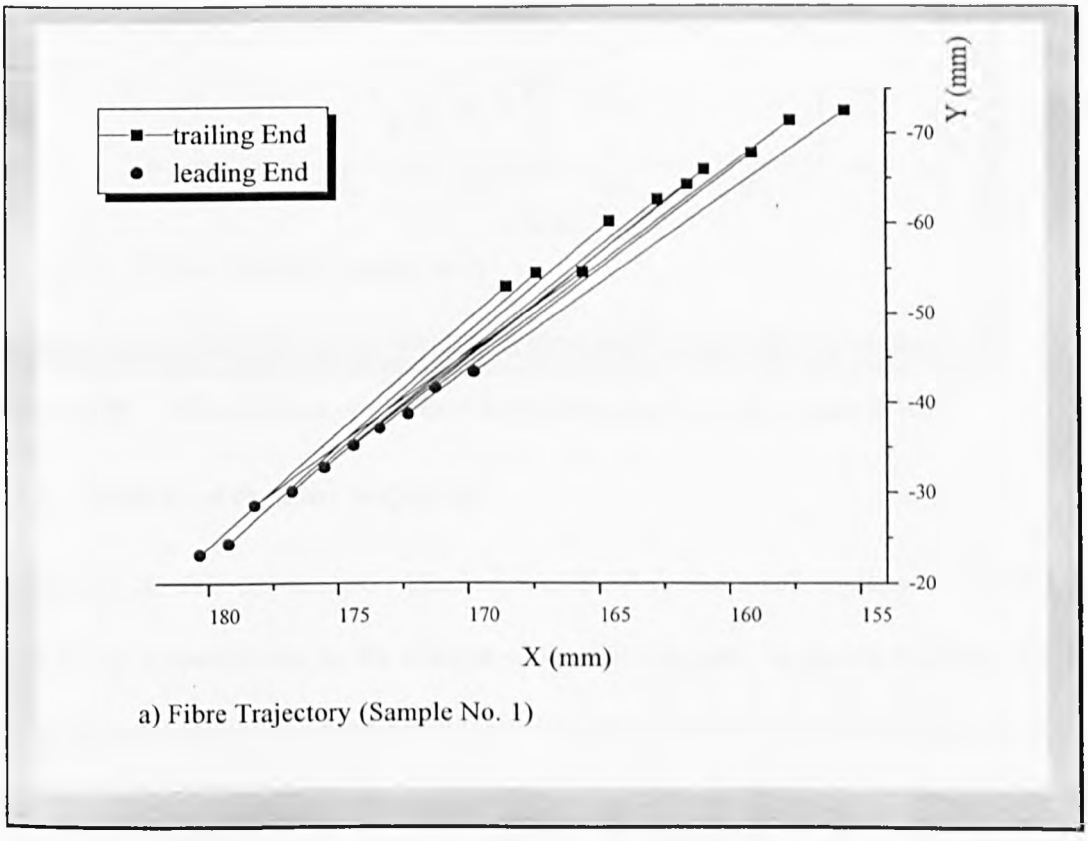

Figure (6.4) Fibre trajectory obtained from photographed fibre (sample No.1)

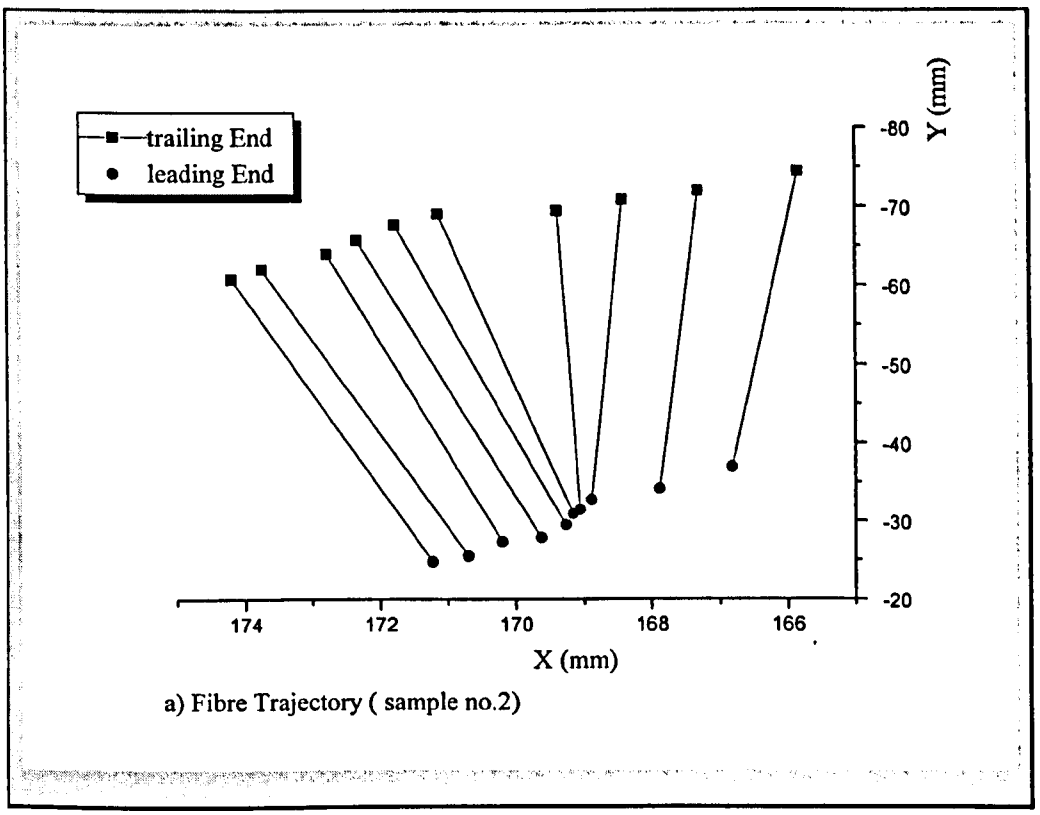

Figure(6.5) Fibre trajectory obtained from photographed fibre (sample No.2)

6.3.2 Analysis of the fibre trajectory

In order to do this the transport channel was divided into small regions by parallel lines drawn perpendicular to the straight edge of the channel, as shown in figure 6.6. The points at which fibres intersected these lines were noted and distances such as da, db, dc in figure 6.6, line 1 were measured and then the average of these distances for each line was taken as being representative of fibre motion in that particular region of the channel. This measurement was carried out for 500 frames in each film. This method of analysis enabled us to have an understanding about the average motion of the fibres throughout the transport channel.

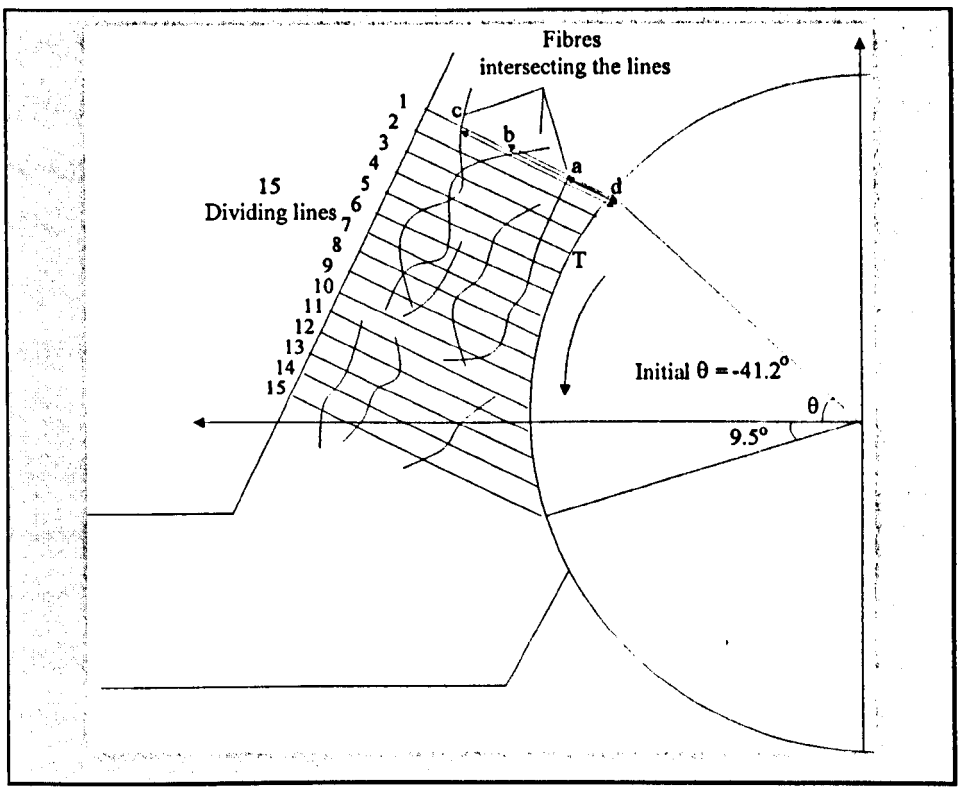

Figure 6.6 Schematic explanation of the fibre analysis method of measuring fibre motion through the transport channel

The distributions of these "intersection distances" (for the case of air-knife tangential to the opening roller surface) for each line are shown in figures 6.7a to 6.7d. It is apparent that at the early sections (1-7) the distributions are positively skewed, while those at later sections (12-15) are negatively skewed with relatively symmetrical distributions being exhibited at the central sections(8-11). This , of course, reflects the fact that fibres tend initially to move close to the opening roller surface and as time goes by they tend to move away from the opening roller.

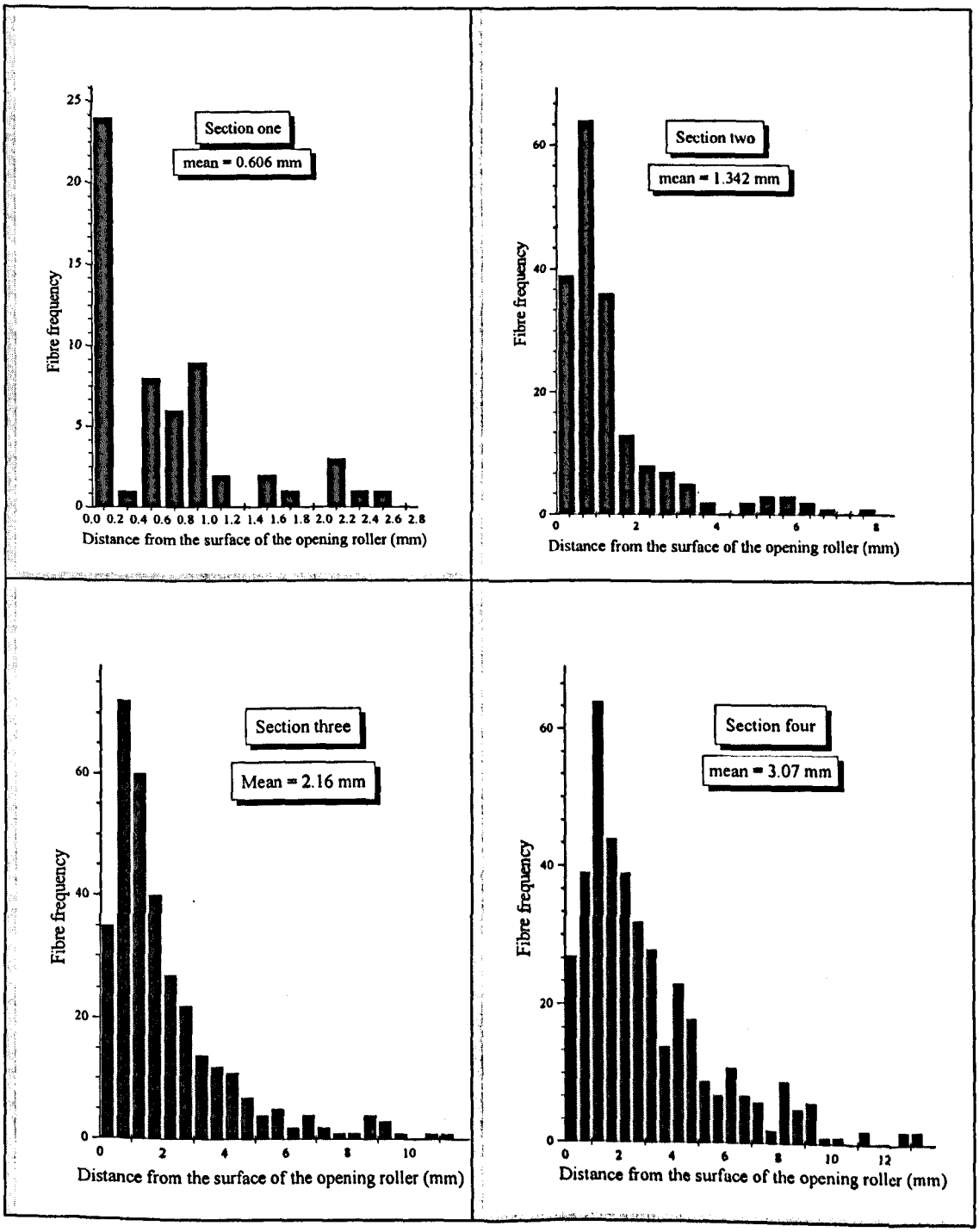

Figure. 6.7a Distribution diagrams for the fibre "intersection distances" from the opening roller (mm): sections 1, 2, 3 and 4

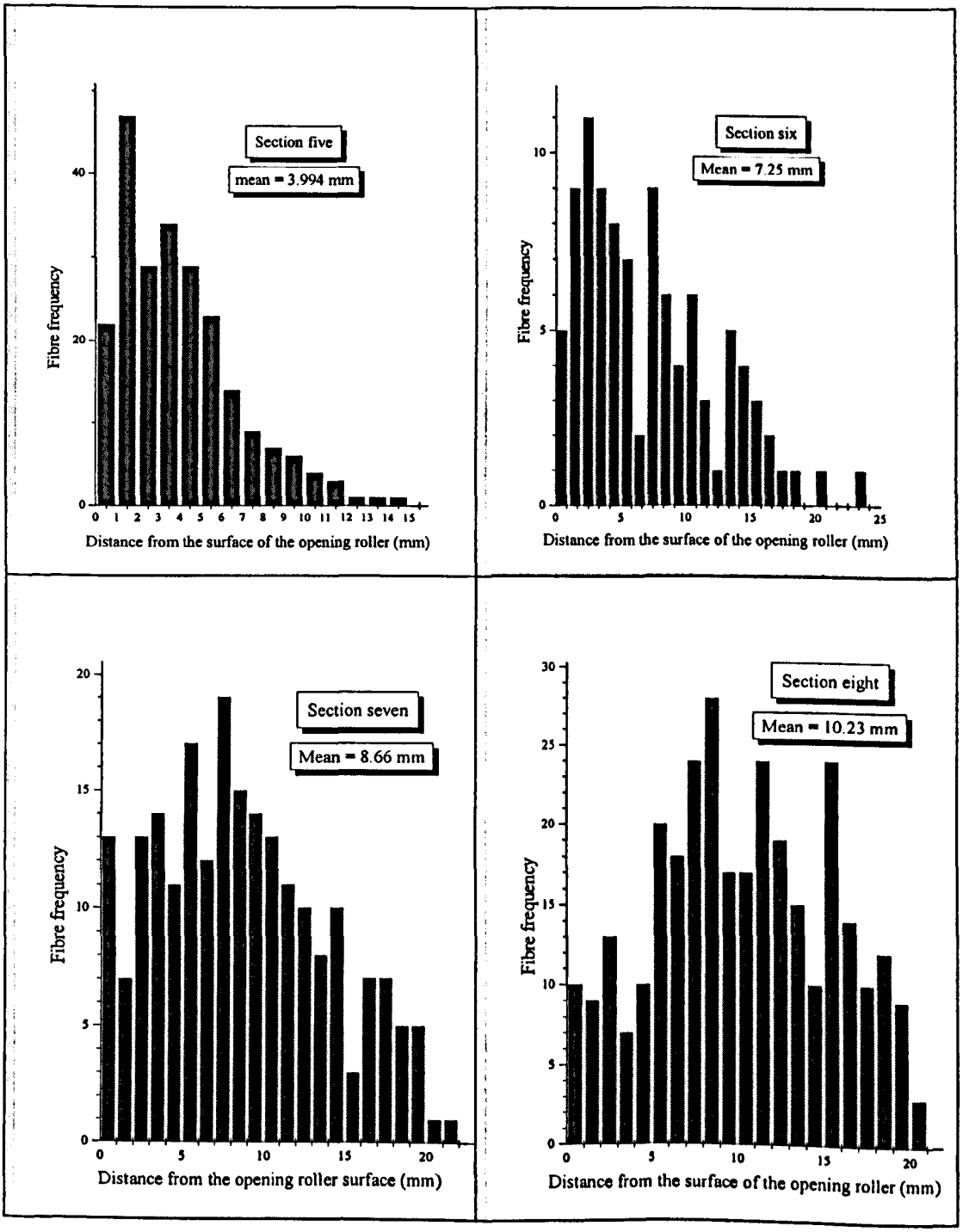

Figure 6.7b Distribution diagrams for the fibre "intersection distances" from the opening roller (mm): sections 5, 6, 7 and 8

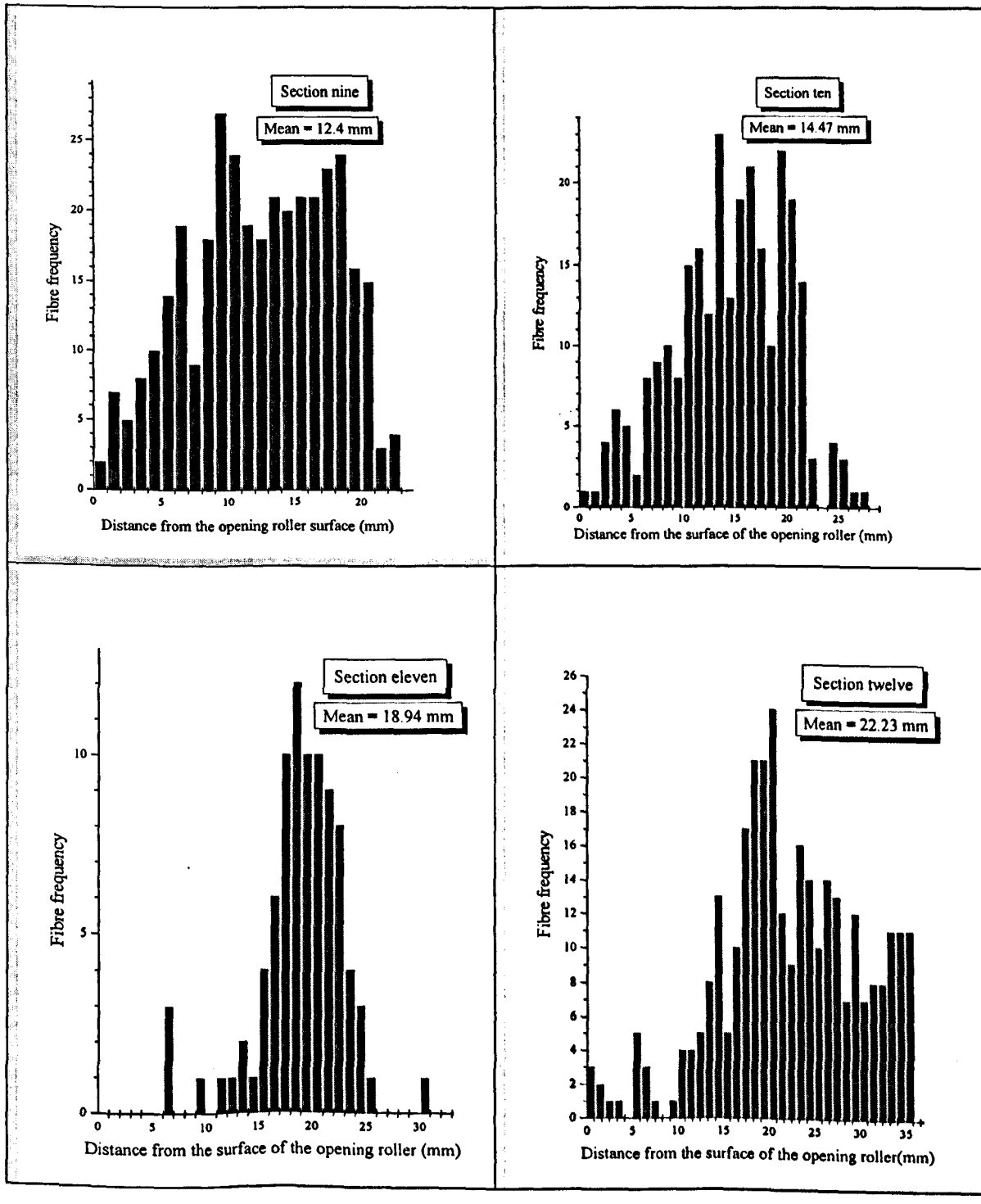

Figure 6.7c Distribution diagrams for the fibre "intersection distances" from the opening roller (mm): sections 9, 10, 11 and 12

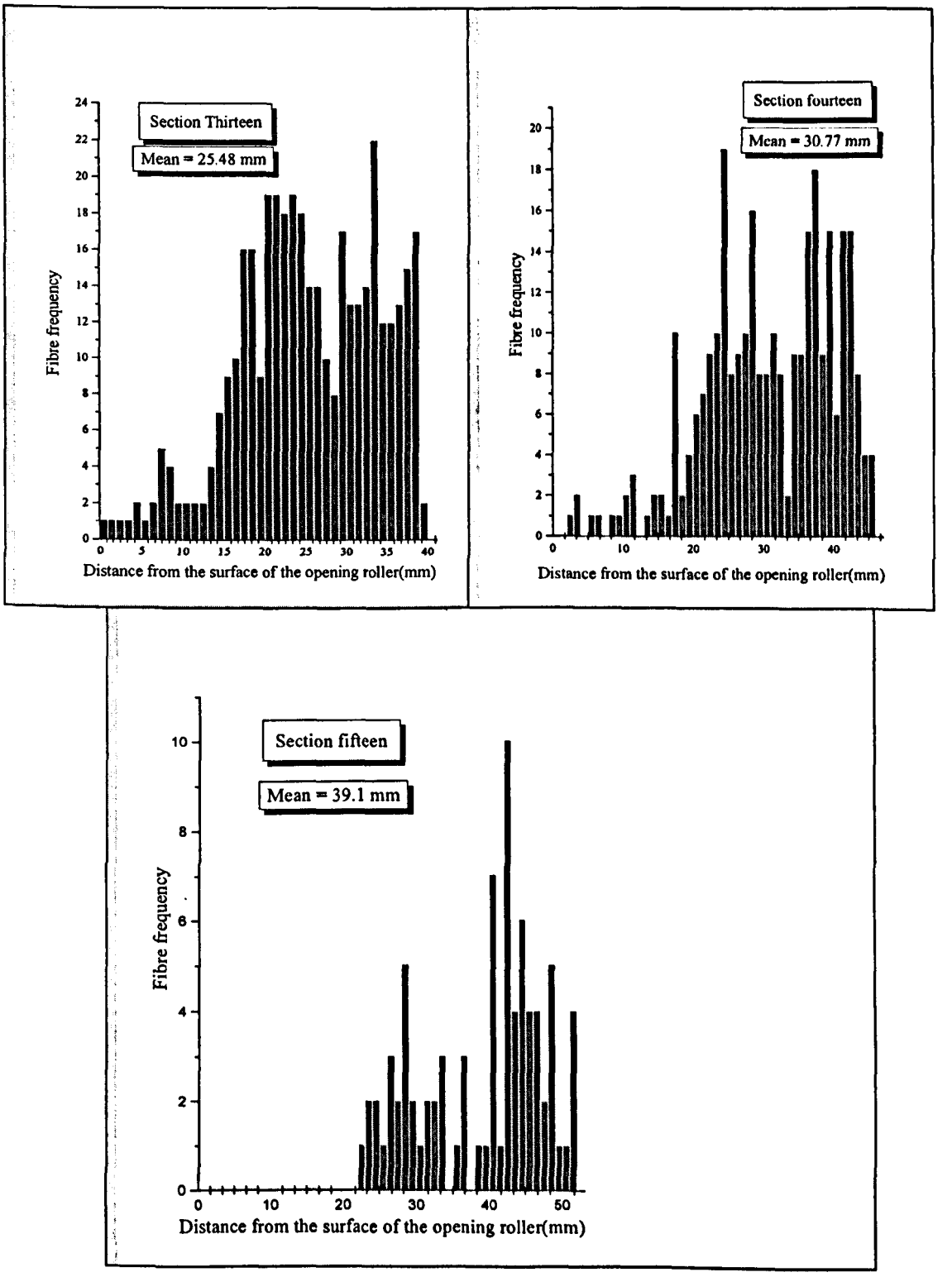

Figure 6.7d distribution diagrams for the fibre "intersection distances" from the opening roller (mm) sections 13, 14, 15

Using these distributions an "average" trajectory can be deduced, and this is shown in figure 6.8.

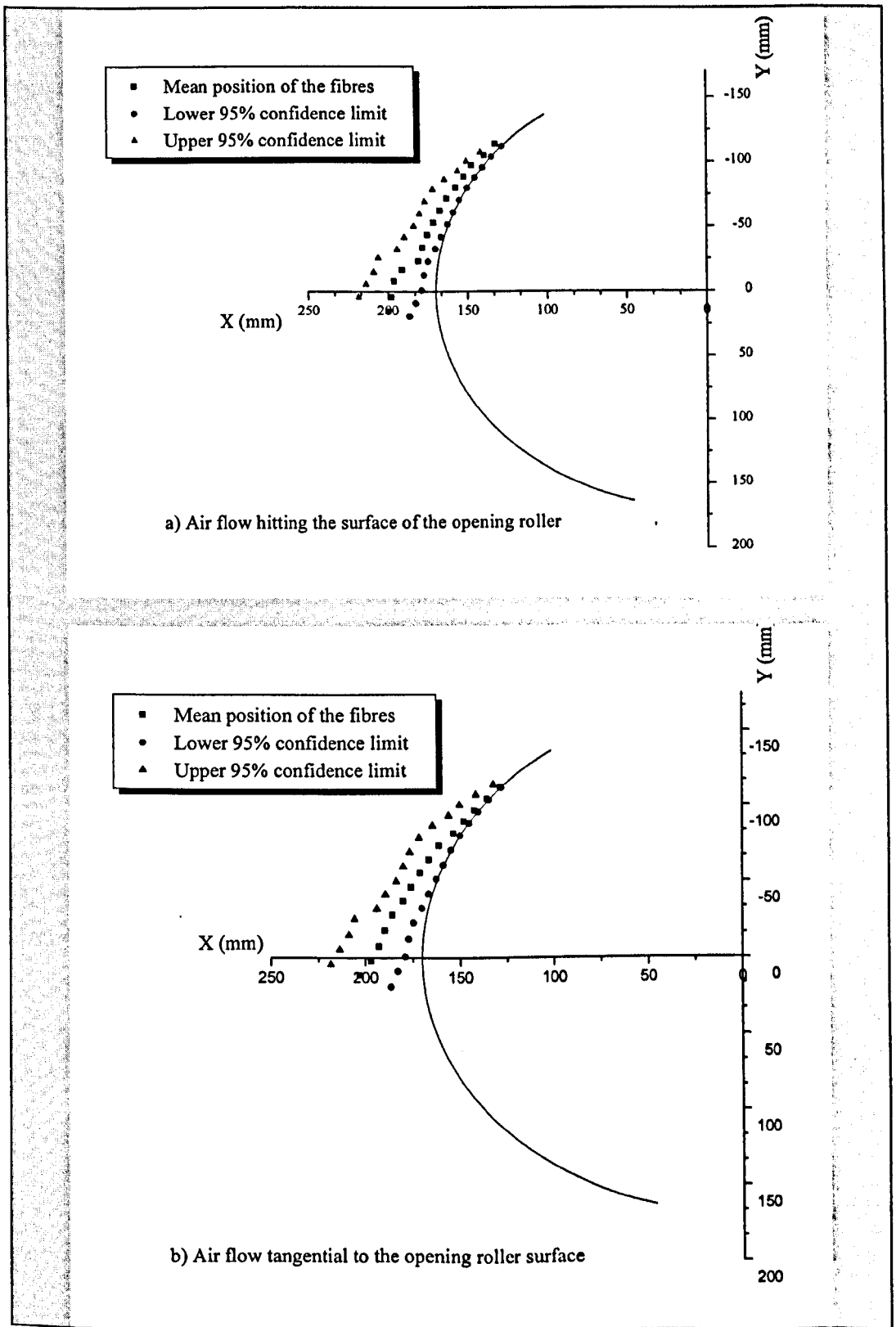

Figure 6.8 Fibre trajectory in the transport channel based on experimental data: a) Air flow hitting the opening roller surface b) Air flow tangential to the opening roller surface

When the air flow is tangential to the opening roller the mean trajectory is smooth, with no discontinuities. However, when the air flow hits the opening roller surface at an angle 15° to the tangential to the surface of the opening roller this is reflected in a change in direction of the path, i.e. in a discontinuity when the angle θ is about -7 degrees, i.e. at about line 11 in figure 5. The fact that the method of analysis can distinguishes the two cases suggests that the approach is a reasonable one.

The distributions can also be used to calculate approximate 95% confidence limits for the trajectories, i.e. limits within which the vast majority of the individual fibre trajectories can be expected to lie. This was done for each distribution corresponding to a given position, a typical example is shown in figure.6.9.

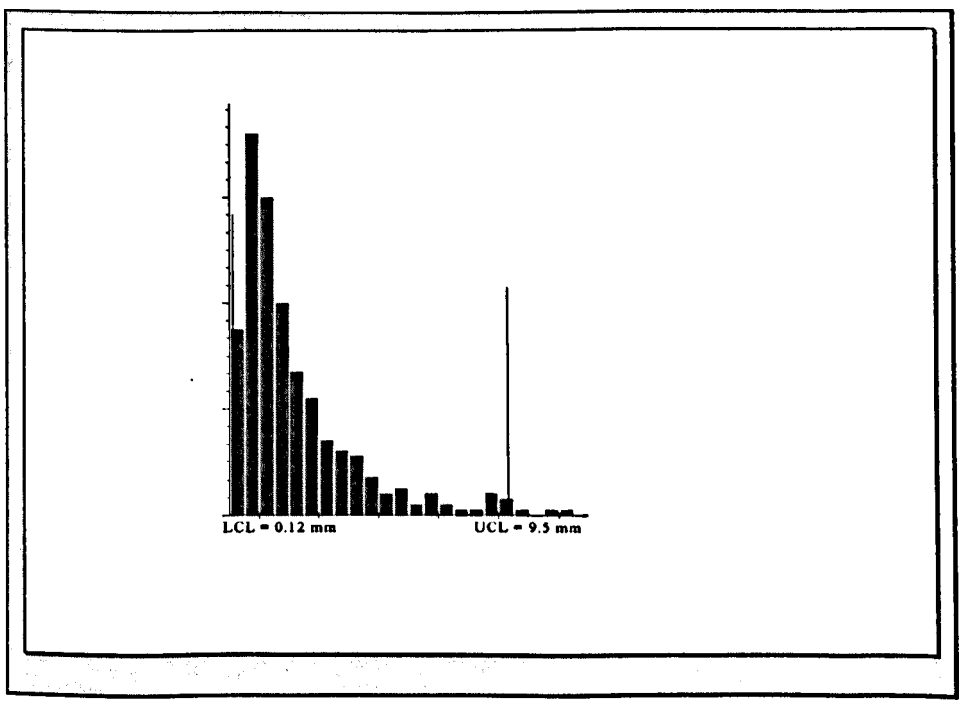

Figure 6.9 Typical distribution used to obtain 95% confidence limit

The 95% confidence limits are marked on this diagram, and are such that 2.5% of the intersection distances are smaller than that the lower confidence limit (LCL), while 2.5% are greater than that the upper confidence limit (UCL). The limits calculated in

this way are shown in figure 6.8, and define a band within which most fibre trajectories are expected to lie.

6.4 Theoretical Results

As explained in Chapter Three, a theoretical model was developed to describe the motion of fibres in the transport channel of the air-laid machine. This model enables us to predict the behaviour of fibre motion for different machine designs, machine parameters and fibre types. In order to solve the equations of fibre motion a series of programs was written in FORTRAN 77 (see Appendix). The programs consist of three main sections which may be summarised as follows:

- Data file reading
- Subroutine FCN
- Subroutine out-put

The data file contains:

- **Machine design parameters** ; opening roller radius (R), length of tooth (L_p), working angle of the card clothing (γ), angle of blower relative to the opening roller surface (β), inlet diameter of the blower (DI), the width of the channel (L_0),
- **Machine parameters** ; velocity of blower (VI), angular velocity of the opening roller (ω),
- **Fibre specifications** ; fibre fineness (dtex) and fibre length (L_f), coefficient of friction between the teeth and the fibres (μ),
- **Initial values** for r, $\dot{r}$, ϕ, $\dot{\phi}$, the position on the tooth where the fibre is placed immediately after entering the transport channel, the initial translational speed of the

fibre, the initial angle between the fibre and the tooth, and the initial rotational speed of the fibre.

An example of the data file which was used is given in table (6.1).

Table (6.2) An Example of the content of data file used to solve the fibre motion equations

Data file content	nag1.data
starting value of time (s)	0.0
final value of time (s)	3.0D-02
length of tooth (mm)	2.0
radius of the opening roller (mm)	170.0
omega (angular velocity of the opening roller rad/s)	11.52
gamma (working angle degrees)	82.0
decitex (fibre fineness)	15
coeff of friction (μ)	0.25
L_f (fibre length mm)	15
PN (pure number - no dimensions)	2.646D-05
PT (pure number - no dimensions)	2.646D-06
theta 0 (degrees)	-45.0
VI (m/s) velocity of blower	25.0
BETA (degrees) direction of blower	65.0
L_0 (narrowest channel width in m)	118.138D-03
DI (inlet width of the blower in m)	0.002

In the FCN subroutine the Nag Library Routine DO2CJF was used to solve the differential equations of fibre motion. This subroutine first computes the fibre velocities V_A, V_B, V_T (normal and tangential to the fibre length respectively). Then these velocities are used to calculate the air resistance terms A_n and A_t, in order to compute these terms the effect of air flow needs to be accounted for. Therefore another subroutine was written to predict the air flow pattern in the system.

Subsequently, four simultaneous equations were solved for F, N, $\ddot{r}$, $\ddot{\phi}$ in the form of a matrix, see section 3.5

In the out-put part of the programme the following information can be obtained:

T ; the travelling time of the fibres.

θ ; the angle between a radius drawn on the drum and the horizontal. θ changes with time as the drum rotates

r ; in the case of motion of the fibres on the tooth, the distance of the fibre contact from the root of the tooth.

$\dot{r}$; in the case of motion of the fibres on the tooth, the translational speed of the fibres.

ϕ ; in the case of motion of the fibres on the tooth, the angle between the fibre and the tooth.

$\dot{\phi}$; in the case of motion of the fibres on the tooth, the rotational speed of the fibre.

X_A, Y_A, X_B, Y_B, X_G, Y_G; co-ordinates of the two ends and centre of gravity of the fibre.

F and N ; the frictional and normal forces acting upon the fibres.

V_A, V_B, V_G ; the velocity of the two ends and centre of gravity of the fibre when it touch the conveyor belt.

φ ; the landing angle of the fibres.

$\dot{\varphi}$; the rotational velocity of the fibres at time of landing on the conveyor belt.

As the boundary conditions for real individual fibres are not known and there is no proper way neither theoretically nor experimentally to determine them, a number of

different cases with different boundary conditions were measured (i.e. different initial values for r, $\dot{r}$, ϕ, $\dot{\phi}$) . These initial values are listed in table (6.3). In the next step the equations were solved for each set of initial values and it was found that the first six set of initial conditions produce results comparable with the experimental data.

Table(6.3) The Initial Values for r, $\dot{r}$, ϕ, $\dot{\phi}$

Case	μ	r_0 (mm)	ϕ_0 (degree)	$\dot{r}_0$ (mm/sec)	$\dot{\phi}_0$ (rad/sec)
1	0.1	1.0	0.0	500.0	50.0
2	0.1	1.0	90.0	0.0	100.0
3	0.1	1.0	115.0	0.0	50.0
4	0.25	1.0	0.0	500.0	100.0
5	0.25	1.0	90.0	0.0	50.0
6	0.25	1.0	115.0	0.0	100.0
7	0.25	1.5	75.0	600.0	50.0
8	0.25	1.5	75.0	600.0	100.0
9	0.25	1.0	74.3	500.0	50.0
10	0.25	1.0	74.3	500.0	100.0
11	0.25	1.0	74.3	600.0	50.0
12	0.25	1.0	74.3	600.0	100.0
13	0.25	1.0	75.0	500.0	50.0
14	0.25	1.0	75.0	500.0	100.0
15	0.25	1.0	75.0	600.0	50.0
16	0.25	1.0	75.0	600.0	100.0
17	0.25	0.0	75.0	0.0	500.0
18	0.25	0.0	75.0	0.0	1000.0
19	0.25	1.0	74.50	0.0	0.0
20	0.25	1.0	74.5.0	1000.0	0.0
21	0.25	1.0	75.0	1000.0	50.0
22	0.25	1.0	75.0	1000.0	70.0
23	0.25	1.0	75.0	1000.0	100.0
24	0.25	1.0	75.0	1500.0	50.0
25	0.25	1.0	75.0	1500.0	70.0
26	0.25	1.0	75.0	1500.0	100.0
27	0.25	1.0	80.0	1000.0	50.0
28	0.25	1.0	80.0	1000.0	70.0
29	0.25	1.0	80.0	1000.0	100.0
30	0.25	1.0	80.0	1500.0	50.0
31	0.25	1.0	80.0	1500.0	70.0
32	0.25	1.0	80.0	1500.0	100.0

The motion of centre of gravity of the fibres for each ot these initial conditions (i.e. case 1-6) are shown in figure (6.10).

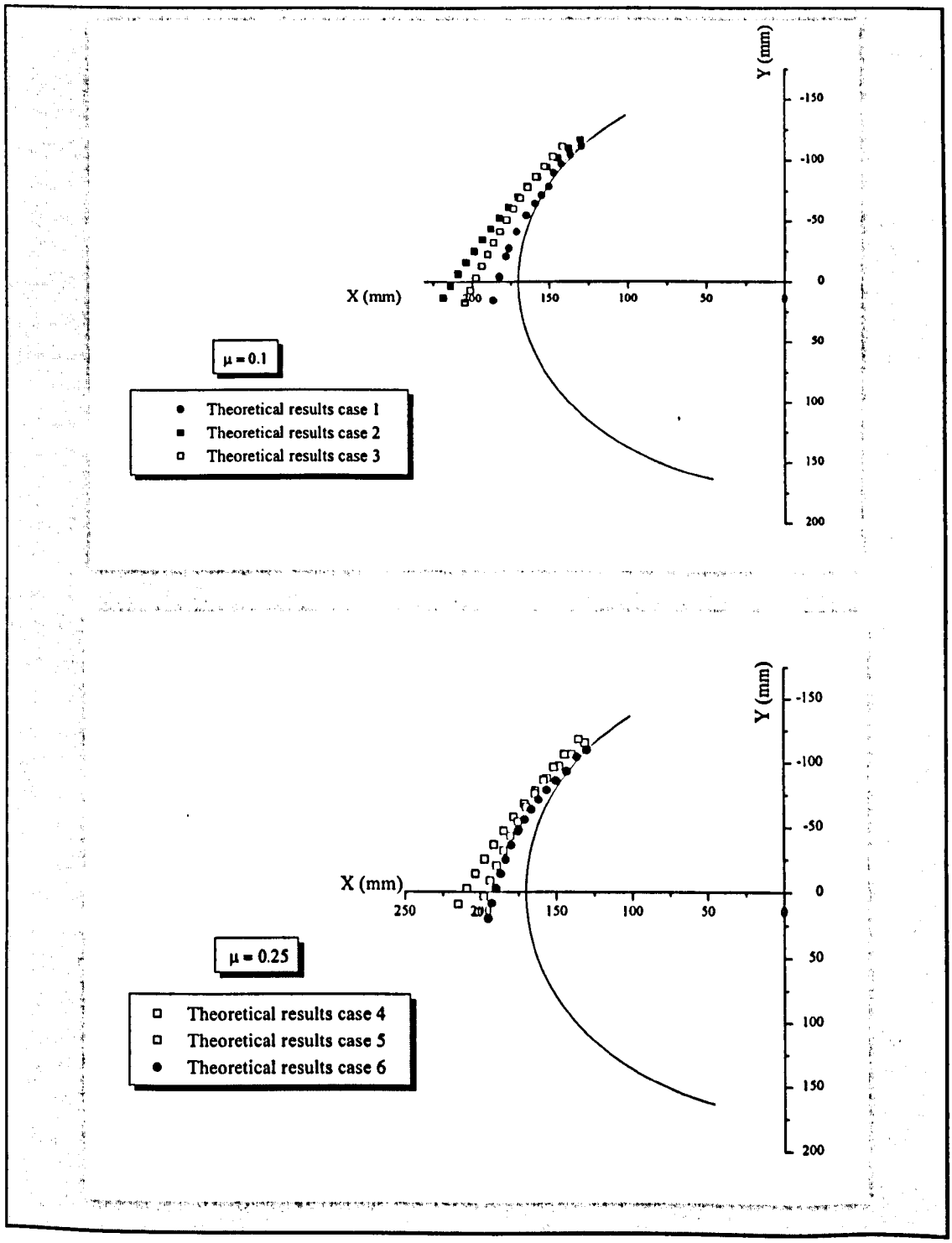

Figure (6.10) The theoretical predition of motion of centre of gravity of fibres with different initial values

6.4.1 The Effect of Some Parameters on the Fibre Motion

The effect of different factors on the fibre motion along the tooth has been investigated. The calculations were most conveniently carried out by using a dimensionless form of the equations of motion, see section 3.4. The following initial values were selected for this investigations (due to the close results of these initial values to the experimental):

r(mm)	$\dot{r}$ (mm / sec)	ϕ (degree)	$\dot{\phi}$ (rad / sec)
1.0	0.0	115.0	0.0

The effects of μ, γ, and L_p on the fibre motion were examined. A typical saw-tooth profile which is usually used on the cylinder of a carding machine is shown in figure(6.11). Here are shown the tooth length L_p and tooth leading angle γ.

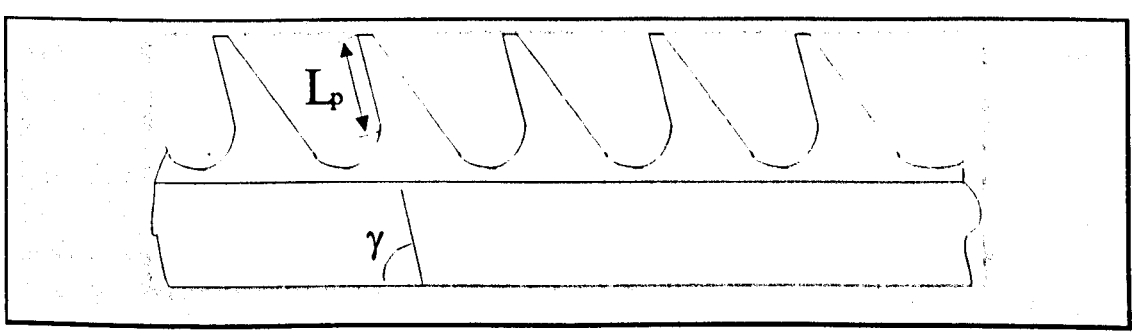

Figure (6.11) The profile of the metallic wire design

The values of 3.5, 2.5, 1.7 mm were chosen for L_p [ECC 97].

The leading or carding angle (γ) was selected in the range 75°-82° [Grimshaw 95].

The coefficient of friction between fibres and teeth (μ) is very difficult to measure. Morton and Hearle (1993) have reported some typical values for ($\mu = \frac{F}{N}$) to express

the magnitude of the friction under particular conditions. In a work done by kaster and emanuel [1964] the μ of wool fibres with carding wires was used in a range of 0.23-028. The coefficient of friction of nylon fibres with steel was also reported between 0.37-0.39 [slade 1998]. Since an absolute value for μ of polypropylene fibre against metal was not found in the literature, a range of three values of 0.1, 0.25, 0.35, were considered in the present study.

The effect of increasing μ is shown in figure(6.12). As would be expected, the higher the coefficient of friction between the fibres and teeth the longer the fibre travels along the tooth before leaving it, at both working angles of the card clothing (γ).

The effect of μ on the fibre velocity is also illustrated in figure (6.13 and 6.14). As μ increases the translational velocity of the centre of gravity of the fibres decreases at high values of L_p , when the terminal velocity is virtually independent of μ. For the rotational velocity of the fibre increasing μ tends to decrease the final rotational velocity except at low values of L_p , when again there is independence for μ.

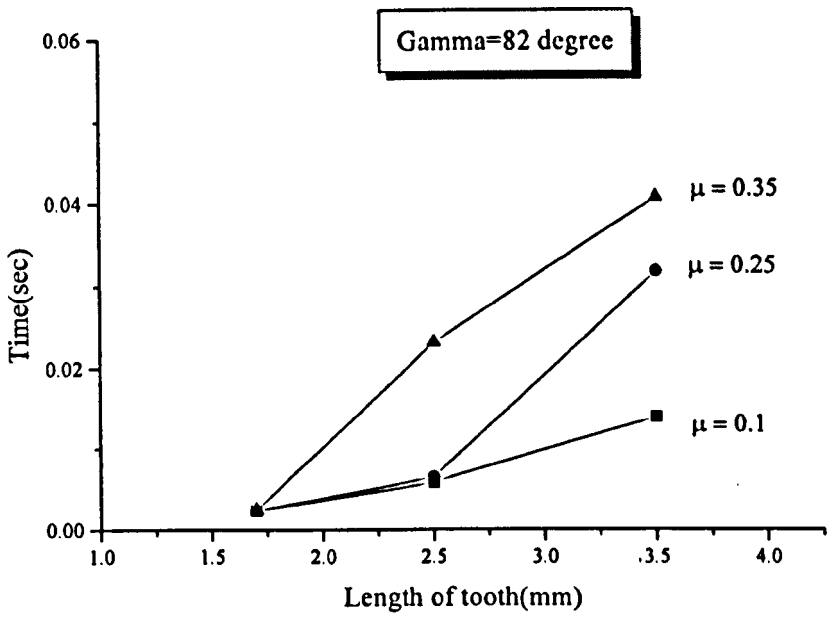

a) Gamma (working angle of card clothing) = 82 degree

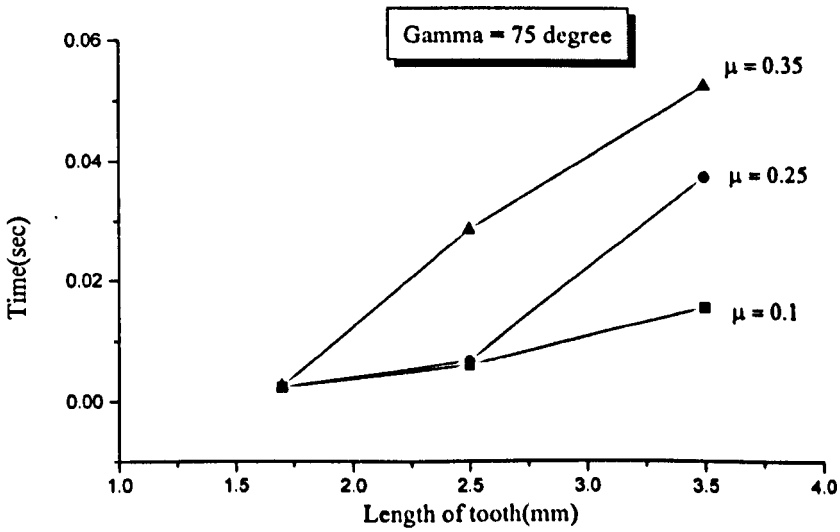

b) Gamma (working angle of card clothing) = 75 degree

Figure(6.12) The effect of γ and μ on the fibre travelling time along the tooth

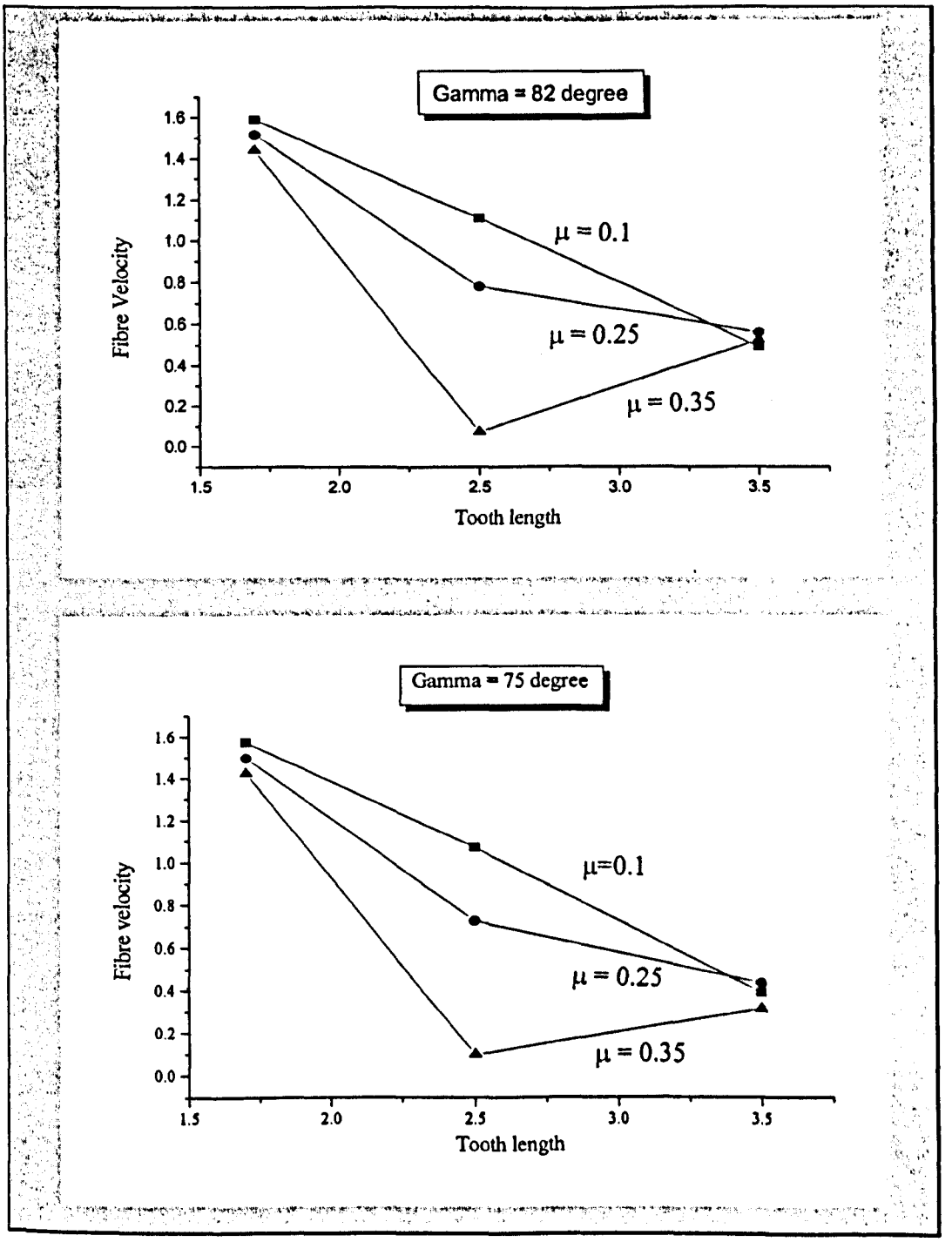

figure (6.13) The effect of μ on the translational velocity of the fibre in different working angle of card clothing (γ)

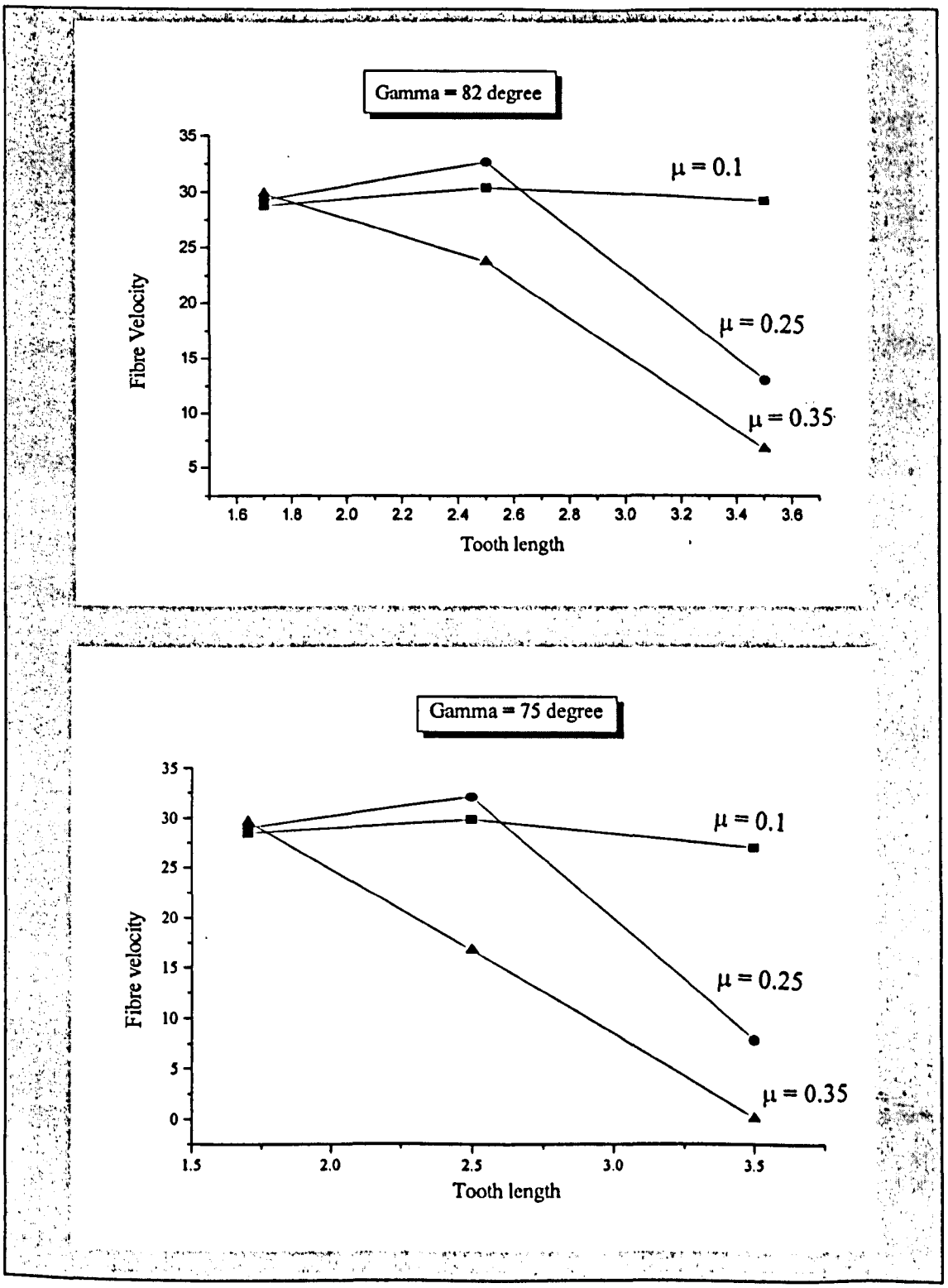

Figure (6.14) The effect of μ on the rotational velocity of the fibre in different working angle of card clothing (γ)

6.5 Comparison between the Theoretical and Experimental Results

The theoretical motion of the fibres is obviously highly dependent on the initial conditions imposed on them while they are on the teeth. In order, therefore, to compare the theory with the experimental results we need to know the appropriate initial conditions such as fibre position, speeds and frictional contact with the teeth. Still photographs (see Fig.5.9) show that fibres are often initially attached to the mid-point of the tooth with the angle (ϕ) between the fibre and tooth, see Fig.(3.2) varying from near 0.0 to 115.0 degrees. However, a problem exists with regard to the initial velocities. $\dot{r}_0$, $\dot{\phi}_0$ and the value of the coefficient of friction between the fibres and the teeth. These can not be easily measured therefore, a numerical approach was tried by considering large number of combination of these factors.

Those giving results comparable with the 95% confidence limits derived above are shown in table I

Table (6.4) The initial values used for calculating the theoretical fibre trajectory

Case	μ	r_0(mm)	δ_0(degrees)	$\dot{r}_0$(mm.s^{-1})	$\dot{\delta}_0$(rad.s^{-1})
1	0.1	1.0	0.0	500.0	100.0
2	0.1	1.0	90.0	0.0	0.0
3	0.1	1.0	115.0	0.0	0.0
4	0.25	1.0	0.0	500.0	100.0
5	0.25	1.0	90.0	0.0	0.0
6	0.25	1.0	115.0	0.0	0.0

and illustrated in figures (6.15a and 6.15b).

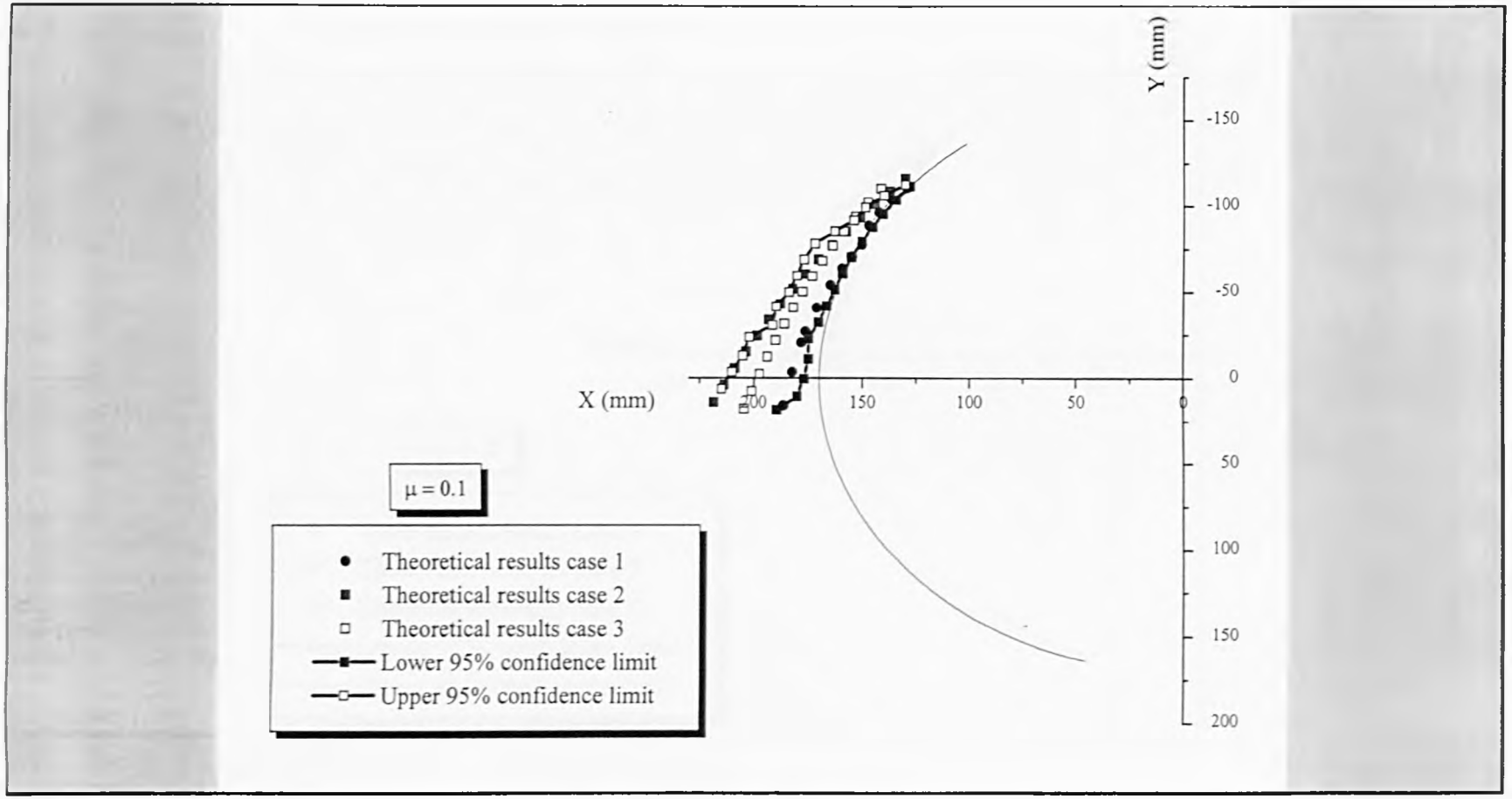

Fig(6.15a) Comparison between the theoretical and experimental results of fibre trajectory in the transport channel of the air-lay machine

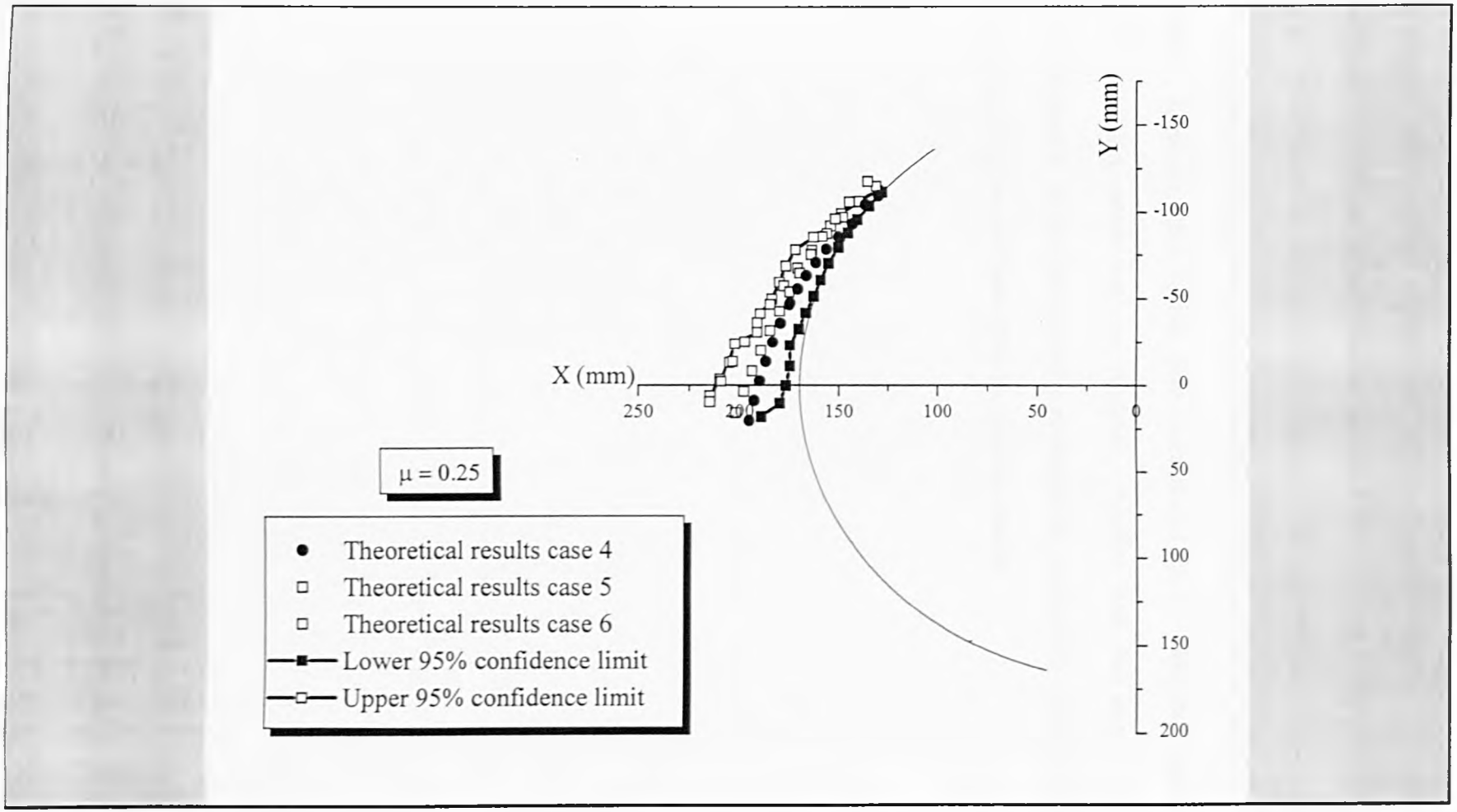

Fig(6.15b) Comparison between the theoretical and experimental results of fibre trajectory in the transport channel of the air-lay machine

As can be seen these theoretical results fall within the 95% confidence limits, suggesting that the theory is capable of giving reasonable results. An experimental approach to determining the initial values would have been preferred to the numerical one. Thus, further experimental investigation of the initial values is recommended, which should involve photographic observation of the position of the fibres on the tooth. However, this would have necessitated more additional photographic instrumentation, which was not available. Another area that may need further consideration is the development of a mathematical relationship which describes the precise nature of the air flow within the transfer channel.

Chapter Seven

Conclusions and Recommendations

6.1 Summary

Air-laid web formation technology is growing in use in the nonwoven industry due to its ability to provide the means of producing webs with equal fibre distribution in all directions , i.e. a totally randomised web.

The objective of the research reported in this thesis was to establish an improved understanding of the air-laid system which could facilitate a better final product in terms of quality and cost.

Reviewing the literature showed that no substantial study of this type (i.e. looking at a process with the aim of making a web with three dimensional fibre arrangement) has previously been made. This work is a beginning to investigate such a complex process by looking at fibre behaviour in the transport channel of the machine. The next stage of the investigation should be characterisation of the fibre behaviour in the landing area, which was beyond the scope of this research basically because of time limit.

To carry out this research an existing air-laid machine was modified so that an acceptable web can be obtained. It is believed that the way in which fibres leave the opening roller and travel in the transport channel to the landing area are the most critical factors in the final product characteristics. Therefore, attempts were made to investigate the fibre dynamics in this zone.

A theoretical model was developed to describe how the fibres move along the tooth of the opening roller clothing and then enter the transport channel. The model enables one

to predict the fibre motion both on and off the tooth and also explains how the fibre specification and machine settings alter its motion. The fibre velocity, acceleration and trajectory can be found through this model.

The conveyance of fibres in the transport channel by the carrier air, in this particular case, was assumed to be a single phase problem. This assumption is not far from reality on account of the fact that fibre flux is much less than the air flux, in other words the effect of fibres on the air flow pattern compared to the effect of air flow on the fibre motion is negligible. Therefore it is reasonable to make the single phase assumption.

The fluid field in the transport channel was assumed to be an inviscid flow (i.e. a flow field in which shearing stresses are negligible) with a linear distribution across the channel width. Although this approximation is a simple one, it has given good results in this research. From the theoretical results, it was found that the initial values (i.e. initial fibre velocity and position) have a substantial effect on the fibre motion.

To investigate the effect of different factors on the fibre motion along the tooth of the opening roller a dimensionless form of the equations was made. The effect of the coefficient of friction between fibres and teeth (μ) on the fibre motion and fibre velocity was demonstrated. It was indicated that the higher the μ the longer the fibres travel along the tooth before leaving it, at both working angles of the card clothing (i.e. $\gamma = 75^0$, $\gamma = 82^0$)

The translational velocity of the centre of gravity of the fibres decreases by increasing μ at high values of the tooth length (L_p), when the terminal velocity is virtually independent of μ. For the rotational velocity of the fibre increasing μ tends to decrease

the final rotational velocity except at low values of L_p , when again there is independence of μ.

In an attempt to validate the theoretical results high speed cine photography was employed. Because of the complexity of the situation and the need of better equipment in terms of powerful light sources and lenses, which were unavailable during the course of this work, satisfactory photographs could not be taken of the motion of fibres along the teeth. Therefore it was decided to take photographs from the transport channel sideways where the fibres are actually off the teeth of the opening roller and travelling through the transport channel

As explained in Chapter 6 it is almost impossible to capture the whole fibre length and follow a particular fibre in successive frames. This caused a difficulty in measuring the velocity of the fibre ends in successive frames, because the measuring points in a frame may move in such a way that they can not be recognised in the next frame (i.e. they may not be identical in successive frames, so that the velocity of a fibre end can not be measured in sequential frames). Alternatively, a method was developed to find the fibre trajectory through the transport channel.

The results show that during air-laying fibres first tend to travel close to the surface of the opening roller and then they start moving away from the opening surface. This trend happens in both machine settings (i.e. where the airflow is tangential to the opening roller surface and also when airflow hits the opening roller surface). Fibres follow a smooth curve where the airflow is tangential to the opening roller surface, whereas in the case of airflow hitting the opening roller surface a discontinuity in the path occurs.

The experimental results obtained may be compared with the theoretical predictions (see fig. 6.11). In this figure the theoretical predictions of the minimum, maximum and average positions of the centre of gravity of the fibres are shown, together with the average movement of the fibres in the experimental results. The theoretical predictions are highly dependent upon the initial conditions and by changing these initial values, the theoretical results could be made closer to the experimental ones. Although it is difficult, with so many variables and assumptions, to isolate the reasons for the differences that do occur, it has been established that there is reasonable agreement between the trend of fibre motion in the transfer channel predicted by theory and that observed experimentally.

7.2 Suggestions for the future work

The following suggestions are made for future work aimed at improving the understanding of air-laid web formation technology leading to the production of a high quality final product.

- The air-laid machine used should be further modified, particularly airflow mechanism. It is suggested that having a blower from the top of the transport channel results in more uniform air flow across the transport zone. Also to be able to process finer fibres the wire clothing of the rollers, especially the licker-in, should be replaced with a clothing with more wire populations.

- In the theoretical model, the air flow pattern was assumed inviscid with a linear distribution across the channel width. For further improvement of this theory a computational fluid dynamic technique can be used to simulate the fluid field. This technique relies on the numerical simulation of the flow field. The equations governing

the fluid flow are generally known for any flow situation. By identifying the boundary conditions and the geometry of the flow zone, the computer program simulates the flow in that specified region. Computational fluid dynamic methods are fairly well established commercially and several computer programs are available such as FIDAP, FLUENT, PHOENICS.

- Through the photographic experiments it is implied that a close-up lens for capturing fibre motion along the tooth and a powerful light source (basically a pulse Laser) should be used for taking satisfactory photographs. By taking such a photographs (i.e. with a sharp picture and enough Depth of Field), it would be possible to analyse the film properly, and then use the results to compare with the theoretical findings and also to get a good approximation for the initial values of the theoretical model.

- From the experiences of the film analysis it is intimated that the analysis of the films can be more conveniently done if the whole fibre length is captured in one frame, provided that the image resolution is sufficient to recognise individual fibres. The advantage of having the whole fibre in one frame is the ability to follow the fibre in successive frames without confusing the fibre ends.

REFERENCES

[Acheson 96] Acheson D J, 'Elementary Fluid Dynamics', Clasendon Press, Oxford, 1996,P 44.

[Bangert 77] Bangert L H, Sagdeo P M, 'On Fiber Alignment Using Fluid Dynamic Forces', *Textile Res. J.*,Dec.1977, 773-780.

[Brown 96] Brown R, Private Communication, Photo-sonics International Ltd., UK.,1996

[Chen 84] Chen K Z, Ph.D Thesis, UMIST, 1984.

[Clark 58] Clark J, 'Apparatus and Method for Manufactureing Fibrous Structure', USP 2 827 668,1958, USA.

[Dedocool 91] Dedocool Instruction Manual ,Dedotec USA,INC.1991

[De maro 70] De maro, 'Photography',Penguin books, 1970

[Edberg 74] Edberg B, Dissertation Gotenberg, 1974.

[ECC 97] English Card Clothing, Commertial brochure 1997.

[Emmanuel 64] Emmanuel M.V. and Kaster, 'Fibre Shedding from the Card Cylinder', *Tech. of Textile Industry U.S.S.R* ,No.2,1964, 44-48.

[Forgacs 59] Forgacs O.L., Mason S.G.,*J. Colloid Sci.*, Vol.14,1959, 473.

[Fehrer 67] Fehrer E, 'Improvements in or Relating to Apparatus for the Manufacture of a Hair or Fibre Web', BP 1 090 827, 1967, Austria.

[Fehrer 93] Fehrer E, 'Apparatus for Making a Nonwoven Web', UK Patent 2 262 $108_{(13)}$ A, 1993, Austria.

[Ghosh 68] Ghosh G C and Bhadur S N, 'Studies on Hook Formation and Cylinder Loading on the Cotton Card', *Text. Res. J*, Vol. 38, 1968, P.533

[Goldstein 38] Goldstein S, 'Modern Developments in Fluid Dynamics', Oxford University Press , London, 1938.

[Grimshaw 95] Grimshaw K 'Trend s in Nonwoven Card Clothing Design For Long Staple Carding',Summer Carding School June 1995, Dept. of Textle Industries.

[Hinds 82] Hinds W. C. ,'Aerosol Technology: Properties, Behaviour, and Measurment of Airbrone Particles, John Wiley and Sons, Inc., New York, NY, USA, 1982.

[Ingham 96] Ingam D B and Elliott L, Private Communication, Dept. of Applied Mathematics University of Leeds, 1996.

[Jantzen 96] Jantzen A, Private Communication, Photographic Analysis Company, New Jersey USA, 1996.

[Jeffery 85] Jeffery A.,'Mathematics for Engineers and Scientists',Third Edit. , VNR, 1985

[Jones 96] Jones T, Private Communication, Dept. of Textiles, UMIST, 1996.

[Kong 96] Kong L.X. ,Platfoot R.A. 'Two-dimensional Simulation of air flow in the Transfer Channel of Open-end Spinning Machine',*Textile. Res. J,* Vol. 66, No.10,1996, 641-650.

[Krause 89] Krause H W, Soliman H A, Stalder H, 'The Yarn Formation in Friction Spinning', *Int. Text. Bul.*,Yarn Forming, No.4, 1989, 31-42.

[Krcma 71] Krcma R., 'Manual of Nonwovens', The Textile Trade Press,1971.

[Kroyer 79] Kroyer K, 'Dry-Laying a Web of Particulate or Fibrous Material', USP 4 144 619, 1979,USA.

[Lawrence 86a] Lawrence C A, Chen K Z, 'Factors Affecting the Spinning of Fine Rotor-Spun Yarns', *J.Text. Inst.*, Vol. 77, No.2, 1986, 139-145.

[Lawrence 86b] Lawrence C A, Chen K Z, 'High Speed Photographic Studies of the Fibre Configuration During Transfer from the Opening Roller of a Rotor-Spinning Unit', *J.Text. Inst.*, Vol. 77, No.3, 1986, 201-211.

[Lawrence 88] Lawrence C A, Chen K Z, 'A Study of Fibre-transfer-channel Design in Rotor-spinning, Part I: The Fibre Trajectory', *J.Text. Inst.*, Vol. 79, No.3, 1988, 367-392.

[Lawrence 96] Lawrence C A, Jiang R K, 'A study of the Mechanics of Fibre Straightening During Deposition in the Disc Spinning Process Part I: Theoretical Considerations', *J. Text. Inst.*, Vol. 87, Part I, No.1, 1996, 23-36.

[Lu 96] Lu F and Moller A, 'New Technology for Microdenier Spunbonds', *Nonwoven World*, Spring 1996, 36-40.

[Lunenschloss 80] Lunenschloss *et al.*, 'Contribution to the Mechanism of the Fibre Separation and Fibre Transport in OE Rotor Spinning', VDI Progress Reports, Series 3. No. 56 , 1980.

[Morton 93] Morton W. E, and Hearle J W S, ' Physical Properties of Textile Fibres', The Textile Institute 1993.

[Munson 98] Munson B R, Young D F, Okiishi T H, 'Fundamentals of Fluid Mechanics', Jhon Wiley & Sons, Inc. New York, USA, 1998, 331, 362.

[Oxford Laser 89] Oxford Laser, 'High Speed Photography, Applications Note No:2', Oxford, UK, 1989.

[Pivko 95] Pivko I B, 'The Air-laid Fabrics business', *Nonwoven World*, April 1995, 81-85.

[Plummer 49] Plummer C H, Truslow N, Frydryk J, 'Method and Apparatus for Making Fabrics', USP 2 676 363, 1949, USA

[Photec manual 91] Photec Instruction Manual, Photonic Systems Inc. New Jersey USA,1991.

[Popov 62] Popov S G, Komarov A M, and Sluchanovskaya Z P, ***Tekstil. Prom.***,Vol.22, No.4, 1962, 77.

[Ray 97] Ray F S, 'High Speed Photography and Photonics`, Focal Press, Oxford, 1997

[Rohlena 75] Rohlena V, *et al.* 'Open-End Spinning`, Elsevier Science Publication Company, Amesterdam,1975.

[Schlichting 79] Schlichting H, 'Boundary-layer Theory` 7th Ed. New York, McGraw-Hill 1979.

[Shariq 96] Shariq K, 'Nonwoven fibres: Trend in Global Supply and Demand`, ***Nonwovens World***, spring 1996, 71-79.

[Shariq 98] Shariq K, 'Nonwoven fabrics: A global Overview`, ***Nonwovens World***, winter 1998, 90-96.

[Slade 98] Slade,P.E, 'Handbook of fibre finish technology`,Marcel Dekker, Inc., 1998, P.12

[Smith 94] Smith A C, Roberts W W, 'Straightening of Crimped and Hooked Fibers in Converging Transport Ducts', ***Textile Res. J.*** Vol.64, No.6, 1994, 335-344.

[Stalder 68] Stalder H, Dissertation ETH Zurich, 1968

[US patent] US patent, 'Machine for Forming Fibre Webs`, 1976.

[Ulku 93] Ulku S, Acar M, King T G, Ozipek B, 'Fibre Alignment and Straightening in opening for open-end spinning`, ***Textile Res.J.***Vol.63, No.6, 1993, 309-312.

[Wolf 90] Wolf H, ByrdV L, 'Flexible Composite and Multicomponent Air-formed Webs`, ***Tappi Journal***, September 1990,159-1661

[Ward 97] Ward D T, 'Energy Consumption in Hydroentanglement`,***ITB Nonwovens***, Vol.43, No. 4, 1997, 38-42.

Wood[80] Wood D E, ' Air-laid Low Density `, nonwoven conference papers, UMIST, 1980, P 89-127.

[Ymamoto 93] Ymamoto S, Matsuoka T, 'A Method for Dynamic Simulation of Rigid and Flexible Fibers in a Flow Field', ***J. chem. Phys.***, 98(1),Jan.1993, 644-650.

[Zhu 93] Zhu R Y, Leaf G A V, Oxenham W, 'Fibre Behaviour in the Twisting Zone of a Friction-Spinning Process`, ***J. Text.Inst.***,Vol.84, No.1, 1993, 57-67

The following programe is a programe written in Fortran 77 in order to solve the equations of motion of the fibres on the teeth of the opening roller of the air-laid machine.

```
*  Program based on D02BDF Example Program Text
*  Mark 14 Revised.  NAG Copyright 1989.
*  but now actually using D02CJF.
*  Modified for fibre problem Nov 1995 - Jul 1996
*
*  Latest version taking account of signs of air resistance

      IMPLICIT NONE

*  Parameter statements
      INTEGER        NEQS, IW
      PARAMETER      (NEQS = 4)
      PARAMETER      (IW = 28 + 21*NEQS)

*  Dimension statements depending on them
      DOUBLE PRECISION Y(NEQS), W(NEQS,IW)

*  External functions and subroutines
      EXTERNAL FCN, OUTPUT, ENDCON
      DOUBLE PRECISION ENDCON

*  Constants in common blocks
      DOUBLE PRECISION PI, LF, BIGR, THETA0, OMEGA, GAMMA
      COMMON /BLOCK1/  PI, LF, THETA0, GAMMA
      DOUBLE PRECISION M, G, PT, PN, THRESH, DTEX
      COMMON /BLOCK2/  M, G, PT, PN, THRESH
      DOUBLE PRECISION MU
      COMMON /FRICTN/  MU
      DOUBLE PRECISION LP
      COMMON /PINLEN/  LP
      DOUBLE PRECISION BETA, VI, L0, DI
      COMMON /AIR/ VI, BETA, L0, DI
      COMMON /NEWBLK/ BIGR, OMEGA

*  Local scalar constants and variables
      DOUBLE PRECISION TOL, T0, TEND
      DOUBLE PRECISION T, R, RDOT, PHI, PHIDOT, U, V, OMEGAF
      INTEGER I, IFAIL
      CHARACTER*1 RELABS, DUMMYC
      CHARACTER*3 RUNNO
      CHARACTER*20 NAME1, NAME2, NAME3
      INTEGER LINENO, LINEN1, LNLEN
```

```
*    Set constants
     PI = 4D0*DATAN(1D0)
     G = 9.81D0
     THRESH = 1D-4
*    Values of RDOT less than THRESH are treated as zero for the purpose
*    of deciding whether the fibre will slip along the pin in the next
*    time-step.  THRESH is about 1/10**6 times typical values of RDOT.

     WRITE (*,*) 'Motion of fibre on pin'
     WRITE (*,*)
     PRINT *, 'Number of line to use in special.data file?'
     READ *, LINENO
     IF (LINENO .LE. 9) THEN
       LNLEN = 1
     ELSE IF (LINENO .LE. 99) THEN
       LNLEN = 2
     ELSE
       LNLEN = 3
     ENDIF
     WRITE(RUNNO, 9) LINENO
  9  FORMAT(I3)
     NAME1= 'dtex11.res.' // RUNNO((4-LNLEN):3)
     NAME2 = 'DTEXNTRP11.res.' // RUNNO((4-LNLEN):3)
     NAME3 = 'VELFILE.' // RUNNO((4-LNLEN):3)
     OPEN (4, FILE=NAME1)
     OPEN (8, FILE=NAME2)
     OPEN (9, FILE=NAME3)
*    Open main data file
     OPEN (3, FILE='nag1.data')
     TOL = 5D-5
     RELABS = 'M'
     WRITE (*,99999) ' Calculation with TOL =', TOL

*    Data file must contain the following 15 numbers:
*    1) starting value of time (s)
*    2) final value of time (s)
*    3) length of pin (mm)
*    4) THE FOURTH VALUE IN THE MAIN DATA FILE IS IGNORED
*    5) THE FIFTH VALUE IN THE MAIN DATA FILE IS IGNORED
*    6) BIG R (mm)
*    7) omega (rad/s)
*    8) gamma  (degrees)
*    9) decitex (mass of 10 Km lenght ,g)
*    10) coeff of friction mu
*    11) Lf (mm)
*    12) PN (pure number - no dimensions)
*    13) PT (pure number - no dimensions)
*    14) theta 0 (degrees)
```

```
*    15) U (m/s)
*    16) V (m/s)
*    17) OMEGAF (radians/s)
*    18) VI (m/s) velocity of blower
*    19) BETA (degrees) direction of blower
*    20) L0 (narrowest channel width - m)
*    21) DI (inlet width - m)


      READ(3,*) T0, TEND, LP, R, PHI, BIGR, OMEGA,
     1        GAMMA, DTEX, MU, LF, PN, PT, THETA0, U, V, OMEGAF,
     2        VI, BETA, L0, DI

*     Override TEND!
      TEND = 5D0
*     Now read special data file for r, phi, rdot, phidot
      OPEN (2, FILE='special.data')

*     Skip past 6 comment lines in file
      DO 1 I=1,6
        READ(2,2) DUMMYC
    2   FORMAT(A)
    1 CONTINUE
      IF (DUMMYC .NE. '*') THEN
        PRINT *, ' Fewer lines beginning * than expected'
        STOP
      ENDIF
*     Read numbered lines until line numbered LINENO is found
    3 READ(2,*,END=4) LINEN1, R, PHI, RDOT, PHIDOT
      PRINT *, 'Have read values', LINEN1, R, PHI, RDOT, PHIDOT
      IF (LINEN1 .NE. LINENO) GOTO 3
      GOTO 5
    4 PRINT *, 'No line numbered ', LINENO, ' in special.data file'
      STOP

    5 CONTINUE

*     Convert angles to radians
      PHI = PI*PHI/180.0D0
      GAMMA = PI * GAMMA /180.0D0
      THETA0 = PI * THETA0 / 180.0D0
      BETA = PI * BETA / 180.0D0

*     Convert lengths to metres
      R = R/1000.0
      RDOT = RDOT/1000.0
      BIGR = BIGR/1000.0
      LF = LF/1000.0
      LP = LP/1000.0
```

```
*    COmpute mass of fibre in Kg
     M = 4*LF*DTEX*1D-7
     PRINT *, '*****************'
     PRINT *, 'The following values have been read:'
     PRINT *, 'r (metres)', R
     PRINT *, 'phi (radians)', PHI
     PRINT *, 'rdot (m/s)', RDOT
     PRINT *, 'phidot (rad/s)', PHIDOT
     PRINT *, '*****************'
     PRINT *
     PRINT *, 'Initial time', T0
     PRINT *, 'FiNAL time', TEND
     PRINT *, 'Length of pin (metres)', LP
     PRINT *, 'big R (metres)', BIGR
     PRINT *, 'omega (rad/sec)', OMEGA
     PRINT *, 'mass ', M, ' Kg'
     PRINT *, 'coeff of friction', MU
     PRINT *, 'Lf (metres)', LF
     PRINT *, 'Pn (think about units: Mass/length**2 ??)', PN
     PRINT *, 'Pt (same units)', PT
     PRINT *, 'theta0 (radians)', THETA0
     PRINT *, 'U (m/s)', U
     PRINT *, 'V (m/s)', V
     PRINT *, 'OMEGAF (rad/s)', OMEGAF

*    Compute initial values of r dot and phi dot

     T = T0

     PRINT *, 'Initial conditions set up, about to start integration'
     PRINT *, ' R RDOT PHI PHIDOT'
     PRINT *, R, RDOT, PHI, PHIDOT

*    Initial values of array Y used by NAG routine:

     Y(1) = R
     Y(2) = RDOT
     Y(3) = PHI
     Y(4) = PHIDOT
     IFAIL = 0
     CALL D02CJF(T, TEND, NEQS, Y, FCN, TOL, RELABS, OUTPUT,
    1          ENDCON, W, IFAIL)
*
     IF (IFAIL.NE.0) THEN
       WRITE (*,99998) ' D02CGF fails. IFAIL =', IFAIL
     ELSE
       PRINT *, ' D02CJF completed!'
       PRINT *, ' Fibre comes off end of pin at time', T
```

```
      PRINT *, ' Values when it comes off:'
      WRITE(4, *) ' D02CJF completed!'
      WRITE(4,*) ' Fibre comes off end of pin at time', T
      WRITE(4,*), ' Values when it comes off:'
      PRINT *, 'THETA=', 180*(THETA0+OMEGA*T)/PI
      CALL OUTPUT(T,Y)
    END IF
*
    STOP
*
99999 FORMAT (1X,A,D9.1)
99998 FORMAT (1X,A,I3)
    END
*
    SUBROUTINE FCN(T,Y,DERIV)
    IMPLICIT NONE
    DOUBLE PRECISION T, Y(4), DERIV(4)

*   Constants in common blocks
    DOUBLE PRECISION PI, LF, BIGR, THETA0, OMEGA, GAMMA
    COMMON /BLOCK1/  PI, LF, THETA0, GAMMA
    DOUBLE PRECISION M, G, PT, PN, THRESH
    COMMON /BLOCK2/  M, G, PT, PN, THRESH
    DOUBLE PRECISION MU
    COMMON /FRICTN/  MU
    COMMON /NEWBLK/ BIGR, OMEGA

*   Variables in common blocks
    DOUBLE PRECISION A(4,4), B(4)
    COMMON /EQNS/    A, B
    DOUBLE PRECISION N, F, R2DOT, PHI2DOT
    COMMON /SOLNS/ N, F, R2DOT, PHI2DOT

*   Local
    DOUBLE PRECISION R, RDOT, PHI, PHIDOT
    DOUBLE PRECISION THETA, PSI, AT, AN, Z
    DOUBLE PRECISION VT, VA, VB
    DOUBLE PRECISION XADOT, YADOT, XGDOT, YGDOT, XBDOT, YBDOT
    DOUBLE PRECISION XA, YA, XG, YG, XB, YB
      DOUBLE PRECISION AIRVXA, AIRVYA, AIRVXG, AIRVYG, AIRVXB,
AIRVYB
    R = Y(1)
    RDOT = Y(2)
    PHI = Y(3)
    PHIDOT = Y(4)

    THETA = THETA0 + OMEGA*T
    PSI = PHI - GAMMA + THETA
```

```
*   First compute the fibre velocities VT, VA, VB

    XA = BIGR * COS(THETA) + R * SIN(GAMMA - THETA)
    XG = XA + LF *SIN(PSI)
    XB = XA + 2*LF*SIN(PSI)

    YA = BIGR * SIN(THETA) + R* COS (GAMMA-THETA)
    YG = YA - LF * COS(PSI)
    YB = YA - 2*LF*COS(PSI)

    XADOT = - BIGR*OMEGA*SIN(THETA) + RDOT * SIN(GAMMA-THETA)
   1          -R*OMEGA*COS(GAMMA-THETA)

    XGDOT = XADOT + LF * COS(PSI) * (PHIDOT + OMEGA)

    XBDOT = XADOT + 2*LF * COS(PSI) * (PHIDOT + OMEGA)

    YADOT = BIGR*OMEGA*COS(THETA) + RDOT*COS(GAMMA-THETA)
   1          + R*OMEGA*SIN(GAMMA-THETA)

    YGDOT = YADOT + LF*SIN(PSI)* (PHIDOT + OMEGA)

    YBDOT = YADOT + 2*LF*SIN(PSI) * (PHIDOT + OMEGA)

    CALL AIRFLO (XA, YA, AIRVXA, AIRVYA, 'A')
    CALL AIRFLO (XG, YG, AIRVXG, AIRVYG, 'G')
    CALL AIRFLO (XB, YB, AIRVXB, AIRVYB, 'B')

    VT = (YGDOT-AIRVYG)*COS(PSI) - (XGDOT-AIRVXG)*SIN(PSI)
    VA = (XADOT-AIRVXA)*COS(PSI) + (YADOT-AIRVYA)*SIN(PSI)
    VB = (XBDOT-AIRVXB)*COS(PSI) + (YBDOT-AIRVYB)*SIN(PSI)

*   Now use VT, VA, VB to compute the air resistance terms AT, AN, Z

    AT = 4*PT*LF*VT**2
    IF (VT .LE. 0D0) AT = -AT

    IF (VA*VB .GE. 0D0) THEN
      AN = (4D0/3D0)*PN*LF*(VA**2+VA*VB+VB**2)
      IF (VA .LT. 0D0) AN = - AN
    ELSE
      AN = 4*PN*LF*(VA**3+VB**3)/(3*ABS(VB-VA))
    ENDIF

    IF (VA*VB .GE. 0D0) THEN
     Z = 2*PN*LF**2*(VB**2-VA**2)/3D0
     IF (VA .LT. 0D0) Z = -Z
    ELSE
     Z = 2*LF**2 *PN*
```

```
     1    (VA**4 - 2*VA**3*VB - 2*VA*VB**3 + VB**4)
     2    / (3*(VA-VB)**2)
*      Above formula produces a positive result if VA*VB < 0
*      (the only cases in which it is used). This is correct
*      if VA < 0 < VB, wrong if VB < 0 < VA.  So
       IF (VA .GT. 0D0) Z = -Z
      ENDIF

*     We have to solve 4 simultaneous equations
*     for N, F, R2DOT, PHI2DOT
*     The first three eqns are always the same
*     The fourth depends on whether the fibre is slipping along the pin
*
*     The 4 equations can be thought of as the matrix equation Ax=b
*     where x is the column vector (N, F, R2DOT, PHI2DOT).

*     Set up first equation (N = ...)

      A(1,1) = 1
      A(1,2) = 0
      A(1,3) = 0
      A(1,4) = -M*LF*COS(PHI)

      B(1) = M*G*SIN(GAMMA-THETA) - M*BIGR*OMEGA**2*COS(GAMMA)
     1     - 2*M*OMEGA*RDOT + AN*COS(PHI)
     2     - (AT + M*LF*(PHIDOT + OMEGA)**2) * SIN(PHI)

*     Set up second equation (F + m r2dot = ...)

      A(2,1) = 0
      A(2,2) = 1.
      A(2,3) = M
      A(2,4) = M*LF*SIN(PHI)

      B(2) = M*G*COS(GAMMA-THETA) + M*BIGR*OMEGA**2*SIN(GAMMA)
     1     + M*R*OMEGA**2 - AN*SIN(PHI)
     2     - (AT + M*LF*(PHIDOT+OMEGA)**2) * COS(PHI)
*     PRINT *,  'VA VB VT', VA, VB, VT
*     PRINT *, 'AN AT Z/LF', AN, AT, Z/LF
*     PRINT *, 'B2 terms',
*     1  M*G*COS(GAMMA-THETA) , M*BIGR*OMEGA**2*SIN(GAMMA),
*     2     + M*R*OMEGA**2, - AN*SIN(PHI),
*     3     - (AT + M*LF*(PHIDOT+OMEGA)**2) * COS(PHI)

*     Set up third equation (moments about G)

      A(3,1) = LF*COS(PHI)
      A(3,2) = -LF*SIN(PHI)
      A(3,3) = 0
```

```
      A(3,4) = M * LF**2 / 3D0

      B(3) = -Z

*     Now for the fourth equation

      IF (ABS(RDOT).GT. THRESH) THEN
*       The fibre  is definitely slipping.
*       It will continue for a while yet.
*       Set up fourth equation according to direction of slip.
        IF (RDOT .GT. 0) THEN
          PRINT *, 'Slipping forwards'
          CALL SETUP4 (+1)
        ELSE
          PRINT *, 'Slipping backwards'
          CALL SETUP4 (-1)
        ENDIF
*       Call subroutine to solve equations for N, F, R2DOT, PHI2DOT
        CALL SOLVEQ
      ELSE
*       In the immediate past the fibre has not been
*       slipping along the pin.  First assume that it
*       will continue not to slip in the immediate future.
*       So set up the fourth equation as r2dot = 0 and solve the set.
        PRINT *, 'Try no slip'
        CALL SETUP4(0)
        CALL SOLVEQ

*       Are the resulting values of F and N consistent with
*       the assumption?

        IF (ABS(F) .LE. MU*ABS(N)) THEN
*         The hypothesis of no slipping turns out to be consistent.
*         The values we have just computed are the true ones
*         Force RDOT to be exactly zero
*         RDOT = 0
          PRINT *, ' this works'
        ELSE
*         Hypothesis is wrong: there is slipping.
*         Is it in direction of increasing or decreasing r?
*         The value of F that we have just computed is the
*         value that would have been needed to keep r2dot=0.

          IF (F.GT.0) THEN
*           slipping in the +r direction.
*           set up fourth equation accordingly
            PRINT *, 'Must be forward slip'
            CALL SETUP4 (+1)
          ELSE
```

```
*          slipping in the -r direction
           PRINT *, 'Must be backward slip'
           CALL SETUP4 (-1)
         ENDIF
         CALL SOLVEQ
       ENDIF
     ENDIF

     DERIV(1) = RDOT
     DERIV(2) = R2DOT
     DERIV(3) = PHIDOT
     DERIV(4) = PHI2DOT
     WRITE(*,101), T, 180*THETA/PI, 1000*R, RDOT, R2DOT, 180*PHI/PI,
    1    180*PSI/PI, PHIDOT, PHI2DOT, 1000*N, 1000*F, F/(MU*ABS(N))
 101  FORMAT ('T=', F7.5, ' THETA=', F6.2, ' R=', F4.2, ' RDOT=', F7.5,
    1     ' R2DOT=', F11.5, ' PHI=', F6.2, ' PSI=', F6.2,
    1     ' PHIDOT=', F7.2, ' PHI2DOT=', F9.2,/ ' N=', F6.3,
    1     ' F=', F6.3, ' F/Fmax=', F5.2)
     PRINT *, 'B(1)=', B(1), ' B(2)=', B(2), ' F+mr2dot', F + M*R2DOT
     RETURN
     END
*
*
     SUBROUTINE SETUP4 (SLIP)
     IMPLICIT NONE
     INTEGER SLIP
     DOUBLE PRECISION A(4,4), B(4)
     COMMON /EQNS/ A,B
     DOUBLE PRECISION MU
     COMMON /FRICTN/ MU
*    Set up fourth equation in manner indicated by SLIP
*    First 3 equations already set up
*    All versions of eqn 4 have 0 on right and do not involve phi2dot
     IF (SLIP .EQ. 0) THEN
*       No slipping
*       Equation is r2dot = 0
        A(4,1) = 0
        A(4,2) = 0
        A(4,3) = 1
        A(4,4) = 0
        B(4) = 0
     ELSE IF (SLIP .GT. 0) THEN
*       Slipping in direction of increasing r
*       So F = mu ABS(N)
*       But as N < 0, this means F = - mu N
*       or mu N + F = 0
        A(4,1) = MU
        A(4,2) = 1
        A(4,3) = 0
```

```
      A(4,4) = 0
      B(4) = 0
    ELSE
*     Slipping in direction of increasing r
*     So F = - mu ABS(N)
*     But as N < 0, this means F = + mu N
*     or -mu N + F = 0
      A(4,1) = -MU
      A(4,2) = 1
      A(4,3) = 0
      A(4,4) = 0
      B(4) = 0
    ENDIF
    RETURN
    END
SUBROUTINE SOLVEQ
    IMPLICIT NONE
    DOUBLE PRECISION A(4,4), B(4)
    COMMON /EQNS/   A, B
    DOUBLE PRECISION N, F, R2DOT, PHI2DOT
    COMMON /SOLNS/ N, F, R2DOT, PHI2DOT
    DOUBLE PRECISION ANS(4), TRIFAC(4,4), WKS1(4), WKS2(4)
    INTEGER IFAIL
    IFAIL = 0
    CALL F04ATF(A, 4, B, 4, ANS, TRIFAC, 4, WKS1, WKS2, IFAIL)
    IF (IFAIL .NE. 0) THEN
      PRINT *, 'Fail to solve simulaneous equations!'
      PRINT *, 'F04ATF IFAIL =', IFAIL
      STOP
    ENDIF
    N = ANS(1)
    IF (N .GT. 0) THEN
      PRINT *, 'N computed to be > 0'
      PRINT *, 'This may mean fibre slips off pin sideways!'
      STOP
    ENDIF
    F = ANS(2)
    R2DOT = ANS(3)
    PHI2DOT = ANS(4)
    RETURN
    END
*
*
    SUBROUTINE OUTPUT (T, Y)
    IMPLICIT NONE
    DOUBLE PRECISION T, Y(4)
    DOUBLE PRECISION PI, LF, BIGR, THETA0, OMEGA, GAMMA
    COMMON /BLOCK1/  PI, LF, THETA0, GAMMA
    COMMON /NEWBLK/ BIGR, OMEGA
```

```
      DOUBLE PRECISION XA, YA, XG, YG, XB, YB, R, PHI, THETA, PSI
      DOUBLE PRECISION RDOT, PHIDOT
      DOUBLE PRECISION XADOT, YADOT, XGDOT, YGDOT, XBDOT, YBDOT

      R = Y(1)
      RDOT = Y(2)
      PHI = Y(3)
      PHIDOT = Y(4)
      THETA = THETA0 + OMEGA*T
      PSI = PHI - GAMMA + THETA

      XA = BIGR*COS(THETA) + R*SIN(GAMMA-THETA)
      YA = BIGR*SIN(THETA) + R*COS(GAMMA-THETA)

      XG = XA + LF*SIN(PSI)
      YG = YA  -LF*COS(PSI)

      XB = XA + 2*LF*SIN(PSI)
      YB = YA - 2*LF*COS(PSI)

      XADOT = - BIGR*OMEGA*SIN(THETA) + RDOT * SIN(GAMMA-THETA)
     1          -R*OMEGA*COS(GAMMA-THETA)

      XGDOT = XADOT + LF * COS(PSI) * (PHIDOT + OMEGA)

      XBDOT = XADOT + 2*LF * COS(PSI) * (PHIDOT + OMEGA)

      YADOT = BIGR*OMEGA*COS(THETA) + RDOT*COS(GAMMA-THETA)
     1          + R*OMEGA*SIN(GAMMA-THETA)

      YGDOT = YADOT + LF*SIN(PSI)* (PHIDOT + OMEGA)

      YBDOT = YADOT + 2*LF*SIN(PSI) * (PHIDOT + OMEGA)

      WRITE(9,1113) T, XADOT, YADOT, XGDOT, YGDOT, XBDOT, YBDOT
      WRITE (9,1114), SQRT(XADOT**2+YADOT**2),
     1          SQRT(XGDOT**2+YGDOT**2),
     2          SQRT(XBDOT**2+YBDOT**2)
      WRITE(9,1115)

C     PRINT *, 'T  THETA(DEG) R(MM)  RDOT(MM/S)',
C     1      ' PHI(DEG)  PHIDOT(RAD/S)'
      WRITE(8,1111) T, 180.0D0*THETA/PI, 1000*Y(1),
     1          1000*Y(2),  180.0D0*Y(3)/PI, Y(4)
C     WRITE(4,*) 'X(MM)      Y(MM)'
      WRITE(4,1112) T, 1000*XA, 1000*YA, 1000*XG, 1000*YG,
     1          1000*XB, 1000*YB
      T = T + 1D-4
      RETURN
```

```
1111  FORMAT(F7.6, 1X, F8.3, 1X, F5.3, F18.3, 4X, F12.3, F16.3)
1112  FORMAT(F7.6, 1X, F10.5, 1X, F10.5, 1X, F10.5, 1X, F10.5,
     1      1X, F10.5, 1X, F10.5)
1113  FORMAT(F6.4, 6(X,F10.5))
1114  FORMAT(10X,3(F10.5, 11X))
1115  FORMAT()
      END
*
*
      DOUBLE PRECISION FUNCTION ENDCON (T,Y)
*     Ending condition - fibre reaches end of pin
      IMPLICIT NONE
      DOUBLE PRECISION T, Y(4)
      DOUBLE PRECISION LP
      COMMON /PINLEN/ LP
      ENDCON = LP - Y(1)
*     Y(1) is R, so ENDCON = 0 when fibre falls off end of pin
      RETURN
      END
```

This program solves the equations of motion of the fibres in the transport channel of the air-laid machine.

```
*   Program based on D02BDF Example Program Text
*   but now actually using D02CJF.
*   Modified for fibre problem Nov 1995
*   Mark 14 Revised.  NAG Copyright 1989.
    IMPLICIT NONE
*   .. Parameters ..
    INTEGER          NOUT
    PARAMETER        (NOUT=6)
    INTEGER          NEQS, IW
    PARAMETER        (NEQS=6)
    PARAMETER        (IW=28 + 21*NEQS)
*   .. Local Scalars ..
    DOUBLE PRECISION PI, TOL, T, TEND
    INTEGER          IFAIL
*   .. Local Arrays ..
    DOUBLE PRECISION W(NEQS,IW), Y(NEQS)
*   Y(1) = XG
*   Y(2) = X DOT
*   Y(3) = YG
*   Y(4) = Y DOT
*   Y(5) = PSI
*   Y(6) = PSI DOT
*   .. External Functions ..
    DOUBLE PRECISION X01AAF
    EXTERNAL         X01AAF
*   .. External Subroutines ..
    EXTERNAL         D02BDF, FCN, OUT, G, OUTPUT, HITBLT
    DOUBLE PRECISION T0, R, RDOT, PHI, PHIDOT, THETA, THMG
    DOUBLE PRECISION BIGR, OMEGA, GAMMA, M, LF, LP, PN, PT, II
    DOUBLE PRECISION HITBLT,G, DTEX
          DOUBLE PRECISION DUMMY1, DUMMY2, DUMMY3, DUMMY4,
   DUMMY5,
     1          DUMMY10, DUMMY14, DUMMY15, DUMMY16, DUMMY17
    DOUBLE PRECISION XG, XDOT, YG, YDOT, PSI, PSIDOT, PI
    CHARACTER*1 RELABS
    CHARACTER*3 RUNNO
    CHARACTER*20 NAME1,NAME2, NAME3
    INTEGER LINENO, LNLEN
    COMMON LF, PT, PN, M, H
    DOUBLE PRECISION BETA, VI, L0, DI
    COMMON /AIR/ VI, BETA, L0, DI
    COMMON /NEWBLK/ BIGR, OMEGA
*   .. Executable Statements ..
```

```
      PI = 4D0*DATAN(1D0)
      WRITE (NOUT,*) 'D02CJF Example Program Results'
      WRITE (NOUT,*)
      PRINT *, 'Number of case?'
      READ *, LINENO
      IF (LINENO .LE. 9) THEN
        LNLEN = 1
      ELSE IF (LINENO .LE. 99) THEN
        LNLEN = 2
      ELSE
        LNLEN = 3
      ENDIF
      WRITE(RUNNO, 9) LINENO
    9 FORMAT(I3)
      NAME1= 'dtexnew.results.' // RUNNO((4-LNLEN):3)
      NAME2= 'dtexnew.ends.' // RUNNO((4-LNLEN):3)
      NAME3= 'VELFILE.offpin.' // RUNNO((4-LNLEN):3)
      OPEN (4, FILE=NAME1)
      OPEN (8, FILE=NAME2)
      OPEN (9, FILE=NAME3)
*     Open main data file
      OPEN (3, FILE='nag1.data')
      M = 75
      PI = X01AAF(T)
      TOL = 5D-5
      RELABS = 'A'
      WRITE (NOUT,99999) ' Calculation with TOL =', TOL

*     Data file must contain the following 15 numbers:
*     1) starting value of time (s) (IGNORED)
*     2) final value of time (s)    (IGNORED)
*     3) length of pin (mm)         (IGNORED)
*     4) THE FOURTH VALUE IN THE MAIN DATA FILE IS IGNORED
*     5) THE FIFTH VALUE IN THE MAIN DATA FILE IS IGNORED
*     6) BIG R (mm)
*     7) omega (rad/s)
*     8) gamma  (degrees)
*     9) mass of fibre (kg)
**    10) coeff of friction mu      (IGNORED)
*     11) Lf (mm)
*     12) PN (pure number - no dimensions)
*     13) PT (pure number - no dimensions)
**    14) theta 0 (degrees)         (IGNORED)
**    15) U (m/s)                   (IGNORED)
**    16) V (m/s)                   (IGNORED)
**    17) OMEGAF (radians/s)        (IGNORED)
*     18) VI (m/s) velocity of blower
*     19) BETA (degrees) direction of blower
*     20) L0 (narrowest channel width - m)
```

```
*    21) DI (inlet width - m)


     READ(3,*) DUMMY1, DUMMY2, DUMMY3, DUMMY4, DUMMY5, BIGR,
    1       OMEGA, GAMMA, DTEX, DUMMY10, LF, PN, PT, DUMMY14,
    2       DUMMY15, DUMMY16, DUMMY17, VI, BETA, L0, DI

     PRINT *, ' Please supply values for T THETA R RDOT PHI PHIDOT'
     PRINT *, ' at time fibre comes off pin'
     PRINT *, ' from last line of relevant NRTP results file:'

     READ *, T0, THETA, R, RDOT, PHI, PHIDOT
     TEND = 1D1

     PRINT *, 'Depth to belt (H) (mm):'
     READ *, H

*    Convert angles to radians
     THETA = PI*THETA/180D0
     PHI = PI*PHI/180.0D0
     GAMMA = PI * GAMMA /180.0D0
     BETA = PI * BETA /180.0D0

*    Convert lengths to metres
     R = R/1000.0
     RDOT = RDOT/1000.0
     BIGR = BIGR/1000.0
     LF = LF/1000.0
     LP = LP/1000.0
     H = H/1000.0
*    Compute mass in Kg
     M = 4 * LF * DTEX *1D-7

     PRINT *, '*****************'
     PRINT *, 'The following values have been read:'
     PRINT *, 'r (metres)', R
     PRINT *, 'phi (radians)', PHI
     PRINT *, 'rdot (m/s)', RDOT
     PRINT *, 'phidot (rad/s)', PHIDOT
     PRINT *, '*****************'
     PRINT *
     PRINT *, 'Initial time', T0
     PRINT *, 'FiNAL time', TEND
     PRINT *, 'big R (metres)', BIGR
     PRINT *, 'omega (rad/sec)', OMEGA
     PRINT *, 'm mass (kg)', M
     PRINT *, 'Lf (metres)', LF
     PRINT *, 'Pn (think about units: Mass/length**2 ??)', PN
     PRINT *, 'Pt (same units)', PT
```

```
      PRINT *, 'Vi (m/s)', VI
      PRINT *, 'beta (radians)', BETA


*     Compute initial values of r dot and phi dot

      PSI = THETA - GAMMA + PHI
      PSIDOT = OMEGA + PHIDOT
      THMG = THETA - GAMMA

      XG = BIGR*COS(THETA) - R*SIN(THMG) + LF*SIN(PSI)
      XDOT = - BIGR*OMEGA*SIN(THETA) - RDOT*SIN(THMG)
     1       -R*OMEGA*COS(THMG) + LF*PSIDOT*COS(PSI)

      YG = BIGR*SIN(THETA) + R*COS(THMG) - LF*COS(PSI)
      YDOT = BIGR*OMEGA*COS(THETA) + RDOT*COS(THMG)
     1      - R*OMEGA*SIN(THMG) + LF*PSIDOT*SIN(PSI)

      T = T0

      PRINT *, 'Initial conditions set up, about to start integration'

      PRINT *, ' Consistency checks on initial conditions'
      PRINT *, ' will be put here later'

*     Initial values of array Y used by NAG routine:

      Y(1) = XG
      Y(2) = XDOT
      Y(3) = YG
      Y(4) = YDOT
      Y(5) = PSI
      Y(6) = PSIDOT

      PRINT *, 'At start of computation, X XDOT Y YDOT PSI PSIDOT are'
      PRINT *, Y

      IFAIL = 0
      CALL D02CJF(T, TEND, NEQS, Y, FCN, TOL, RELABS, OUTPUT, HITBLT,
     1           W, IFAIL)
*
      IF (IFAIL.NE.0) THEN
        WRITE (NOUT,99998) ' D02CGF fails. IFAIL =', IFAIL
      ELSE
        PRINT *, ' D02CJF completed!'
        PRINT *, ' Fibre touches belt at time', T
        PRINT *, ' Values when it touches:'
        WRITE(4, *) ' D02CJF completed!'
        WRITE(4,*) ' Fibre touches belt at time', T
```

```
      WRITE(4,*), ' Values when it touches:'
      CALL OUTPUT(T,Y)
    END IF
*
    STOP
*
99999 FORMAT (1X,A,D9.1)
99998 FORMAT (1X,A,I3)
    END

*
    SUBROUTINE FCN(T,Y,DERIV)
    IMPLICIT NONE
*   .. Parameters ..
    INTEGER      NEQS
    PARAMETER    (NEQS=6)
*   .. Scalar Arguments ..
    DOUBLE PRECISION T
*   .. Array Arguments ..
    DOUBLE PRECISION DERIV(NEQS), Y(NEQS)
*   Local scalars ...
    DOUBLE PRECISION M, LF, H
    DOUBLE PRECISION G, I, PN, PT
    DOUBLE PRECISION XG,YG, XDOT,YDOT, PSI,PSIDOT
    DOUBLE PRECISION VT, VA, VB
    DOUBLE PRECISION AN, AT, Z
       DOUBLE PRECISION AIRVXA, AIRVYA, AIRVXG, AIRVYG, AIRVXB,
AIRVYB
    COMMON LF, PT, PN, M, H
*   .. Executable Statements ..

    XG = Y(1)
    XDOT = Y(2)
    YG = Y(3)
    YDOT = Y(4)
    PSI = Y(5)
    PSIDOT = Y(6)

    G = 9.81D0
    CALL AIRFLO (XG - LF*SIN(PSI), YG+LF*COS(PSI), AIRVXA, AIRVYA,
   1  'A')
    CALL AIRFLO (XG, YG, AIRVXG, AIRVYG, 'G')
    CALL AIRFLO (XG + LF*SIN(PSI), YG - LF*COS(PSI), AIRVXB, AIRVYB,
   1 'B')
    VT = (YDOT-AIRVYG)*COS(PSI) - (XDOT-AIRVXG)*SIN(PSI)
    VA = (XDOT-AIRVXA)*COS(PSI) + (YDOT-AIRVYA)*SIN(PSI) - LF*PSIDOT
    VB = (XDOT-AIRVXB)*COS(PSI) + (YDOT-AIRVYB)*SIN(PSI) + LF*PSIDOT

    AT = 4*PT*LF*VT**2
```

```
      IF (VT .LE. 0D0) AT = -AT

      IF (VA*VB .GE. 0D0) THEN
        AN = (4D0/3D0)*PN*LF*(VA**2+VA*VB+VB**2)
        IF (VA .LT. 0D0) AN = - AN
      ELSE
        AN = 4*PN*LF*(VA**3+VB**3)/(3*ABS(VB-VA))
      ENDIF

      IF (VA*VB .GE. 0D0) THEN
        Z = 2*PN*LF**2*(VB**2-VA**2)/3D0
        IF (VA .LT. 0D0) Z = -Z
      ELSE
*       Z = -2*LF**2 *PN*
*     1    (VA**4+10*VA**3*VB+12*VA**2*VB**2+10*VA*VB**3+VB**4)
*     2    / (3*(VA-VB)**2)
*
        Z = 2*LF**2 *PN*
     1    (VA**4 - 2*VA**3*VB - 2*VA*VB**3 + VB**4)
     2    / (3*(VA-VB)**2)
        IF (VA .GT. 0D0) Z = -Z

      ENDIF
      PRINT *, 'VA=', VA, ',  VB=', VB, ',  VT=', VT
      PRINT *, 'AN=', AN, ', AT=', AT, ',  Z=', Z
*     PRINT *, 'Components of Xdotdot:'
*     PRINT *, ' From transverse air resistance', AT*SIN(PSI)/M
*     PRINT *, 'From normal air resistance', -AN*COS(PSI)/M
      I = M *LF**2/3D0

      DERIV(1) = XDOT
      DERIV(2) = (AT * SIN(PSI) - AN*COS(PSI))/M
      DERIV(3) = YDOT
      DERIV(4) = G - (AT * COS(PSI) + AN * SIN(PSI))/M
      DERIV(5) = PSIDOT
      DERIV(6) = -Z/I
      print *
*     PRINT *, 'Y"/X"', DERIV(4)/DERIV(2)
      Print *, 'T=', T, '  X=', xg, '  Y=', yg
      print *, 'psi(deg)=', 180*psi/3.14159
      print *, 'xdot=', xdot, '  ydot =', ydot
      print *, 'air vel', airvxg, airvyg
      print *, 'rel to air xdot=', xdot -airvxg, ' ydot=',
     1             ydot -airvyg
      print *, 'x-comp of an', -AN*COS(PSI)/M
      print *, 'x-comp of At', AT*SIN(PSI)/M
      print *, 'x2dot=', deriv(2)
      print *, 'y-comp of An', -AN*SIN(PSI)/M
      print *, 'y-comp of At', -AT*COS(PSI)/M
```

```
      print *, 'y2dot=', deriv(4)
      print *
      RETURN
      END



      SUBROUTINE OUTPUT (T, Y)
      IMPLICIT NONE
      INTEGER NEQS
      PARAMETER(NEQS=6)
      DOUBLE PRECISION T, Y(NEQS)
      DOUBLE PRECISION XG, XGDOT, YG, YGDOT, PSI, PSIDOT, PI
      DOUBLE PRECISION LF, PT, PN, M, H
      DOUBLE PRECISION XADOT, XBDOT, YADOT, YBDOT
      COMMON LF, PT, PN, M, H
      PI = 4D0*DATAN(1D0)
      XG = Y(1)
      XGDOT = Y(2)
      YG = Y(3)
      YGDOT = Y(4)
      PSI = Y(5)
      PSIDOT = Y(6)

      XADOT = XGDOT - LF*PSIDOT*COS(PSI)
      YADOT = YGDOT - LF*PSIDOT*SIN(PSI)

      XBDOT = XGDOT + LF*PSIDOT*COS(PSI)
      YBDOT = YGDOT + LF*PSIDOT*SIN(PSI)

      WRITE(9,1113) T, XADOT, YADOT, XGDOT, YGDOT, XBDOT, YBDOT
      WRITE (9,1114), SQRT(XADOT**2+YADOT**2),
     1          SQRT(XGDOT**2+YGDOT**2),
     2          SQRT(XBDOT**2+YBDOT**2)
      WRITE(9,1115)

      PRINT *, 'T  XG  XGDOT YG  YGDOT  PSI(deg) PSIDOT(rad/s)'
      WRITE(4,1111) T,  1000*XG, 1000*XGDOT, 1000*YG, 1000*YGDOT,
     1          180D0*PSI/PI, PSIDOT
      WRITE(8,1112) T, 1000*(XG + LF*SIN(PSI)), 1000*(YG-LF*COS(PSI)),
     1            1000*XG, 1000*YG,
     2          1000*(XG - LF*SIN(PSI)), 1000*(YG+LF*COS(PSI))
      T = T + 1D-3
      RETURN
1111  FORMAT(F7.6, 3(X,F8.3, X, F11.3))
1112  FORMAT(F7.6,6(X,F8.3))
1113  FORMAT(F6.4, 6(X,F10.5))
1114  FORMAT(10X,3(F10.5, 11X))
```

```
1115 FORMAT()
     END

     DOUBLE PRECISION FUNCTION HITBLT (T,Y)
     IMPLICIT NONE
     INTEGER NEQS
     PARAMETER (NEQS = 6)
     DOUBLE PRECISION T, Y(NEQS)
     DOUBLE PRECISION LF, YG, PSI, PT, PN, M, H
     COMMON LF, PT, PN, M, H
     YG = Y(3)
     PSI = Y(5)
     HITBLT = H - MAX (YG - LF * COS(PSI), YG + LF * COS(PSI))
*    HITBLT=0 when fibre hits belt
     RETURN
     END
```

This program calculates the air flow in the transport channel of the air-laid machine

```
SUBROUTINE AIRFLO (X, Y, AIRVX, AIRVY, POINT)
    IMPLICIT NONE
    CHARACTER*1 POINT
    DOUBLE PRECISION X, Y, AIRVX, AIRVY
    DOUBLE PRECISION BETA, VI, L0, DI
    COMMON /AIR/ VI, BETA, L0, DI
    DOUBLE PRECISION BIGR, OMEGA
    COMMON /NEWBLK/ BIGR, OMEGA
    DOUBLE PRECISION U, V, AIRVU, AIRVV, L
    double precision typvel
    typvel = vi * di/ l0
    U = X*SIN(BETA) - Y*COS(BETA)
    V = X*COS(BETA) + Y*SIN(BETA)
*   print *, 'entering airflo for ', point
    IF (U .GT. BIGR + L0) THEN
*     AIRVU = - 20*VI
*     AIRVV = 0
      Print *, ' !!!!!!!!!!!!!!!!! hits side of channel!'
      print *, 'x,y,u,v=', x,y,u,v
      airvu = -typvel
      airvv = typvel
    ELSE IF (U**2 + V**2 .LT. BIGR**2) THEN
*     AIRVU = 20*(U/BIGR)*VI
*     AIRVV = 20*(V/BIGR)*VI
      print *, ' !!!!!!!!!!!!!!!!! hits drum !'
      airvu = typvel
      airvv = typvel
    ELSE IF (V .LT. BIGR) THEN
*     print * , ' >>>> in channel! <<<<<<<<<<<<<<<<<<<<<<'
      L = BIGR + L0 - SQRT (BIGR**2 - V**2)
      AIRVU = 0
      AIRVV = VI*DI / L
    ELSE
*     AIRVU = 0
*     AIRVV = VI/10
      print *, ' !!!!!!!!!!!!!!!!! gets near bend in channel!'
      airvu = 0
      airvv = typvel
    ENDIF
    AIRVX = AIRVU*SIN(BETA) +AIRVV*COS(BETA)
    AIRVY = AIRVV*SIN(BETA) - AIRVU*COS(BETA)
*   print *, 'in airflo, u=', u, '  v=', v
*   print *, 'airvu=', airvu, '  airvv=', airvv
*   print *, 'airvx=', airvx, '  airvy=', airvy
    RETURN
    END
```